# 24th Electromagnetic Induction Workshop

**13-20 August 2018, Helsingør Denmark**

**www.emiw2018.org**

# Abstracts Session 5

## SESSIONS DESCRIPTION

### Session 5. Marine EM

Marine EM encompasses both active and passive soundings of the sub-seafloor from the Arctic to the tropics and from mid-Ocean ridges to continental shelves. We invite contributions from authors working at all scales of marine EM, stretching from large arrays for offshore and amphibious exploration to borehole logging and monitoring. We welcome results of basic and applied research including the challenges inherent in running field campaigns, developing instruments, processing data, estimating errors, and implementing inversion algorithms. We encourage discussions on state-of-the art methods for marine magnetotelluric and controlled source electromagnetic data acquisition, inversion and interpretation as well as where active exploration is heading given recent emphasis in deep-sea mineral deposits, petroleum exploration and shallow water CO2 sequestration.

***Conveners: Romina Gehrmann, Kim Senger, Yuguo Li***

# 1D anisotropic inversion of marine CSEM data

Ming Luo[1*], Yuguo Li[1]
[1] Key Lab of Submarine Geosciences and Prospecting Techniques of Ministry of Education, Ocean University of China, luoming@ouc.edu.cn

## SUMMARY

When interpreting marine controlled-source electromagnetic (CSEM) data sets, it is often assumed that seafloor conductivity structures are electrically isotropic. However, it is commonly known that in the fold and thrust areas hydrocarbon reservoirs are frequently overlain by thick sedimentary sequences including shale and thinly interbedded sandstones. The effect of anisotropy on the marine CSEM responses needs to be addressed, and ignoring anisotropy in interpreting marine CSEM data may lead to a distorted image of seabed conductivity structures, even misinterpretation. In this paper, we present a one-dimensional anisotropic inversion method for frequency domain marine CSEM data sets. The partial derivatives of the electromagnetic fields with respect to both the anisotropic resistivity and thickness are analytically calculated. Both the synthetic and real data sets are inverted for demonstrating the practicality and stability of the presented inversion method.

**Keywords:** Marine CSEM, Anisotropy, Inversion, 1D, Resistivity

## INTRODUCTION

The marine controlled-source electromagnetic (CSEM) method has emerged as a useful geophysical technique for offshore hydrocarbon reservoirs exploration and near-surface investigations. When interpreting marine CSEM data sets, it is often assumed that seafloor structures are electrically isotropic. However, it is commonly known that in the fold and thrust areas hydrocarbon reservoirs are frequently overlain by thick sedimentary sequences including shales and thinly interbedded sandstones. The sedimentary sequences and the thin bedded sand-shale sequences can exhibit macroscopic electrical anisotropy. The effect of anisotropy on the marine CSEM responses needs to be addressed, and ignoring anisotropy in interpreting marine CSEM data may lead to a distorted image of seabed conductivity structures, even misinterpretation (Li and Dai, 2011, Li et al, 2012).

In this paper, we present a one-dimensional anisotropic inversion method for frequency domain marine CSEM data sets. The inversion approach is based on the Gauss-Newton scheme. The partial derivatives of the electromagnetic fields with respect to both the anisotropic resistivity and thickness are analytically calculated. An adaptive selection method of regularization factor, basing on the interrelation between the horizontal resistivity ( $\rho_h$ ) and the vertical resistivity ( $\rho_v$ ) of the inversion model, is proposed to balance the effects of the data misfit and the structural constraint. Both the synthetic and real data sets are inverted for testing the practicality and stability of the presented inversion method.

## THEORY

### Forward modeling

Due to the influence of ocean currents, the transmitter antenna will appear tilting and rotating. Applying superposition principle of electromagnetic field, we extend the scheme of Loseth and Ursin (2007) for calculating CSEM fields from a horizontal dipole source (HED) and/or a vertical dipole source (VED) in stratified media with vertical anisotropy to the general case of arbitrary orientation dipole source.

### Gauss-Newton inversion method

The objective functional is given by

$$\phi(\mathbf{m}) = \| \mathbf{W}_\mathbf{d}(\mathbf{d} - \mathbf{F}(\mathbf{m})) \|^2 + \mu \| \mathbf{W}_\mathbf{m} \nabla \mathbf{m} \|^2 \qquad (1)$$

where $\mathbf{m}$ is the model parameter vector, $\|\cdot\|$ represents the $l_2$ norm, $\mathbf{d} = (d_1, \cdots, d_N)^T$ is the inversion data vector. $\mathbf{F}(\mathbf{m})$ is the forward operator. $\mathbf{W}_\mathbf{d}$ is the data weighted matrix. $\mathbf{W}_\mathbf{m}$ is a diagonal weighting matrix penalizing the model parameter vector.

The regularization parameter is selected as the product of the maximum row sum of the matrix product $[(\mathbf{W}_\mathbf{d}\mathbf{J})^\mathrm{T}(\mathbf{W}_\mathbf{d}\mathbf{J})]$ and a weighting parameter (Newman et al., 1997)

$$\mu = \underset{1 \le m \le M}{Max} \left| \sum_{j=1}^{M} a_{mj} \right| / \chi^{i-1} \cdot \lambda \qquad (2)$$

where $a_{mj}$ is an element of the matrix $[(\mathbf{W}_\mathbf{d}\mathbf{J})^\mathrm{T}(\mathbf{W}_\mathbf{d}\mathbf{J})]$ with $j = 1$ for the first iteration. $\chi$ denotes a cooling

parameter. $\lambda$ is a weighting parameter of the inversion model. $\mathbf{J}$ is the Jacobian matrix

$$\mathbf{J}_i = \nabla_m \mathbf{F}(\mathbf{m}_i) = \left( \frac{\partial \mathbf{F}(\mathbf{m}_i)}{\partial \log_{10} \underline{\underline{\rho}}} \quad \frac{\partial \mathbf{F}(\mathbf{m}_i)}{\partial \log_{10} h} \right)^T \tag{3}$$

The weighting vector $\lambda$ consists of three parts: $\lambda_h = 1$ for the horizontal resistivity, $\lambda_v$ (anisotropic ratio) for the vertical resistivity and $\lambda_t = 1$ for the thickness of each layer. The weighting parameter $\lambda$ in the $k$-th iteration is given by

$$\lambda_k = \begin{cases} \lambda_{h_k} = 1 & m \in \rho_h \\ \lambda_{v_k} = \sqrt{\dfrac{\rho_{v_{k-1}}}{\rho_{h_{k-1}}}} & m \in \rho_v \\ \lambda_{t_k} = 1 & m \in thickness(h) \end{cases} \tag{4}$$

where $m$ is the model parameter and the initial value $\lambda_1$ is set to be 1.

## MODELING

### Sensitivity calculation

To demonstrate the validity of the sensitivity computation procedure and the inversion code, we simulated the five-layer isotropic model displayed in Figure 1a. We evaluate the sensitivities with respect to $\rho_h$ and $\rho_v$ (assuming VTI-anisotropy), and with respect to isotropic $\underline{\underline{\rho}}$. A line of 76 sources are placed 50m above the seafloor (z=950m) and a receiver is located at the seafloor.

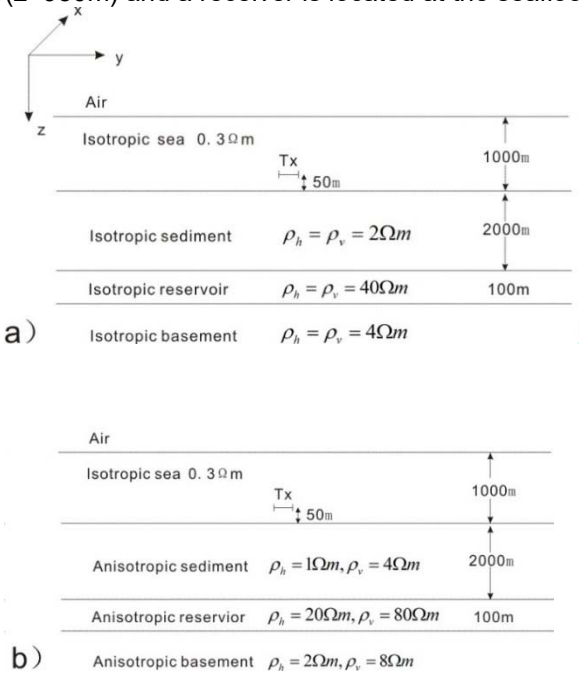


**Figure 1.** 1D isotropic(a) and anisotropic(b) model.

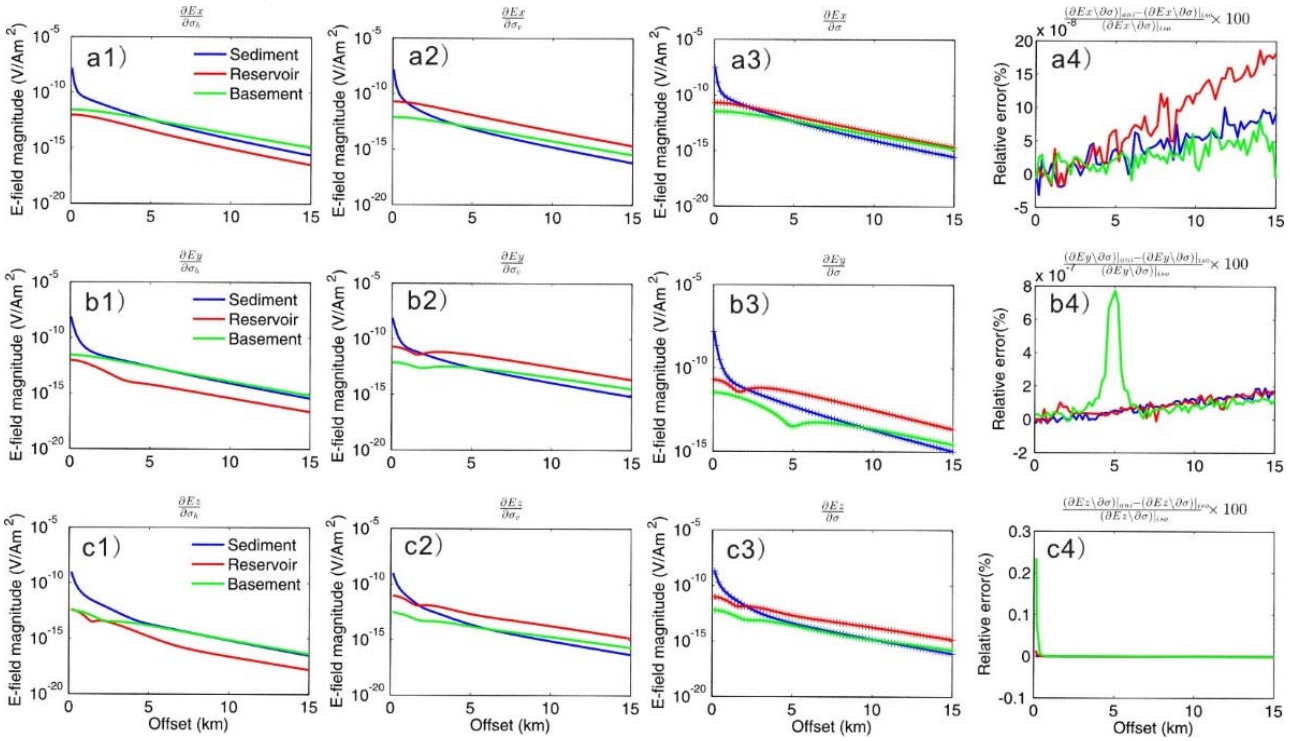


**Figure 2**. Comparison of sensitivities computed from the presented method and the isotropic algorithm (Li and Li, 2016). Frequency is 0.25 Hz. The left three columns show absolute values of sensitivity with respect to the horizontal, vertical and isotropic resistivity, respectively. The far right column shows relative errors between anisotropic and isotropic sensitivities.

For the isotropic model shown in Figure 1a, the isotropic sensitivities are the sums of the sensitivities with respect to both the horizontal and vertical resistivity (Streich et al.,2011). The left two

columns in Figure 2 show the sensitivity to the horizontal and vertical resistivity, respectively, computed by using the presented method. For comaprison, the sensitivity computed from the code of (Li and Li, 2016) is shown in the third column, the relative differences are less than 0.3%.

Figure 3 shows the sensitivities of the horizontal resistivity (a) and vertical resistivity (b) of 1D anisotropic model shown in Figure 1b. One can see that the horizontal electric field is sensitive to the vertical resistivity of the reservoir layer. However, the sensitivity of horizontal electric field with respect to the horizontal resistivity of the reservoir layer is lower than that of both horizontal and vertical resistivities of the sediment layer and that of vertical resistivity of reservoir layer.

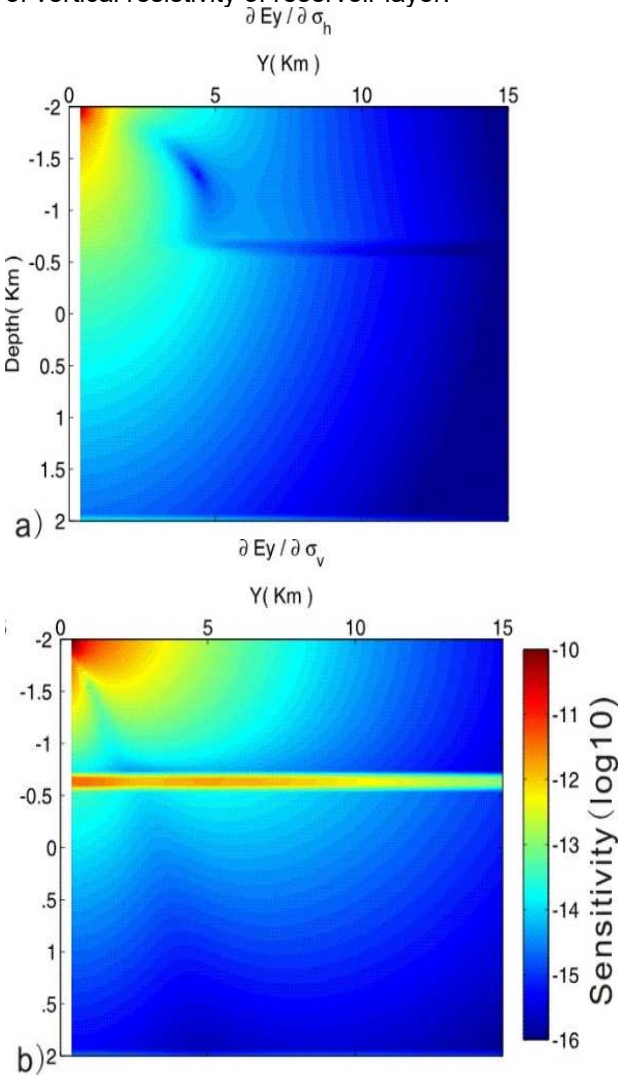


**Figure 3.** Sensitivities of the horizontal resistivity (a) and vertical resistivity (b) of 1D anisotropic model shown in Figure 1b.

**Synthetic data inversion**

We present the inversion results of the synthetic horizontal electric and magnetic fields of the anisotropic model shown in Figure 1b. The signal is excited at 0.25Hz, 0.75Hz and 1.25Hz. 30 transmitters are spaced at 500m interval along the tow line at a height of 50m above the seafloor. A receiver is located at (0,0,0). The initial inversion model is an isotropic half-space of $1\,\Omega m$.

Here we use an eigenparameter analysis method to demonstrate the resolution for multi-frequency data sets. The resistivity and depth of the seawater layer are fixed during the inversion. There are six unknown seafloor resistivities ( $\rho_{h1}, \rho_{v1}, \rho_{h2}, \rho_{v2}, \rho_{h3}, \rho_{v3}$ ) and two unknown thickness of sediment layer and reservoir layer ( $\mathrm{h}_1, \mathrm{h}_2$ ). The content of the Jacobian matrix J for the 1D model shown in Figure.1b is investigated by using a singular-value decomposition (SVD) to represent **J** as a product of three matrices (Inman et al., 1973)

$$\mathbf{J} = \mathbf{USV}^T \qquad (5)$$

where **U** is a $N_d \times N_m$ matrix, $N_d$ and $N_m$ are the length of data vector and model parameter vector, respectively. The diagonal matrix **S** contains the eigenvalues (EVs) of **J**, and the matrix **V** contains the so-called eigenparameteres (EPs).

Figure 4 shows the result of the eigenparameter statistical analysis for the 1D model inversion shown in Figure 1b. The white circles indicate positive components of EP, while the black circles indicate negative components. One can see that EP5 and EP6 (the vertical resistivity and thickness of the reservoir layer) are slightly coupled to each other, while the EPs corresponding the resistivities and the thickness of the sediment layer can be resolved independently, thus the resistivity of the reservoir layers could be recovered during the inversion.

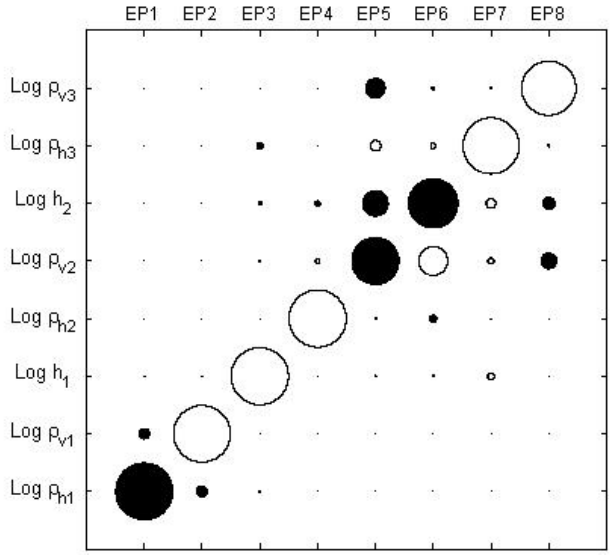


**Figure 4.** Eigenparameter statistical analysis of 1D anisotropic model shown in Figure 1b.

Figure 5a shows the inverted anisotropic seafloor resistivity. The final RMS misfit is 1.025. The dotted lines indicate the true resistivities and the star lines indicate the inversion results. From Figure 5a, one

can see that the horizontal and vertical resistivity of the surrounding sediments, and the vertical resitivity and the thickness of the thin resistivie layer are reconstructed very well, but the horizontal resistivity of the thin resistive layer is badly recovered, which is insensitive known from the analysis of the sensitivities shown in Figure 3.

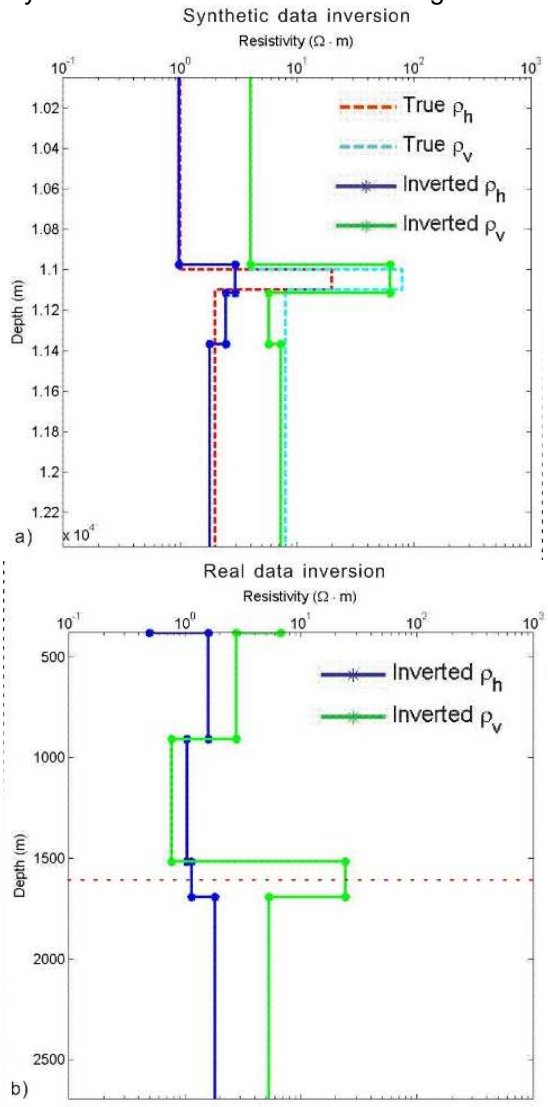


**Figure 5.** The inverted anisotropic seafloor resistivity for the synthetic CSEM data (a) and the Troll field data (b).

### Real data inversion

The presented method is used to invert the Troll field data set in Norway (Morten et al., 2012). 33 electric dipole transmitters with the depth of about z = 300 m are over a 18 km survey line. A receiver is located on the seafloor at about z = 330 m. The frequencies are 0.25Hz, 0.75Hz and 1.25Hz. The horizontal electric field component (Ex) of the full transmitter-receiver ranges are inverted. Figure 5b shows the predicted anisotropic seafloor resistivity. The final RMS misfit is 1.857. The high resistive layer is predicted well. For comparison, the top reservoir depth estimated from a seismic migration profile (red dot line) is also shown. The top depth of the reservoir is approximately estimated.

## CONCLUSIONS

We present an anisotropic Gauss-Newton inversion method for frequency domain marine CSEM data. Both the synthetic and field data inversion examples indicate that the presented inversion method is stable and efficient.

## ACKNOWLEDGEMENTS

The authors thank Electromagnetic Geoservices (EMGS) for permission to use the Troll field data.

## REFERENCES

Loseth L O, Ursin B.Electromagnetic fields in planarly layered anisotropic media. Geophysical Journal International, 2007, 170(1), 44-80.

Yuguo Li, Shikun Dai. Finite element modelling of marine controlled-source electromagnetic responses in two-dimensional dipping anisotropic conductivity structures[J]. Geophys. J. Int., 2011, 185: 622-636.

Li Y, Luo M, Pei J. Adaptive finite element modeling of marine controlled-source electromagnetic fields in two-dimensional general anisotropic media[J]. Journal of Ocean University of China, 2013, 12(1): 1-5.

Li G, Li Y. Joint inversion for transmitter navigation and seafloor resistivity for frequency-domain marine CSEM data. Journal of Applied Geophysics, 2016, 136:178-189.

Morten, J.P., Roth, F., Karlsen, S.A., Timko, D., Pacurar, C., Olsen, P.A., Nguyen, A.K., 2012. Field appraisal and accurate resource estimation from 3D quantitative interpretation of seismic and CSEM data. The Leading Edge 447–456.

Newman, G. A., and Alumbaugh, D. L., 1997, Three-dimensional massively parallel electro-magnetic inversion analysis of a cross-well electromagnetic experiment: Geophysical Journal International, 128, no. 2, 355-363.

Streich R. Sensitivity of controlled-source electro-magnetic fields in planarly layered media[J]. Geophysical Journal International, 2011, 187(2):705-728.

Inman, J.R., Ryu, J., Ward, S.H., 1973. Resistivity inversion. Geophys. 38, 1088 – 1108.

# 2D inversion of MT data measured at Costa Rica Rift

J. Chen[1], M. Jegen[1] and R. Hobbs[2]
[1]GEOMAR Kiel, Germany, jchen@geomar.de, mjegen@geomar.de
[2]Durham University, UK, r.w.hobbs@durham.ac.uk

**ABSTRACT**

Magmatic processes at mid ocean ridges create and shape the Earth's seafloor. Magmatic supply, however, varies spatially and temporally and the crustal manifestation of the magmatic variations is frozen into the crust when it is formed. The upper crustal layer is furthermore overprinted by a secondary alteration caused by hydrothermal interaction, which leads to a chemical alteration and potential reduction in porosity/permeability. Thus, geophysical mapping of changes of crustal characteristics along a profile of crust with increasing age allows for an unraveling of temporal and spatial dynamics of magmatic processes. A geologically interesting region is the Costa Rica Rift (CRR), where Galapagos hotspot magmatism interacts with passive mantle upwelling.

CRR is the eastern most segment of the three spreading centers forming the Galapagos or Cocos-Nazca spreading center, with asymmetrical spreading rates of 3.6 cm/yr to the south and 3.0 cm/yr to the north, and is bounded by the Panama Fracture zone to the east and the Ecuador Fracture zone to the west. In 2015 under the framework of the UK project OSCAR, multidisciplinary data, including seismic, magnetic, gravity, bathymetric and magnetotelluric (MT) and shallow sub-bottom profiler data, along a ~250 km profile from the CRR ridge axis to a ~7 Ma oceanic crust in its southern flank has been acquired. The overall aim of the project is to investigate the effects of the heat loss and hydrothermal circulation on both the solid Earth and the ocean, and to derive a new integrated model of the ocean and hydrothermal circulations at active ocean ridges and ridge flanks.

The collected MT data have been processed using traditional Fourier-based robust processing code BIRRP. 1D conductivity models are obtained with the derived effective impedances at periods larger than 100 s by using OCCAM inversion code. Based on a preliminary 1D inversion of the data, it is observed that magmatic/tectonic processes in this region are different from other oceanic spreading rifts. Global studies on mid-ocean ridges show that after the early cooling stage the transition from resistive depleted mantle to conductive un-depleted mantle occurs at 60 - 90 km depth. At the CRR, however, the transition seems to occur much shallower at 30 - 45 km depth from a younger section (~1 Ma old) to an older section of oceanic crust (~7 Ma old). One possible explanation could be an influence of the Galapagos hotspot on the magmatic processes at the CRR.

In this paper, we want to present the 2D conductivity model of the crust and mantle from magnetotelluric impedances derived from seafloor electric and magnetic time series observations along the profile. In combination with the existing seismic, borehole and heat flow geophysical observations, we investigate the different geophysical signatures of the lithosphere along this profile which may reflect a) a different chemical composition of the mantle when crust was created, b) different thermal regime between the time of the creation (~7 Ma ago) and now, c) presence of increased partial melt fractions further off axis than usual, and/or d) effects of fracture zones on the state of the crust.

**Keywords:** Costa Rica Rift, Galapagos hotspot, marine MT, 2D inversion

# 2D Inversion of time-domain controlled source electromagnetic and differential electrical dipole data based on an update of MARE2DEM to the time-domain

Amir Haroon[1], Marion Jegen-Kulcsar[1], Shuangmin Duan[1], Zahra Faghih[1], Bradley Weymer[1], Sebastian Hölz[1], Bülent Tezkan[2]

[1]GEOMAR – Helmholtz Centre for Ocean Research Kiel, 24148, Germany
[2]Institute of Geophysics and Meteorology, University of Cologne, 50968, Germany

**SUMMARY**

Time-Domain Controlled Source Electromagnetic (TD-CSEM) methods are commonly applied to detect and delineate subsurface resistivity anomalies on land and in the marine environment. The most general form of the application utilises a horizontal electric dipole (HED) current excitation with an alternating waveform ranging from periods of several milliseconds to seconds. TD-CSEM experiments are commonly conducted along transects in a towed inline, or broadside configuration. Therefore, the data is generally sensitive to resistivity variations in the line between the source and the receiver, motivating the development of a 2D inversion for the data interpretation. A 2D inversion for frequency-domain controlled source electromagnetic data has recently become state of the art in academia through the availability of MARE2DEM (developed by Kerry Key, http://mare2dem.ucsd.edu/). This adaptive finite element algorithm allows the interpreter to easily implement the measurement geometry and his/her *a-prior* information into a 2D inversion scheme without much knowledge of the finite element method. Here, we present an update of MARE2DEM that accounts for time-domain data and, additionally, calculates signals for the novel Differential Electrical Dipole (DED) transmitter of the University of Cologne. This novel transmitter/receiver system consists of a double inline dipole current excitation using three electrodes where the central electrode has one polarity, and the two outer electrodes have the other polarity. In theory, the excited EM field is thereby focused underneath the transmitter making the method more sensitive towards lateral resistivity variations compared to the conventional HED systems. We use synthetic 2.5D forward and inverse modelling studies to validate the accuracy and applicability of the time-domain development and underline the necessity of using a 2D inversion algorithm for interpreting DED data. We apply the algorithm to two separate case studies targeting fresh groundwater reservoirs in shallow marine environments near the coast of Israel (DED) and New Zealand (HED).

**Keywords:** Time-Domain CSEM, 2D finite element inversion, Offshore Groundwater

# 3D Electromagnetic Imaging of the Santos Basin by Marine Magnetotelluric Studies

Paula Lima Ribeiro and Sergio Luiz Fontes
Department of Geophysics, Observatorio Nacional/MCTIC, Brazil, paulalribeiro4@gmail.com

## SUMMARY

Seismic imaging is generally poor when salt, basalt and carbonates are present in sedimentary basins. To circumvent this problem, the EM techniques have assumed an important role in petroleum exploration. In offshore environments, the advances in technology have enabled the application of the magnetotelluric method in such cases. The potential hydrocarbon accumulation in Brazilian offshore sedimentary basins is associated to the tectonic-stratigraphic evolution of the eastern continental margin of Brazil, whose origin is related to the breakup of the supercontinent Gondwana that caused the rifting process. Accumulation of sediments started with fluvial-lacustrine deposits, followed by an evaporitic stage until reaching marginal basin stages. Within this scenario, the Santos Basin, one of the widest basins in South Atlantic, has already become an important productive basin in Brazil based particularly in subsalt oil accumulations. The first large Marine Magnetotelluric (MMT) campaign in Brazil was performed in Santos Basin in 2007 by WesternGeco Electromagnetics in collaboration with Petrobras and Observatorio Nacional. It comprised 96 MMT stations sampled at 62.5 Hz and typical acquisition times of 3 days, displaced along 3 NW-SE profiles. Previous analysis of these data was carried out by using a 2D approach based on the structural trend suggested by gravity and magnetic data. A joint inversion with multiple geophysical data (magnetotelluric, seismic, magnetic and gravity) was also performed. It was possible to map main structures such as the top of the basement and the base of the salt. However, having complex structures implies the strong 3D dimensionality of the electrical data in this region (confirmed by using dimensionality tools), justifying further studies. Considering that 3D inversion codes have become more efficient, we propose in this study a three-dimensional analysis using the ModEM software to better recover the salt geometry. Work is in progress and it is expected to further enhance the MMT imaging.

**Keywords:** Marine Magnetotelluric data – 3D inversion – Santos Basin

# 3D modeling of marine CSEM using survey decomposition and local meshes

D. Yang[1], K. Key[2]
[1] Lamont-Doherty Earth Observatory, Columbia University, yangdikun@gmail.com
[2] Lamont-Doherty Earth Observatory, Columbia University, kkey@ldeo.columbia.edu

## SUMMARY

The 3D modeling of marine EM data from distributed arrays of sources and receivers often requires a massive mesh that arises from both the high density of small cells needed for rapidly decaying signals as well as from the large computational domain needed for wide survey extents. In this work, we present a general approach for decomposing a large survey to many small "atomic" problems, each of which only models the data for a single source (S) and single receiver (R) at a single frequency (F). Each S-R-F combination is then modelled using a local mesh customized to the frequency and S-R geometry. A local mesh has a refined core volume encompassing the S-R region and pads out to a distance where the field is practically vanished. According to the skin effect, high frequency data require smaller cells but falls off more quickly; low-frequency and long-offset data need a larger domain but they can be modelled with a coarser mesh. As a result, the decomposition produces a large number of independent small local meshes with similar number of cells. Such a fine-grained and embarrassingly parallelizable decomposition allows a variety of parallel solving strategies to be utilized in a scalable manner. Another benefit is that because a typical local meshes contains no more than $10^5$ cells, a parallel direct solver is a more accurate and efficient choice when compared to iterative solvers. Our approach is demonstrated with a 3D synthetic reservoir model and a deep-towed survey using ocean bottom receivers.

**Keywords:** three-dimensional; marine CSEM; numerical simulation; decomposition

## INTRODUCTION

The marine controlled source electromagnetic (CSEM) method is a technology widely used to characterize the upper few kilometers of the continental margins and oceanic crust. A typical survey consists of a deep-towed horizontal electric dipole source and an array of electric dipole receivers deployed on the seafloor (Figure 1).

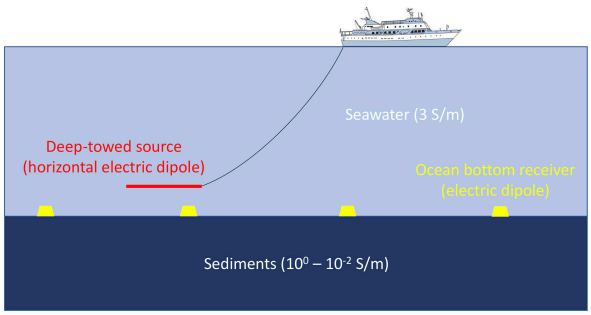


**Figure 1.** Configuration of a deep-towed marine CSEM survey modelled in this study.

3D modeling of marine CSEM has been a computational challenge because of the scale contrast – the 3D mesh needs to be fine enough to capture rapidly decaying signals and to be wide enough to cover the entire survey area, which in some cases can span a few hundred kilometers. Such a one-size-fit-all mesh may require millions to billions of cells and may exceed currently available computational resources. Further, the numerical solution often scales poorly as the survey area expands and the number of parallel processors increases.

One approach that has been investigated for the improvement of the scalability in the past decade is to carry out EM modeling on separate simulation meshes, each of which only models a subset of the entire survey. By paying some extra bookkeeping cost in handling multiple meshes, a massive Maxwell matrix on a single large mesh can avoided. This general idea can be implemented differently. For example, Commer and Newman (2008) makes simulation meshes based on the source location and adapts the cell size to frequencies. Zhdanov et al. (2014) uses the integral equation moving footprint method, which is equivalent to making a new simulation mesh when the footprint moves. Haber et al. (2018) uses a locally refined octree mesh for a source and set of receivers.

In our implementation, we adopt the concept of "atomic" survey decomposition (SD) applied to airborne and land EM (Yang and Oldenburg, 2016). An atomic decomposition breaks down any CSEM survey to a collection of mini-surveys, each of which only concerns a dipole source (S) and a dipole receiver (R) at a certain frequency or time (F/T).

Then every mini-survey is assigned a customized mesh and is modelled independently. The final result is a simple assembly or superposition (for non-dipole source or receiver) of the mini-survey results. The most important feature of SD is that it promotes very fine-grained decomposition using S-R-F combinations, as modeling more than one S, R or F in a subproblem is considered not optimal.

In the following, we demonstrate how a synthetic marine CSEM survey can be decomposed and modelled. Some techniques that are critical in SD implementation, like local mesh and conductivity upscaling, are also introduced.

## Survey Decomposition

The goal of SD is to break down the original problem that is poorly scaled into many independent subproblems that are as small as possible. A marine CSEM survey is typically made with a dipole source and dipole receivers, so its decomposition is straightforward. For the configuration in Figure 1, each SD subproblem models data from a particular electric dipole source at an ocean bottom receiver at one of the operating frequencies.

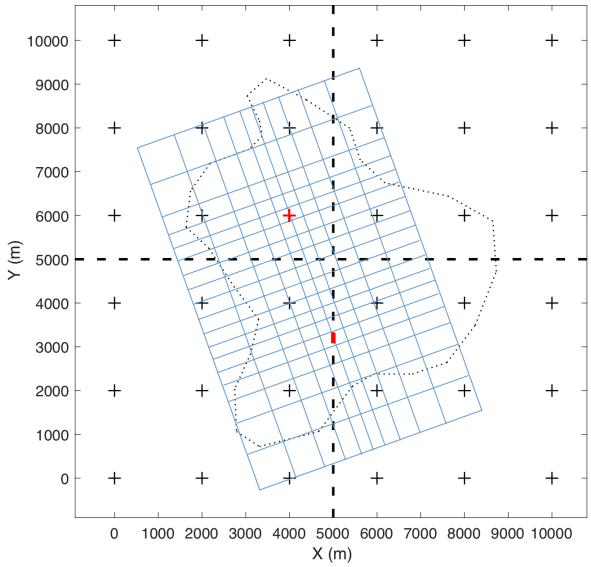


**Figure 2**. Synthetic survey (cross: receiver; dash: source) and the reservoir model (dotted). The blue grid illustrates a local mesh designed specifically for the source-receiver pair in red.

Our synthetic model consists of three background layers: air ($Z > 0$ m), seawater ($0 > Z > -1000$ m) and subseafloor sediments ($Z < -1000$ m). We insert a hydrocarbon reservoir layer ($10^{-2}$ S/m) in the sediments from -1800 to -2000 m at depth with an irregular horizontal shape (Figure 2). The receivers are deployed on an equal-spaced grid. Every receiver measures the horizontal components of electric field data (Ex and Ey). A 200-m long horizontal dipole source is towed along two perpendicular lines 100-m above the seafloor. In practice, the relative position and orientation of the source and receivers can be arbitrary. In this example, there are 36 receivers, 48 source locations and 5 frequencies (0.1, 0.2, 0.4, 0.8, 1.6 Hz), giving 8640 possible S-R-F subproblems in total. We note this is a sparse example for the purpose of demonstration. Actual surveys can be much larger in both area and the number of S-R-F combinations.

## Local Mesh

Most of the computational efficiency comes as a result of "local mesh" – a spatial discretization scheme that only serves a subset of data. Any type of mesh can be used. In Zhang and Key (2016), a local mesh is a portion of a coarse starting tetrahedral mesh that is adaptively refined around a subset of sources and receivers, building on the earlier 2D method in Key and Ovall (2011). Haber et al. (2018) uses a moving refinement in an octree mesh to simulate the sources and receivers at different locations. Here we use rectilinear grid for local meshes and the finite difference method, similar to Commer and Newman (2008), but with some extension and modification.

Because in SD every local mesh only concerns one source and one receiver, only the region around and between them needs to be refined. To minimize the size of each individual local mesh, we allow the rotation of local coordinate system so the source and the receiver can be made in-line with the local grid. With local mesh rotation, there is only one refined core volume in a local mesh, so the number of cell for a rectilinear mesh is not much more than for an unstructured mesh (for example see the blue mesh grid in Figure 2).

By using a rectilinear grid mesh, we benefit from its simplicity and robust performance. Generally, only two parameters need to be determined when making a mesh – the smallest cell size and the distance to the boundary of the simulation domain. Both of them depend on the operating frequency and the S-R offset. For high-frequency and/or short-offset data, the field decays rapidly, so cells need to be small near S-R, but the modeling domain can be truncated earlier. For low-frequency and/or long-offset data, the local mesh requires a large domain, but the grid can be coarser. It is possible to automatically find the optimal cell sizes and boundary distance with an adaptive trial-and-error method (Yang and Oldenburg, 2016). But our tests

show that for marine problems, a local mesh can be created using some empirical parameters estimated from analytic or 1D solutions. A rectilinear local mesh with a reasonable trade-off between accuracy and cost often contains $10^4$ – $10^5$ cells, typically solvable within a minute using parallel direct solvers that are faster and more accurate than iterative solvers. Keeping the size of local meshes within the sweet spot of direct solvers is another motivation for atomic decomposition.

After the data are calculated on local meshes, they are rotated back to the original coordinate system. The final step of coordinate transform and collecting modeling results from parallel workers often takes an insignificant amount of time.

## Conductivity Upscaling

A local mesh only has fine cells near the location of the source and the receiver. For bulky cells far away, finding a conductivity value that effectively represents the macroscopic property of fine-scale structure in those cells is a non-trivial problem often called upscaling or homogenization.

The simplest solution is to volume-average the materials enclosed by a local mesh cell, then assign the averaged value to the cell center. We have tested this method and found that it is very fast if the original model is held in a structured mesh axis-conformal to the local mesh or the global and local meshes are perfectly nested. However, it has some restrictions. First, our local meshes may rotate different angles relative to the original coordinate system, so meshes are usually not conformal or nested. Second, averaging to cell center based on relative volumes does not take into account anisotropy introduced by upscaling. For example, in Figure 3, Cell 2 is split equally by $\sigma_1$ and $\sigma_2$ in the original model. Assigning the average of $\sigma_1$ and $\sigma_2$ at the cell center implies the conductivities in x and y are the same, although it is obvious that the average should be arithmetic in x and harmonic in y.

In Commer and Newman (2008), the electric field is defined on cell edges, so to get current density, conductivities are averaged to edges using a control volume crossing the neighboring cell (the red and green box for edge conductivity at Ex and Ey respectively). We extend their approach by using a point cloud to facilitate the upscaling calculation.

The first step is to initiate an array of points to fill each local mesh cell. Then the points are coordinate transformed to the original coordinate system. A query procedure returns the conductivities at those points in the original model. Those conductivity-assigned points form a 3D cubic lattice structure within each cell. The effective conductivity of the lattice can be rigorously calculated by solving a dc resistivity problem. For fast approximation, we assume the current only flows along the edge direction. For example, in Figure 3 if we need to find an edge conductivity at Ex, the points in the red box only carry current along x direction. Without cross-current, the lattice in the red box is a series-parallel combination circuit. Its effective edge conductivity can be easily calculated by doing arithmetic average in y (parallel circuit) and then harmonic in x (series circuit). Similarly, the lattice in the green box for Ey is first arithmetically averaged in x, then harmonically in y.

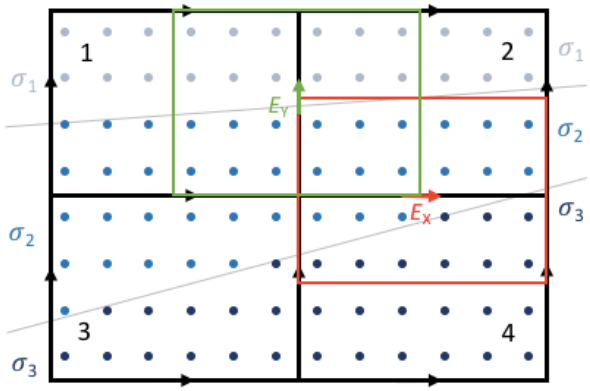


**Figure 3**. Averaging conductivity from the original model ($\sigma_1$, $\sigma_2$, $\sigma_3$ with the grey lines as the interfaces) to a local mesh using point cloud.

Our approach has some improvement. First, it does not require the original model to be held in an axis-conformal or nested mesh. In the example in Figure 3, the original model is only a description of spatial division. For example, the grey line between $\sigma_2$ and $\sigma_3$ can be the seafloor bathymetry. We only require that the original model can return conductivity values when probed by points. Second, we have the flexibility of adjusting the density of point cloud. In a highly stratified sedimentary environment with many thin layers, we may use more point in the vertical direction than in the horizontal directions to better capture the intrinsic anisotropy.

## Result

Upon decomposition, we have 8640 S-R-F subproblems in total. Although some of them may not be practically useful (e.g. too long offset at high frequency), we model all of them for the purpose of understanding the computational performance. All the procedures, including the decomposition, coordinate transform, conductivity upscaling and local mesh modeling, are carried out in a shared

memory parallel environment with 8 cores. The largest mesh contains 79764 cells and its solve time is about 40 s. All processors are running at 100% capacity for the most part with a short idle time when finishing up. In the future, we plan to scale up the number of processors in a large-scale distributed memory platform, so the total computing time will be close to the time required to solve a single local mesh.

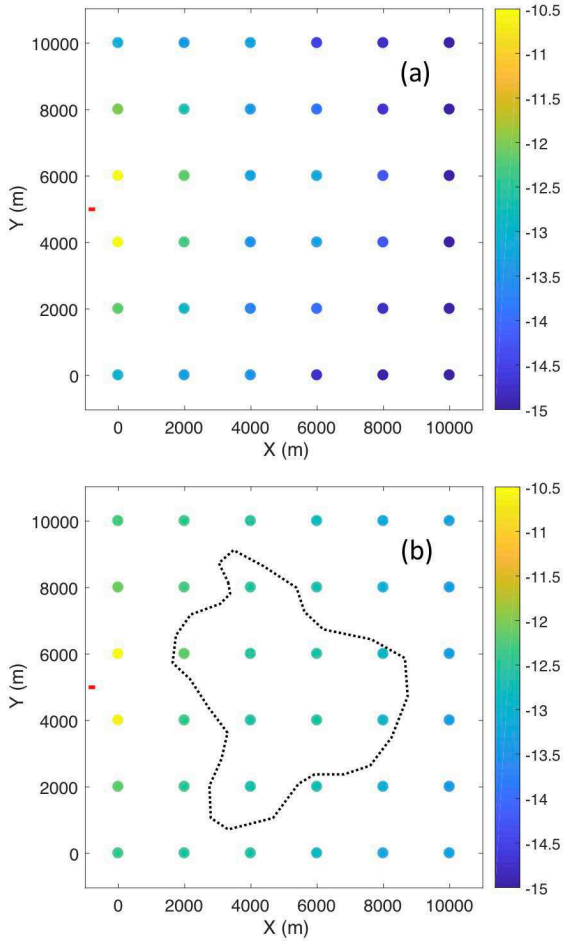


**Figure 4**. 3D modeling data (a) without and (b) with the reservoir layer. The red line indicates the source location. Shown are amplitude of Ex in log(VA$^{-1}$m$^{-2}$)).

Figure 4 shows the modelled Ex amplitude data from the first source location at 0.2 Hz. The presence of the reservoir enhances the responses at most receiver locations. The 3D effect is evident as a stronger E-field is observed at the receivers whose S-R line does not cross the reservoir at all.

## Conclusions

3D marine CSEM modeling is still challenged by high computational cost because we often demand high-resolution results over a large survey area. We propose an approach of "divide and conquer". Using the concept of atomic survey decomposition, the original marine CSEM problem is considered as an assembly of many mini-surveys, each of which only measures data from one dipole source (S) at one dipole receiver (R) at one frequency (F). Then every S-R-F combination is assigned a specifically optimized mesh, called local mesh, on which the forward calculation is carried out.

Because S-R-F subproblems and local meshes are independent, they are solved in an embarrassingly parallel environment. The computation is well load-balanced because the local meshes are about the same size. Further speed up is possible by adding more processors and using a distributed parallel scheme.

## Acknowledgements

DY is sponsored by the NSERC Postdoctoral Fellowship from the Government of Canada and the Electromagnetic Methods Research Consortium at Columbia University. DY also thanks Dr. Dieter Werthmüller for providing *empymod* for 1D solutions.

## References

Commer M, Newman GA (2008) New advances in three-dimensional controlled-source electromagnetic inversion. Geophys. J. Int. 172: 513–535

Haber E, McMillan M, Kary B, Marchant D (2018) 3D inversion of large scale marine controlled-source electromagnetics. ASEG Extended Abstracts 2018(1): 1–5

Key K, Ovall J (2011) A parallel goal-oriented adaptive finite element method for 2.5-D electromagnetic modelling. Geophys. J. Int. 186(1): 137–154

Yang D, Oldenburg D (2016) Survey decomposition: A scalable framework for 3D controlled-source electromagnetic inversion. Geophysics 81(2): E69–E87

Zhang Y, Key K (2016) MARE3DEM: A three-dimensional CSEM inversion based on a parallel adaptive finite element method using unstructured meshes. SEG Technical Program Expanded Abstracts 2016: 1009–1013

Zhdanov MS, Endo M, Cox LH, Čuma M, Linfoot J, Anderson C, Gribenko AV (2014) Three-dimensional inversion of towed streamer electromagnetic data. Geophysical Prospecting 62(3): 552–572

# A Preliminary study on air wave separation from Marine CSEM Data by using Fictitious Wave Domain Modelling

Jie Lu [1], Yuguo Li [1,2]
[1] College of Marine Geo-sciences, Ocean University of China, Qingdao 266100, China
[2] Key Lab of Submarine Geo-sciences and Prospecting Techniques of Ministry of Education, Ocean University of China, Qingdao 266100, China

## SUMMARY

Frequency domain marine CSEM responses are seriously influenced by the seawater layer. The diffusive Maxwell equations can be transformed into wave equations in fictitious wave domain (FWD) based on the correspondence principle. In fictitious wave domain, the propagation of the EM fields can be analyzed and investigated, and air waves can be separated from the other types of waves.

**Keywords:** Fictitious wave domain, air wave, marine CSEM, shot gather

## INTRODUCTION

The marine controlled-source electromagnetic (CSEM) method is considered as a geophysical tool for offshore hydrocarbon exploration and reservoir prospect evaluation. The marine CSEM method is a low frequency method. Hence the displacement currents are negligible and the governing equation of marine EM fields is the diffusive equation. Recently, the fictitious wave domain (FWD) method has been proposed for marine CSEM simulations (Mittet 2010, 2015). The FWD method transforms the diffusive Maxwell's equations to a set of hyperbolic equation by the application of the correspondence principle (Hoop 1996). Connections between EM fields in diffusion frequency domain and EM waves in fictitious time domain are thus established. The fictitious EM wave equations can be efficiently solved by using the finite difference time domain (FDTD) method. The resultant EM fields are completely wave-alike (Mittet, 2010) and hence propagate like waves. The propagation behavior and character of the fictitious EM waves have not yet been well investigated.

In this paper, we investigate and analyze the propagation characteristics of the electromagnetic fields in FWD with the use of the wave propagation theory. We simulate marine CSEM responses in the FWD by using the high-order FDTD method with adoption of the complex frequency shifted perfectly matched layer (CFS-PML) boundary condition (Lu et al., 2018). The propagation characteristic of EM waves in the FWD are demonstrated with several numerical examples.

## FICTITIOUS WAVE DOMAIN TRANSFORMATION

Assuming a time variation $e^{-i\omega t}$, the frequency domain Maxwell equations in the quasi-stationary approximation are

$$\nabla \times \mathbf{H}(\omega) - \sigma \mathbf{E}(\omega) = \mathbf{J}(\omega), \quad (1)$$

$$\nabla \times \mathbf{E}(\omega) - i\omega\mu \mathbf{H}(\omega) = 0, \quad (2)$$

where $\omega = 2\pi f$ is angular frequency, $\mathbf{J}$ is electric current density and $\sigma$ is conductivity.

Mittet (2010) defined the fictitious dielectric permittivity $\varepsilon'$ and the fictitious angular frequency $\omega'$ as follows

$$\varepsilon' = \frac{\sigma}{2\omega_0}, \quad (3)$$

$$\omega' = (i+1)\sqrt{\omega\omega_0}, \quad (4)$$

Eqs. (1) and (2) in diffusion frequency domain can then be transformed to a set of coupled hyperbolic partial differential equations in the fictitious wave frequency domain (Mittet 2010, 2015; Kusuda et al., 2014):

$$\nabla \times \mathbf{H}'(\omega') + i\omega\varepsilon' \mathbf{E}'(\omega') = \mathbf{J}'(\omega'), \quad (5)$$

$$\nabla \times \mathbf{E}'(\omega') - i\omega'\mu \mathbf{H}'(\omega') = 0, \quad (6)$$

where $\omega_0$ is a transform factor.

The governing equations in the fictitious wave time domain can be written as:

$$\nabla \times \mathbf{H}'(t') - \varepsilon' \boldsymbol{\partial}_{t'} \mathbf{E}'(t') = \mathbf{J}'(t'), \quad (7)$$

$$\nabla \times \mathbf{E}'(t') + \mu \boldsymbol{\partial}_{t'} \mathbf{H}'(t') = 0, \quad (8)$$

In the homogeneous media without source, $\mathbf{E}'$ and $\mathbf{H}'$ satisfy:

$$\nabla^2 \mathbf{H}'(t') - \mu\varepsilon' \frac{\partial^2 \mathbf{H}'(t')}{\partial t'^2} = 0, \quad (9)$$

$$\nabla^2 \mathbf{E}'(t') - \mu\varepsilon' \frac{\partial^2 \mathbf{E}'(t')}{\partial t'^2} = 0, \quad (10)$$

Eqs. (9) and (10) indicate that EM fields in FWD satisfy the wave equations. The fictitious wave velocity of EM fields

$$c' = \sqrt{\frac{1}{\mu\varepsilon'}} = \sqrt{\frac{2\omega_0}{\mu\sigma}}. \quad (11)$$

is a function of both the conductivity and the

transform factor $\omega_0$. For a given model, it is only dependent on $\omega_0$.

EM field in FWD can be transformed back to the frequency domain:

$$\mathbf{E}(\omega) = \int_0^T \mathbf{E}'(\mathrm{t}')\, e^{-\sqrt{\omega\omega_0}t'} e^{i\sqrt{\omega\omega_0}t'} \mathbf{d}t', \quad (12)$$

$$\mathbf{H}(\omega) = \sqrt{\frac{2\omega_0}{-i\omega}} \int_0^T \mathbf{H}'(\mathrm{t}')\, e^{-\sqrt{\omega\omega_0}t'} e^{i\sqrt{\omega\omega_0}t'} \mathbf{d}t', \quad (13)$$

## EM WAVE PROPAGATION PATHS AND SHOT GATHER

We investigate the propagation characteristics of EM fields in the FWD.

**Model 1 - The whole space seawater model**
Assume that the whole space is full of seawater and the conductivity is 3.2S/m, and the fictious wave velocity is 1.768 km/s if $\omega_0 = 2\pi$ (Fig. 1a). There is only the Direct Wave (DW) from the source to the receiver.

**Model 2 - A two half-space model**
This model contains a layer of infinite seawater, underlain by the half-space sediments on the bottom. The conductivity of sediments is 1.0S/m. The marine CSEM data was created by a unit horizontal electric dipole (HED), oriented along the x-axis, located at a height of 100m above the seafloor. The EM receivers are located on the seafloor (Fig. 1b). There are two types of waves: the Direct Wave (DW) and the seabed refracted wave (BRW), traveling from the source downward through seawater incident at the critical angle to the seabed and then along the seabed to the receiver.

**Model 3 - A half-space seawater model**
It contains a layer of infinite seawater, overlain by the half-space air on the top of it (Fig. 1c). The infinite seawater generates three types of waves: (a) the direct wave (DW); (b) the air refracted wave (ARW), which has been called 'air wave' in the frequency domain; (c) when the wave travelling upward from the source strikes the air-sea interface with an angle other than zero degree, it is reflected off from the air-sea interface, and back the seawater to the receiver. We call it the air reflected wave (ALW). Fig. 2 shows the normalized shot gather for the fictitious horizontal electric component at 0.1 Hz and 1.0 Hz. For comparison, the right-hand side of the theoretical travel time curves is over plotted. One can see that ARW can be separated from DW and ALW for offset larger than 4.0 km. Assuming that the upper limit of the inverse Fourier transform T=2.2 s in (12), one can calculate the 'air wave' field.

**Model 4 - Three-layer homogeneous seawater model**
This model consists of an infinite air and a layer of 1.0km seawater, overlying on the half-space sediments (Figure 1d). Compared to Model 3 (Fig. 1c), Fig. 1d illustrates the two additional waves: the seabed refracted wave (BRW) and multiple waves (MBW), including multiple seabed refracted and reflected waves, initially travelling from source downward/upward to the seabed/sea-air interface. The multiple waves are repeatedly reflected by the two interfaces, before reaching a receiver.

**Model 5 - A four-layer reservoir model with infinite seawater**
This model consists of an infinite seawater and a thin resistive layer, which is embedded into the seabed sediments (Fig. 1e). Compared to model 2 (Fig. 1b), Fig. 1e illustrates the additional wave: the oil wave (OW), which is related to the top and bottom of the reservoir.

**Model 6 - A five-layer reservoir model**
This model contains a thin resistive layer (Fig. 1f). Assuming that the conductivity is 3.2S/m in the seawater, 1.0S/m in the sediment and 0.01S/m in the reservoir. The fictitious wave velocity is 1.768km/s in the seawater, 3.162km/s in the seafloor sediment and 31.622km/s in the reservoir layer, if $\omega_0 = 2\pi$, respectively. The fictitious velocity in the reservoir layer is much higher than in the sediment layer. Compared to the three-layer homogeneous seafloor model (Fig. 1d), this model generates multiple oil waves, contributed by the reflections resulted from both the air-sea and seabed interfaces (Fig. 1f).

## AIR WAVE SEPARATION

Fig. 3a and b show the amplitude and phase of the horizontal electric field component for six models (Fig. 1) calculated by using the quasi-analytical solution presented in Li and Li (2016). Fig. 3c and d show the amplitude and phase of various types of waves: DW, ALW, ARW, BRW, MBW, OW and MOW.

For marine CSEM surveying, we are interested in OW and MOW. For offset less than 3.0 km, DW and BRW are the primary wave. For offset ranging from 3.0 km to 9.0 km, OW and MOW dominate the response, but BRW, MBW and ARW are not negligible.

## CONCLUSIONS

Transforming Maxwell equations into wave equations provides a new possibility for efficient investigating and analyzing the properties of the marine electromagnetic fields. The propagation of the EM fields can be analyzed in the fictitious time domain and each type of waves has its finite velocity and propagation path. And various wave fields can be separated from each other.

## ACKNOWLEDGEMENTS

This work is financially supported by the National Natural Science Foundation of China (No. 411304420).


## REFERENCES


Hoop A T. (1996) A general correspondence principle for time - domain electromagnetic wave and diffusion fields[J]. Geophysical Journal International, 127(3): 757-761.

Kusuda K, Mikada H, Goto T, et al. (2014) Improvement of methane hydrate detection using marine CSEM in the fictitious wave domain[C]//The 18th International Symposium on Recent Advances in Exploration Geophysics (RAEG 2014).

Mittet R. (2010) High-order finite-difference simulations of marine CSEM surveys using a correspondence principle for wave and diffusion fields FDTD simulation of marine CSEM surveys[J]. Geophysics, 75(1): F33-F50.

Mittet R. (2015) Seismic wave propagation concepts applied to the interpretation of marine controlled-source electromagnetics[J]. Geophysics, 80(2): E63-E81.

Li Y, Li G. (2016) Electromagnetic field expressions in the wavenumber domain from both the horizontal and vertical electric dipoles[J]. Journal of Geophysics and Engineering, 13(4): 505.

Lu J, Li Y, Du Z. Fictitious Wave Domain modeling and analysis of marine CSEM data. Geophysical Journal International, under revision


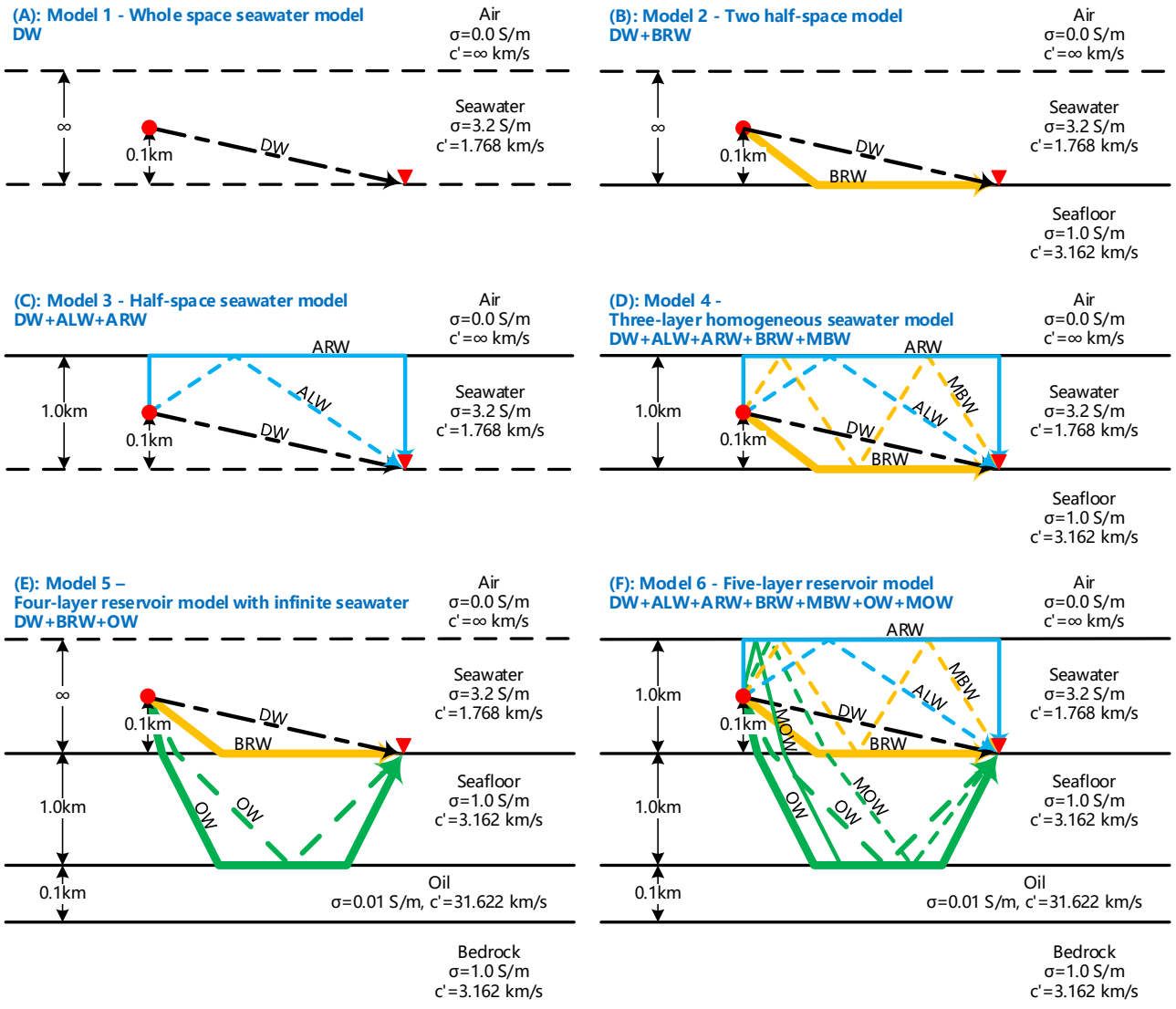


**Figure 1.** Marine conductivity models and wave propagation paths.

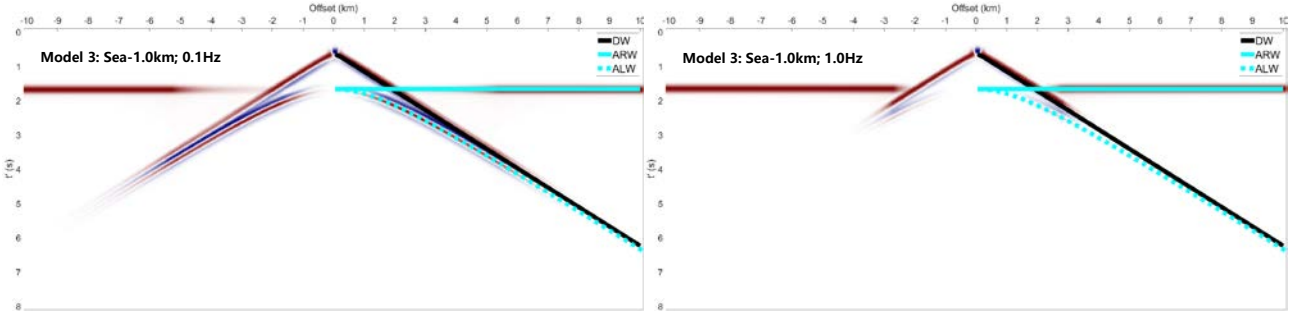


**Figure 2.** Normalized shot gather of the horizontal electric component for Model 3 (Fig. 1c) at 0.1 Hz and 1.0 Hz.

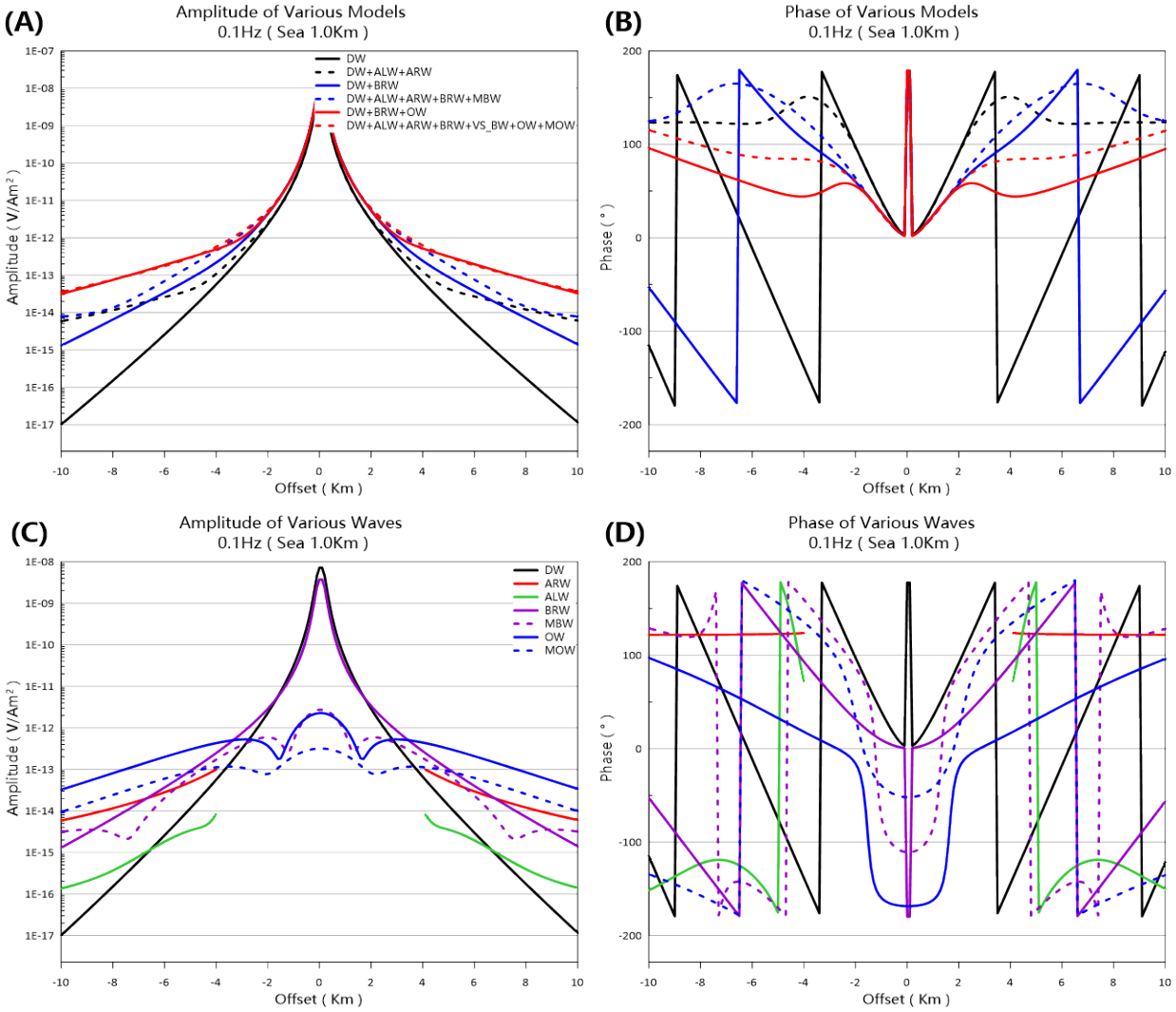


**Figure 3**. The amplitude (A) and phase (B) of horizontal electric component for models shown in Fig. 1 at 0.1 Hz; Amplitude (C) and phase (D) of various types of waves: DW, ALW, ARW, BRW, MBW, OW and MOW.

# An adaptive finite-element method for 3D time-domain CSEM modeling

Z. Hui[1*], C. Yin[1], Y. Liu[1], B. Zhang[1], X. Ren[1], J. Li[1], and J. Cai[1]
[1]College of Geo-exploration Science and Technology, Jilin University. Email: yuminhzj1115@163.com

**SUMMARY**

We use the adaptive unstructured finite-element method to fulfil 3D modeling for time-domain marine controlled-source electromagnetic (MCSEM) system. To discretize the time, we use the implicit backward Euler technique. By using an adaptive method based on the continuity of normal current for the posterior errors estimation, we can obtain an effective mesh for accurate modeling of multichannel MCSEM. To further improve the efficiency, we run a random choice in the process of mesh integration. We use MUMPUS to solve the equations system that needs only to decompose the matrix once for the same time interval. To check the accuracy of our algorithm, we compare our results with the semi-analytical solution for a half-space under the ocean. Numerical experiments for a topographic ocean bottom with a resistive body embedded show that ocean topography can have large influence on MCSEM responses, by subtracting the responses from the topographic ocean bottom the resistive target underneath can be easily identified.

**Keywords:** Time-domain; marine CSEM; adaptive unstructured finite-element

## INTRODUCTION

Marine controlled-source electromagnetic (MCSEM) method is an important means for marine exploration. It can obtain the electrical information of the submarine strata so as to evaluate the seabed geology and the resistive oil & gas reservoir. Compared with the frequency-domain method, the time-domain method is more effective for shallow water exploration.

In recent years, due to the increase in computational speed, many 3D forward modeling techniques have been introduced into MCSEM (Avdeeva 2007; Swidinsky 2010; Um et al. 2010). With increasing model complexity, the advantage of unstructured finite-element (FE) method become more and more obvious because of its capability to simulate complex models. The accuracy of calculation for the FE method depends on the quality of grids. To obtain effective mesh for accurate modeling, scholars (Ren et al. 2010; Ren et al. 2013, Yin et al. 2016) used adaptive methods to refine the mesh. While those are all for the frequency-domain EM or DC, we represent an adaptive method for multichannel MCSEM modeling in time-domain.

We use the adaptive unstructured finite-element method to calculate the 3D time-domain MCSEM responses. For the time discretization, we use implicit backward Euler method, which is stable and accurate for large time intervals. For the adaptive method, the posterior errors estimation based on the continuity of normal current is adopted. To improve efficiency while maintaining accuracy, we use a random choice technique. Further, we use the MUMPUS solver to solve the equations system that needs only to decompose the matrix once when the time interval is not changed, which enhances the modeling speed. To verify the accuracy of our algorithm, we check our model results against semi-analytical solutions for a half-space under the ocean. We further study the EM responses characteristic of topographic ocean floor and the resistive target under the seafloor.

## METHODS

*Unstructured vector finite-element method*

The EM diffusion equation in time-domain is written as

$$\nabla\times[\frac{1}{\mu}\nabla\times\mathbf{e}(\mathbf{r},t)]+\sigma\frac{\partial\mathbf{e}(\mathbf{r},t)}{\partial t}+\frac{\partial\mathbf{j}_s(\mathbf{r},t)}{\partial t}=0 \quad (1)$$

where $\mathbf{e}(\boldsymbol{r},t)$ is the electric field for time $t$ and position r, $\mu$ and $\sigma$ are respectively the magnetic permeability and conductivity, $\mathbf{j_s}$ is the current source. We divide the model domain into elements and for each element, the electric field is expressed as

$$\mathbf{e}^e(\boldsymbol{r},t)=\sum_{i=1}^{6}e_i^e(t)\mathbf{n}_i^e(\boldsymbol{r}) \quad (2)$$

where $\mathbf{n}_i^e(\boldsymbol{r})$ denotes the vector basis function, $e_i^e(t)$ is the electric field on i-th edge.

Substituting Eq. (2) into (1) and using the Galerkin's method, we obtain the FE governing equation for each element, i.e.

$$\mathbf{A}^e \frac{d\mathbf{e}^e(t)}{dt} + \mathbf{B}^e \mathbf{e}^e(t) + \mathbf{S}^e = \mathbf{0} \quad (3)$$

The (*i,j*) element of A and B and i-th element of S can be expressed as

$$\mathbf{A}^e_{i,j} = \iiint_{V^e} \sigma^e \mathbf{n}^e_i(\boldsymbol{r}) \cdot \mathbf{n}^e_j(\boldsymbol{r}) dV \quad (4)$$

$$\mathbf{B}^e_{i,j} = \frac{1}{\mu^e} \iiint_{V^e} \nabla \times \mathbf{n}^e_i(\boldsymbol{r}) \cdot \nabla \times \mathbf{n}^e_j(\boldsymbol{r}) dV \quad (5)$$

$$\mathbf{S}^e_i = \iiint_{V^e} \mathbf{n}^e_i(\boldsymbol{r}) \cdot \frac{\partial \mathbf{j}_s(\boldsymbol{r},t)}{\partial t} dV \quad (6)$$

Using backward Euler method to Eq. (3), we have

$$(3\mathbf{A} + 2\Delta t\mathbf{B})\mathbf{e}^{i+2} = \mathbf{A}(4\mathbf{e}^{i+1} - \mathbf{e}^i) - 2\Delta t\mathbf{S}^{i+2} \quad (7)$$

Combining Eq. (7) for all elements, we obtain

$$\mathbf{Ke} = \mathbf{b} \quad (8)$$

where **K** is the coefficient matrix, **e** is electric field on the edge, **b** is the term connected with transmitting source and the electric fields at the previous two moments. For the step-off waveform, we use FE for DC solutions to obtain the initial electric field.

*Posterior errors estimation*

Assume *f* as the interface between tetrahedron $T_i$ and $T_j$ and define electric field in tetrahedron $T_i$ and $T_j$ as $\mathbf{e}_i$ and $\mathbf{e}_j$, then the continuity of normal current is written as

$$\mathbf{n}_f \cdot (\sigma_i \mathbf{e}_i - \sigma_j \mathbf{e}_j) = 0 \quad (9)$$

where $\mathbf{n}_f$ is the normal vector of the interface. Due to the fact that the FE solutions exist errors, Eq. (9) may not be equal to zero. The difference of two sides in Eq. (10) is

$$\eta_i^2 = \sum_{m=1}^{4} \left\| \mathbf{n}_m \cdot (\sigma_i \mathbf{e}_i - \sigma_j \mathbf{e}_j) \right\|_{L^2, T_i} \quad (10)$$

where *m* denotes the surface number of element *i,* while *j* denotes the tetrahedron that has interface *m* with tetrahedron *i.*

*Adaptive process*

In our modeling, we run the following adaptive process: 1) Read the information of initial mesh. Define the maximum number of iteration Ndmax, the maximum number of grids Nsmax, and the minimum volume Vmin; 2) When the number of iteration Nd is less than Ndmax and the number of grids Ns is less than Nsmax, calculate for each element the relative posterior errors $\beta_e = \frac{\eta_e}{\eta_{max}}$ for each time channel ($\eta_{max}$ is the maximum posterior errors for all elements in a single time channel); 3) In accordance with $\beta_e$, set a threshold for this time channel so that the number of grids is just less than a certain proportion of the total grid number; 4) For some channel, if $\beta_e > \beta_t$ and $V > V_{\min}$, record this element. Record all units that need refinement for all channels and randomly select a certain percentage of grids for refinement; 5) Calculate the responses using the new mesh. Compare the results with the former one. If the difference is less than a threshold, stop this process, otherwise, go to step 2).

## RESULTS

For checking the accuracy, we compare our results with the semi-analytical solutions for a half-space model. The depth of sea is 400m. The resistivity for air, sea and sediments are, respectively, $10^8\Omega\cdot$m, 0.3Ω·m, and 1.0Ω·m. The transmitting source is an electric dipole of 300m along in x-direction. The current is 1A. The transmitter and receivers are, respectively, 50m and 30m above the sea bottom. Figure 1 shows the comparison. From the figure, one sees that the maximum relative error between the two solutions is less than 1.8%. Figure 2 shows the posterior errors for different time channels. From the figure, one sees that the grids near the source need to be refined for early channels and the grids away from the source need to be refined for later time channels.

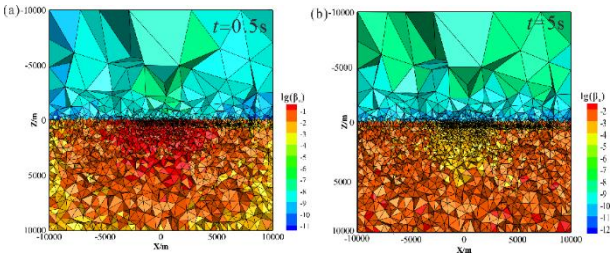


**Figure 2.** Posterior errors for different time channel.

Further, we design a resistive abnormal body embedded under a topographic seafloor to study reservoir detectability by MCSEM. Fig.3 (a) shows the topographic seabed. The size of anomalous body is 3000m×2000m×200m that is located at (4000m, 0m, 1500m). The survey line ranges from x=1000m ~ 8000m at y=0m and the distance between neighbor stations is 100m. Figures 3 (b), (c), and (d) show the EM responses, respectively, for the pure terrain, the total response and the percentage anomaly (define as the relative anomaly with respect to the background response of the topographic ocean). From Figure 3, one sees that topography has big influence on MCSEM responses. In comparison to total response, the abnormal body can be easily identified from the percentage anomaly.

## CONCLUSIONS

The adaptive unstructured FE method can obtain good results for MCSEM forward modeling in time-domain. A topographic seafloor has large influence on MCSEM responses. The anomaly of the target can be overwhelmed, however, when we subtract the topographic response and calculate the percentage anomaly, we can easily identify the resistive target. In practical survey, the ocean topography can be determined by sonar sounding before MCSEM survey, so we can calculate the response of topographic ocean and subtract to easily identify the resistive oil reservoirs.

## ACKNOWLEDGEMENTS

The paper was financially supported by the Key National Research Project of China (2016YFC0303100，2017YFC0601900) and the National Natural Science Foundation of China (41530320, 41774125).

## References

Avdeeva A, Commer M, Gregory A., et al (2007) Hydrocarbon reservoir detectability study for marine CSEM methods: time-domain versus frequency-domain.SEG Tech Program Expand Abstr pp: 628-632.

Ren Z, Kalscheuer T, Greenhalgh S, et al. (2013) A goal-oriented adaptive finite-element approach for plane wave 3D electromagnetic modeling. Geophysical Journal of International 194: I700-718.

Ren Z, Tang J (2010) 3D direct current resistivity modeling with unstructured mesh by adaptive finite-element method. Geophysics 75(1): H7-H17.

Swidinsky A, Edwards RN (2010) The transient electromagnetic response of a resistive sheet: an extension to three dimensions. Geophysical Journal International 182: 663-674.

Um SE, Harris JM, Alumbaugh DL (2010) 3D time-domain simulation of electromagnetic diffusion phenomena: A finite-element electric-field approach. Geophysics 75(4): F115-F126.

Yin C, Zhang B, Liu Y, et al. (2016) A goal-oriented adaptive finite-element method for 3D scattered airborne electromagnetic method modelling. Geophysical 75(4): E337-E346.

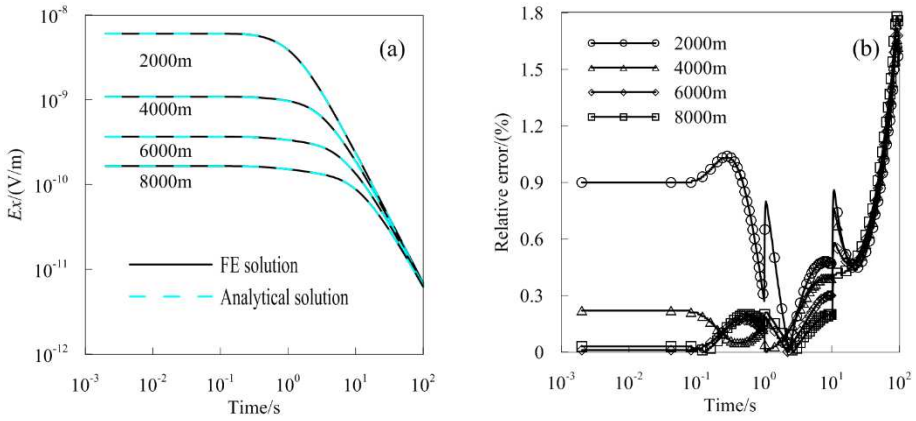


**Figure 1** Accuracy verification

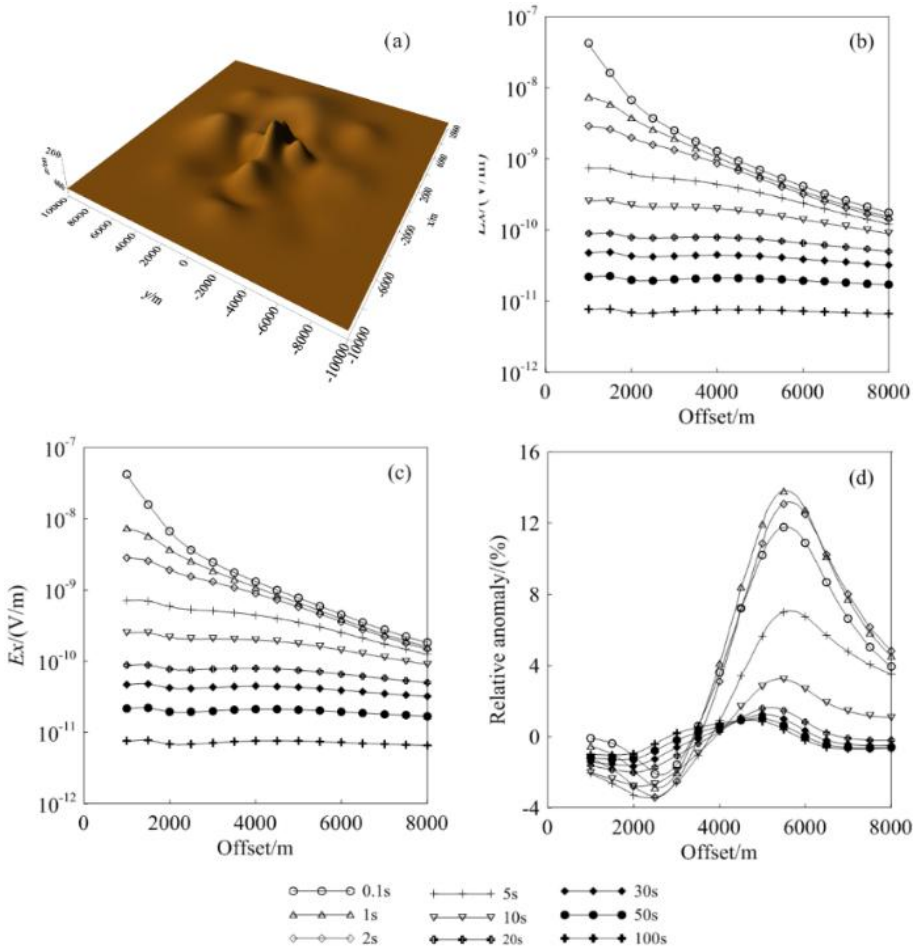


**Figure 3** MCSEM responses for a resistive target buried under a topographic ocean floor.

# Characterization of marine hydrothermal deposits from petrophysics and frequency-domain central loop electromagnetic soundings

H. Müller[1], K. Reeck[2] and K. Schwalenberg[3]
[1]BGR - Federal Institute for Geosciences and Natural Resources, hendrik.mueller@bgr.de,
[2]Geomar Helmholtz Centre for Ocean Research, kreeck@geomar.de
[3]BGR - Federal Institute for Geosciences and Natural Resources, katrin.schwalenberg@bgr.de

## SUMMARY

The development of geophysical methods for the assessment of spatial extent, composition, and inner structure of seafloor massive sulfide (SMS) deposits is crux to evaluate their resource potential for future deep-sea mining prospects. Challenges to acquire high resolution near-surface electromagnetic (EM) data in such geologically and morphologically complex marine environments have been addressed by our recent development of the deep-sea profiler GOLDEN EYE that utilizes a frequency-domain EM in-loop sensor, 3.5m in diameter. This system has been used to map active and relict hydrothermal vent fields in the German License-Areas for polymetallic sulfides at the Central- and Southeastern-Indian-Ridge in 2015 and 2017. Aside from technological developments, new data processing routines and methods to unravel the conductivity-depth-distribution, induced polarization and magnetic susceptibility are important milestones. This paper will address a combined interpretation of marine field data and petrophysical laboratory analysis.

In-situ magnetic susceptibility, electric conductivity and chargeability data of the Edmond hydrothermal area were resolved from half-space models with complex and frequency-dependent conductivity (Figure 1). Lateral dimensions of active and inactive (partly buried) hydrothermal deposits were clearly mapped and classified by EM derived petrophysical properties. In contrast to time-domain data where chargeability often contributes with negative sign and counteracts the conductivity signal, both, chargeability and conductivity, amplify the signal amplitude with specific frequency and phase dependency.

The subsurface architecture is approximated from 1D inversion and 3D gridding techniques. The volume of sulfide-bodies and mineral characteristics were derived from marine field data in combination with electrical impedance spectroscopy and rock magnetic analysis of 33 inch-sized SMS samples from the working-area. Cross-plots of conductivity versus chargeability, time-constant and porosity confine pore-fluid and sulfide-mineral contributions. Our findings emphasize the benefit of combined susceptibility-conductivity-chargeability modelling to retrieve a comprehensive image of compelling near-surface properties, to localize high-grade ores and to derive the subsurface-architecture of hydrothermal deposits.

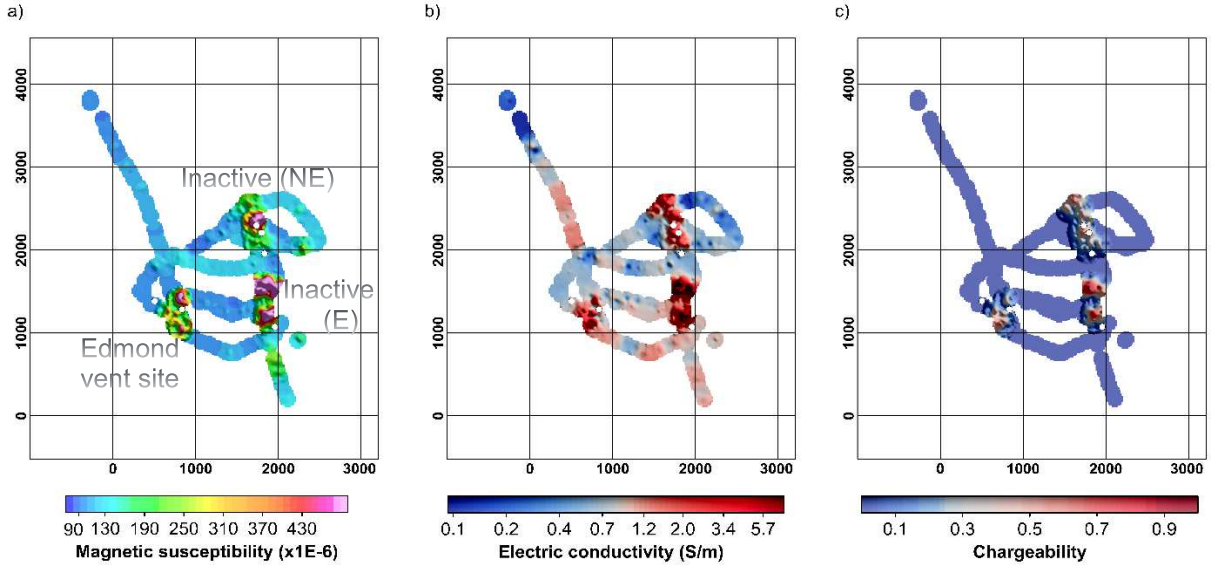


**Figure 1**. Maps of apparent magnetic susceptibility (a), electric conductivity (b) and chargeability (c) depict the lateral extends and characteristics of active and inactive hydrothermal mineral deposits of the Edmond vent site (23°53' S, 69°36' E) in 2900 to 3300 m water depth. White dots mark sample locations; X and Y in meters.

**Keywords:** Marine Near-Surface EM, Mineral Deposits, Frequency-Domain EM, Chargeability, Petrophysics

# Controlled Source Electromagnetics data analysis to evaluate fluid flow pathways associated with CCS sites

Naima K. Yilo[1], Romina Gehrmann[1] , Jonathan M. Bull[1], Timothy A. Minshull[1] , Axel Tcheheumeni Djanni[1] and Christian Berndt [2]
[1]Southampton University, N.K.Yilo@soton.ac.uk
[2]GEOMAR, N.K.Yilo@soton.ac.uk

**SUMMARY**

In April 2017 a controlled source electromagnetic survey was completed in the Central North Sea at the Scanner Pockmark, an area affected by wide-spread shallow gas. The seismic and CSEM experiments targeted a vertical fluid conduit identified on seismic reflection data (a “gas chimney”) laying underneath the Scanner pockmark. Chimney structures are commonly observed within sedimentary basins, and if they have high permeability, may be a potential risk for Carbon Capture and Storage sites if the reservoir seal is broken. Marine CSEM is a geophysical tool used to detect changes in electric resistivity below the seafloor related to features of geological interest. It is highly sensitive to electrically resistive targets such as hydrocarbons.
We will present CSEM data acquired and discuss the effect of noise and a preliminary interpretation of the electrical resistivity of the subsurface and how this relates to the geological processes.
A Deep-towed Active Source Instrument (DASI) powered from the ship with a deep-tow cable was towed 20-40 m above the sea bottom across an array of multicomponent receivers separated 500 m. The receiver array was composed of: 14 free-fall ocean bottom electric field receivers, placed on the seabed, and two three-axial Vulcan receivers towed behind the source. The CSEM survey was carried out in water depths <150 m, with the source towed along 12 profiles, in a star pattern over the Scanner Pockmark. The survey covers 4 azimuths that will aid resistivity anisotropy analysis over this chimney structure. The 14 ocean bottom instruments were equipped with two orthogonal horizontal 12 m electrodes. Six instruments were equipped with vertical 1.5 m electrodes, as the effect of the signal propagating through air is less prominent in the vertical component than the horizontal component of the electric field.
Several sources of environment noise are known to have significant impact on CSEM data quality in shallow water. The most significant ones being swell, surface wave, atmospheric noise and motion induced noise due to tidal currents. The presented data contains high intensity noise at low frequencies only in the horizontal component of the electric field. This demonstrated that the implementation of carbon fiber and fairings on the vertical electrodes was effective in significantly reducing the motion induced noise in the vertical electric field. The sources of noise are investigated by correlating the receiver data with oceanographic information. Additionally, higher frequency atmospheric noise generated in both the magnetosphere and ionosphere is clearly observed in the data.

**Keywords:** CSEM, electromagnetic methods, shallow water, electric resistivity, noise.

# Creating an Oceanic Lithosphere and Asthenosphere Reference Model

J. MacFarlane[1], G. Heinson[2]
[1] Department of Earth Sciences, University of Adelaide, Adelaide SA 5005,
Jake.Macfarlane@adelaide.edu.au
[2] Department of Earth Sciences, University of Adelaide, Adelaide SA 5005,
Graham.Heinson@adelaide.edu.au

**SUMMARY**

Both continental and oceanic MT programs are naturally bounded by the continental shelf and electrically-conducting seawater. Within a few hundred kilometres of the coastline, long-period MT data may be strongly influenced by induction in the seawater, a phenomenon known as the coast-effect. Thus, 3D inversion of gridded long-period MT data for continental and oceanic lithosphere models requires good constraints on the resistivity of the seawater, oceanic crust and upper mantle, and into the asthenosphere.

In this paper, we discuss the concept of a one-dimensional resistivity structure representative of the entire Pacific Ocean and suggest that other studies from the region vary from this resistivity structure due to the horizontal adjustment distance. This is the horizontal distance away from a major contrast in electrical conductance at which the anomalous EM fields are attenuated by a factor of 1/e from a one-dimensional response. This distance can range from hundreds of kilometers for continental crust to thousands of kilometers for oceanic crust and is largely dependent on the conductance of the continental and oceanic lithosphere, as well as the resistivity of the upper crust.

**Keywords:** Magnetotellurics, Oceanic Lithosphere, Horizontal Adjustment Distance

## INTRODUCTION

Large-scale grids of long-period magnetotelluric (MT) data are being collected across the globe in programs such as AusLAMP and the USArray. Such data are being used to generate 3D models of electrical resistivity of the continental lithosphere and asthenosphere to depths of several hundred kilometres.

It has been known for some time using long-offset marine controlled source EM measurements that the oceanic lithosphere can be extremely resistive, of order at least $10^4$ Ω.m (compared to $10^1$ - $10^3$ Ω.m for the continent) directly beneath the oceanic Moho and probably to a depth of about 50 km or so, at which point conduction increases with temperature (Cox et al., 1986). The consequence of a resistive oceanic upper mantle is that the contrast in electrical conductance at the ocean-continent boundary affects measurements hundreds of kilometres inland and thousands of kilometres out on the ocean floor. Smooth models, therefore, may not capture the significance of this boundary.

In this poster, we define a one-dimensional resistivity structure for the Pacific oceanic lithosphere to better constrain the horizontal adjustment distance. Furthermore, we propose MT studies from this region vary from our one-dimensional resistivity structure because of the horizontal adjustment distance, first identified by Ranganayaki and Madden (1980) and later developed by Weaver and Dawson (1992) to include frequency dependence.

## METHOD

A thin-sheet model was constructed by producing a 301 x 301 grid with a grid spacing of 100 km which overlies an azimuthally projected map of the Pacific Ocean and surrounding lithospheric crust (Figure 1). This projection allows us to maintain the distance from our projection centre (Hawaii) to the surrounding coastline. The ocean depth was coarsely gridded at intervals of 500 m, 1000 m, 1500 m, and 5000 m (Figure 2). Despite this coarse gridding, a significant portion of the coast-effect is caused by the 500 m depth interval.

To define the resistivity structure, we compared the resistivity structures of previous MT studies from the Pacific Ocean (Figure 1) to the resistivity structure generated by global C-responses (Grayver et al., 2017) and the resistivity curve calculated from the hydrous olivine electrical conductivity law (Gardes et al., 2014) (Figure 2). From this, we defined a resistivity structure which approximately represents the majority of the MT studies from the region.

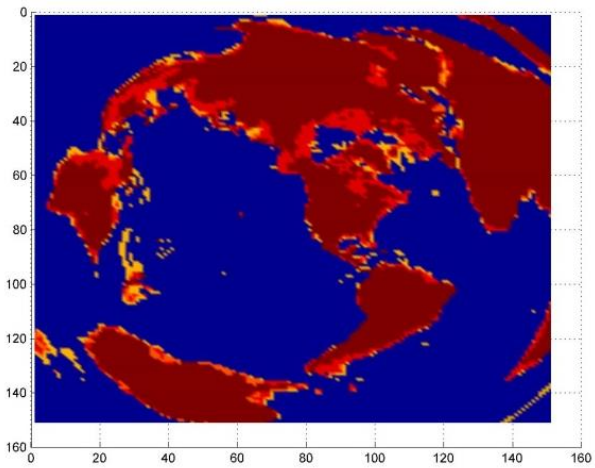

**Figure 1.** Structure for the thin-sheet modeling algorithm.

To investigate the horizontal adjustment in the Pacific Ocean we constructed a simple analytical model of a coastline as shown in Figure 3. The model consists of a surface thin-sheet layer with finite conductance given by the term $\tau$ with subscripts o and c for ocean and continent respectively. On the left side, typical ocean depths of 5 km with seawater resistivity of 0.3 Ω.m leads to a conductance of $\tau_0 \approx 16{,}500$ S; by contrast the conductance of 5 km of continental crust is between $\tau_c \approx 500$ S.

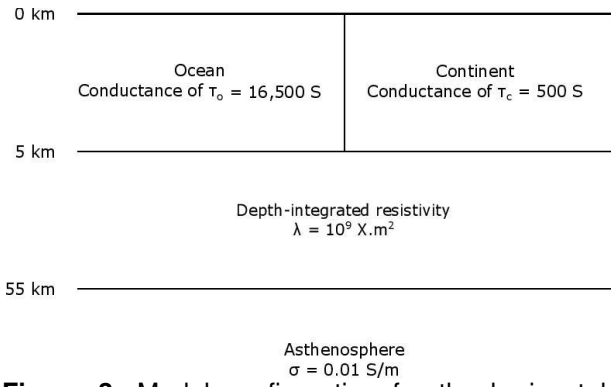


**Figure 3:** Model configuration for the horizontal adjustment distance.

The layer beneath is the parameter $\lambda = 10^9$ Ω.m$^2$ which defines the resistivity-thickness product. Beneath this layer is the asthenosphere defined by a resistivity of $\Omega = 10^1$ Ω.m (and conductivity $\sigma = 10^{-1}$ S/m).

Weaver and Dawson define the term α as:

$$\alpha = \sqrt{\omega\mu\sigma} \qquad (1)$$

where ω is the angular frequency, and μ is the magnetic permeability of free space. With this definition, they then define

$$\chi_j = \frac{1}{\lambda\alpha} - \sqrt{\frac{1}{(2\lambda\alpha)^2} - \frac{1}{\tau_j\lambda} + i\alpha^2} \qquad (2)$$

In Equation 2, the index j refers to either the ocean or continental side. Weaver and Dawson (1992) then derive an accurate approximation of the horizontal adjustment distance d as

$$d_j = \frac{\sqrt{\tau_j\lambda}}{\mathrm{Re}\sqrt{1 - {}^{\tau_j\chi_j}/_{\sigma}}} \qquad (3)$$

By comparison, Ranganayaki and Madden (1980) used a simpler term for the horizontal adjustment distance r given by

$$r_j = \sqrt{\lambda\tau_j} \qquad (4)$$

This expression is effectively an upper bound of d as it has no frequency dependence.

Using values as defined in Figure 3, we can plot the adjustment distance on land and to sea for long-period MT $10^1$ -$10^4$ s.

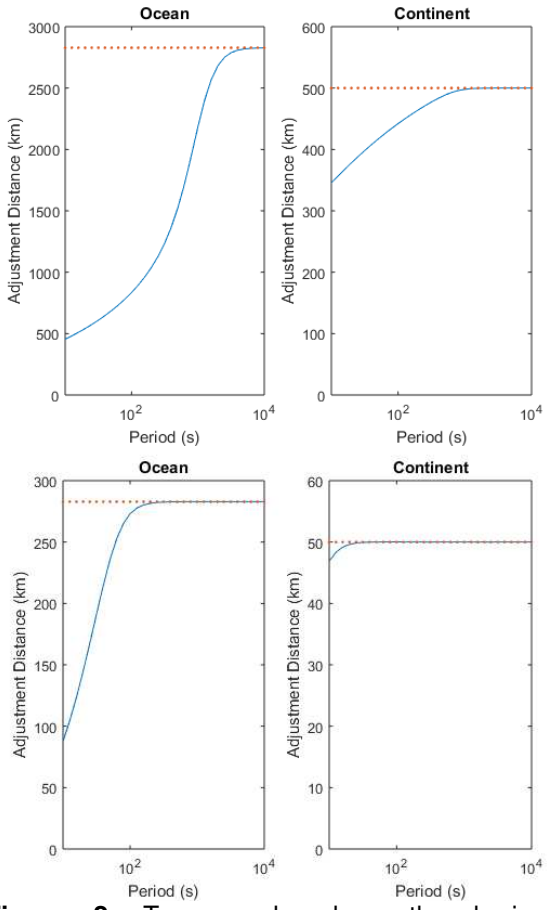


**Figure 2.** Top panels show the horizontal adjustment distance for the case of $\lambda = 5 \times 10^8$ Ω.m$^2$ (oceanic upper mantle dominant) for the ocean and continental sides; the two right-hand panels show the case of $\lambda = 5 \times 10^6$ Ω.m$^2$ (continental crust dominant). In all panels, the blue

lines show the frequency dependent adjustment distances from Equation 3 and the red dots are for the frequency-independent limit from Equation 4.

## RESULTS

Figure 5 displays the apparent resistivity calculated by the thin sheet algorithm compared to measured MT responses from the APPLE experiment.

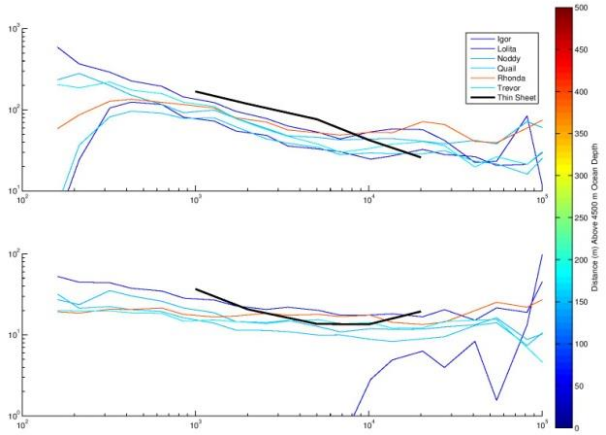


**Figure 5:** Resistivity curves for the APPLE experiment plotted alongside resistivity curves output by the thin-sheet modeling algorithm

Figure 6 displays the region of interest with previous MT studies marked by triangles. When the coastlines are considered, it becomes apparent that a significant number of these studies are within the range defined by the horizontal adjustment distance in Figure 4 for 1,000 s.

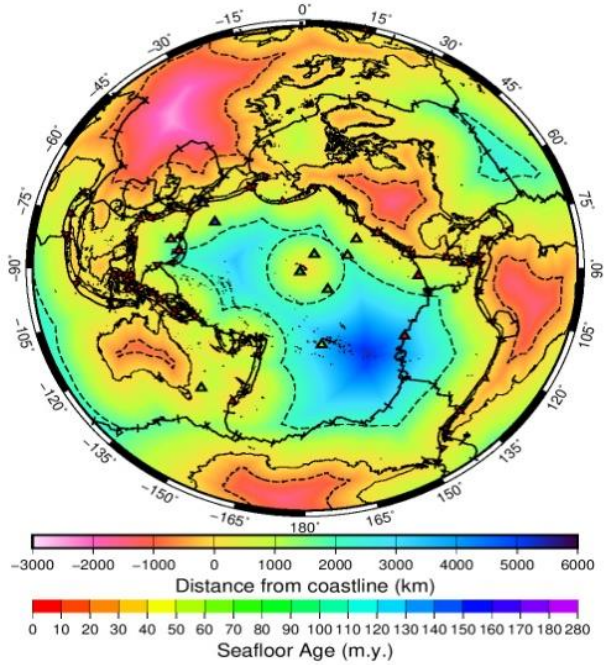


**Figure 6:** Azimuthally equidistant projection of the Pacific Ocean centered on Hawaii with previous MT studies marked as triangles. Contours represent the adjustment distance calculated in Figure 4 at 1,000 s. Triangles represent MT surveys with the colour representing the age of the oceanic lithosphere. Map coloured with respect to distance from the coastline.

## CONCLUSIONS

Results show that for a relatively simple average model derived from previous MT studies situated within the Pacific Ocean is capable of approximately reproducing MT responses measured during the APPLE experiment. Variability within APPLE experiment responses is likely the result of variations on the seafloor causing inconsistent MT instrument depths. This reduced depth causes MT responses of any given period to sample variable amounts of the highly conductive sea water which then manifests itself in highly variable apparent resistivity curves at shorter periods.

## ACKNOWLEDGEMENTS

We thank the University of Adelaide for supporting a PhD scholarship to fund this research.

## REFERENECS

Baba K, Tada N, Matsuno T, Liang P, Li R, Zhang L, Shimizu H, Abe N, Hirano N, Ichiki M, Utada H, (2017) Electrical conductivity of old oceanic mantle in the northwestern Pacific I: 1-D profiles suggesting differences in thermal structure not predictable from a plate cooling model. Earth Planets and Space,69(1): 111.

Cox CS Constable SC Chave AD Webb SC (1986), Controlled-source electromagnetic sounding of the oceanic lithosphere. Nature: 320: 52-54.

Gardés, E Gaillard F. Tarits P (2014). Toward a unified hydrous olivine electrical conductivity law. Geochem Geophys Geosystems, 15(12): 4984-5000.

Grayver, AV Munch FD Kuvshinov AV Khan A Sabaka TJ Tøffner-Clausen L (2017) Joint inversion of satellite-detected tidal and magnetospheric signals constrains electrical conductivity and water content of the upper mantle and transition zone. Geophys Res Lett 44: 6074–6081

Kelbert A Meqbel N Egbert GD Tandon K (2014) ModEM: A modular system for inversion of electromagnetic geophysical data: Computers and Geosciences, 66: 40-53.

Naif S Key K Constable S Evans RL (2013) Melt-rich channel observed at the lithosphere–asthenosphere boundary. Nature, 495(7441), p.356.

Ranganayaki RP Madden TR (1980) Generalized thin sheet analysis in magnetotellurics: an extension of Price's analysis: Geophys J Roy Astron Soc 60: 445-457.

Sarafian E Evans R Collins JA Elsenbeck J Gaetani GA Gaherty JB Hirth G Lizarralde D (2015) The electrical structure of the central Pacific upper mantle constrained by the NoMelt experiment. Geochem Geophys Geosystems, 16(4): 1115-1132.

Weaver JT Dawson TW (1992) Adjustment distance in TM mode electromagnetic induction: Geophys J Int 108: 293-300.

.

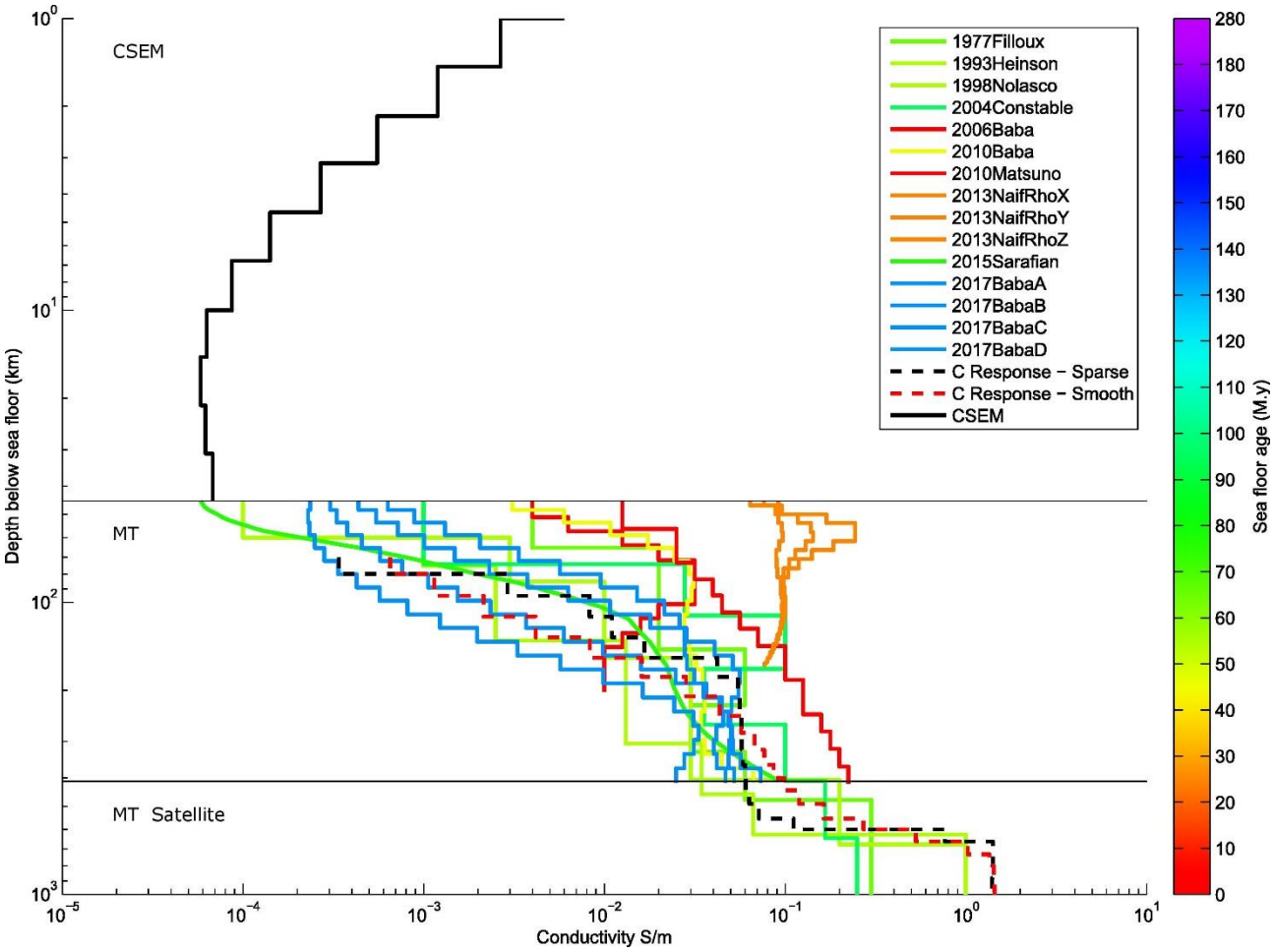


**Figure 2:** Resistivity curves from multiple sources plotted versus depth. Resistivity curves from MT studies are coloured with respect to the seafloor age on which MT study was conducted.

# Exploring ocean circulation's geoelectric fields with Pacific Ocean submarine voltage cables

N. R. Schnepf[1], M. Nair[2], N. P. Thomas[3] and A. Kuvshinov[4]
[1]University of Colorado Boulder/CIRES, CO, USA, Neesha.Schnepf@colorado.edu
[2]CIRES/National Center for Environmental Information, NOAA, Boulder, CO, USA, Manoj.C.Nair@noaa.gov
[3]University of Maryland, College Park, MD, USA, npthomas@terpmail.umd.edu
[4]Institute of Geophysics, ETHZ, Zürich, Switzerland, kuvshinov@erdw.ethz.ch

**SUMMARY**

Marine electromagnetic (EM) signals largely depend on three factors: oceanic transport (i.e., depth-integrated flow), the local main magnetic field, and the local seawater conductivity (which in turn depends on the local temperature and salinity). Thus, there is interest in using marine EM signals to study oceanic state properties, as well as monitor the inter-annual variability of these properties.

Seafloor telecommunication cables can be used to analyze marine EM signals because these cables measure voltage differences between their two ends. Data from such cables can provide information on the depth-integrated transport occurring in the water column above the cable. However, these time-varying data are a superposition of all EM fields present at the observatory, no matter what source (eg. Earth's core, lithospheric/mantle induction, the ocean, or near-Earth space) or process created the field (eg. ocean tides versus ocean circulation). The main challenge in using such submarine voltage cables to study ocean circulation is properly isolating its signal.

Here, we analyze voltage data from Pacific Ocean submarine voltage cables located in the Kuroshio Current and California Current, and compare the observed inter-annual voltage variations with those from a 3-D EM induction model driven by the latest version of the Estimating the Circulation & Climate of the Ocean (ECCO) model. We only use seafloor data from geomagnetically quiet days (Ap index < 20) to effectively remove EM noise caused by solar disturbances in near-Earth space. We then evaluate and discuss the implications of using voltage data across ocean basins to study and monitor ocean flow.

From our preliminary results, the correlation between measured and predicted voltage data is encouraging. Stronger correspondence between observations and predictions may indicate inter-annual ocean flow is detectable in the voltage cables.

**Keywords:** marine electromagnetism, ocean circulation, submarine voltage cables, geoelectric fields

# Investigation of the Namibian continental margin by integrating Magnetotelluric, Gravity and Seismic data in a Joint Inversion approach

G. Franz[1], M. Jegen[1], M. Moorkamp[2] and A. Avdeeva[3]
[1]GEOMAR Helmholtz Centre for Ocean Research Kiel, gfranz@geomar.de, mjegen@geomar.de
[2]Ludwig-Maximilians-University Munich, max.moorkamp@geophysik.uni-muenchen.de
[3]Complete MT solutions, avdeevaanna@gmail.com

**SUMMARY**

The source of magmatic features along the Namibian continental margin, and therefore the processes which lead to the opening of the South Atlantic ocean, are still debated controversially. One big question is weather hotspot volcanism was fed by a deep reaching plume or by heterogeneities of the middle and upper mantle.

In an attempt to gain a better understanding of the involved magmatic processes, a 3D inversion of magnetotelluric (MT) data with integration of seismic and gravity constraints was conducted. In a first step, integration was accomplished by adding a cross-gradient constraint of the density model to the inversion, which enforces model resemblance at structural boundaries. The impact of the cross-gradient constraint with a preexisting density model limited to this model's resolution, because the cross-gradient only works at structural boundaries within the constraint model. Its benefits include enhancing of resistivity structures in the inversion model. Additionally, the density constraint does not overprint resistivity structures which are not imaged by gravimetric methods (i.e. resistivity variations due to mineral composition).

In the second step, we present preliminary results of a true joint inversion with MT-, vertical gravity-, and first arrival seismic data. By adjusting not only the resistivity model to the MT data and constraining it to structural boundaries, we now integrate gravity and seismic data to achieve an improved earth model.

An observed high resistivity anomaly below the continental margin and Walvis Ridge coincides well with seismically observed high velocity underplating. This feature is interpreted to mark magmatic intrusions from a plume source, initiating continental breakup. The eastern termination of the high resistivity structure correlates with the onset of seaward dipping reflectors in seismic data. Therefore, it marks the transition from continental to oceanic regime (continent-ocean boundary). The theory of a plume source of the magmatic features is supported by the local planar extent of roughly estimated 70 000 km² and the deep reaching form of the underplating. This form with three arms at a 120° spread is suggestive for the rift arms of a hot spot impingement into the crust. However, since the aforementioned amount of intrusive material is rather small for the impact of a broad plume head, the preferred model includes a plume that stopped ascending in the mid-mantel. The underplated magmatic features would then be fed by smaller plumes or hotspot-like dikes rising from this deep mantle plume. A continental breakup solely driven by plate-forces is unlikely for the South Atlantic, as lithospheric thinning and subsequent magmatism would have resulted in a larger volcanic area due to mantle heterogeneities, than the observed local magmatic underplating.

**Keywords:** passive margins, marine magnetotellurics, Walvis Ridge, electromagnetic inversion, magmatic intrusions

# Large submarine aquifers on the US Atlantic continental shelf

C. Gustafson[1], K. Key[1], R. Evans[2], and D. Blatter[1]
[1]Lamont-Doherty Earth Observatory, Columbia University, cdg2152@columbia.edu
[2]Woods Hole Oceanographic Institution

## SUMMARY

Submarine groundwater beneath continental shelves may be a significant global phenomenon, yet little is known about the distribution of these fresh and brackish water bodies. Borehole data provide direct evidence of submarine groundwater, but their sparse locations are unable to characterize the lateral extent of offshore aquifers. Here, we present data from a pilot study of large-scale electromagnetic (EM) surveying of offshore groundwater on the US Atlantic continental shelf. We collected a total of 410 line kilometers of surface-towed controlled source EM data and 18 stations of passive magnetotelluric data in shore perpendicular surveys located off New Jersey and off Martha's Vineyard. Our data reveal laterally continuous low conductivity zones consistent with brackish aquifers within the top 500m of sediment that extend up to 98 km offshore, providing the first constraints on the lateral distribution of this groundwater. The distributions of brackish and saline water imaged via EM methods are consistent with co-located borehole measurements from IODP Expedition 313 off New Jersey. Furthermore, combining our EM results with seismic stratigraphic interpretations reveals structural controls on freshwater distribution.

**Keywords:** Marine EM, Joint Inversion, Submarine Groundwater

## INTRODUCTION

Fresh and brackish waters have been identified in boreholes drilled on continental shelves worldwide, yet their distribution, origin, and interactions with the surrounding submarine environments is not yet well understood (Post et al. 2013). One modeling study estimates $3 \times 10^5$ km$^3$ of freshwater may exist within continental shelves (Cohen et al. 2010), but considerable uncertainty exists due to a lack of observational data. Brackish and briny waters have been observed in several boreholes drilled on the US Atlantic continental shelf. The earliest indications come from a scattering of boreholes made across the margin in the 1970's as part of the Atlantic Continental Margins Coring (AMCOR) project (Hathaway et al. 1979). A more focused drilling survey, IODP Expedition 313 (Mountain et al. 2010), off the coast of New Jersey identified a more complex groundwater system within the shelf, revealing sharply alternating layers of saline and fresh water within the top 600m of sediment (Mountain et al. 2010; Lofi et al. 2013).

## MARINE EM SURVEY AND METHODS

In order to investigate the distribution of submarine groundwater in continental shelves, we collected controlled source electromagnetic (CSEM) and magnetotelluric (MT) data to image electrical resistivity structure of shallow crust off the coasts of central New Jersey and Martha's Vineyard. The New Jersey survey was colocated with IODP Expeditions 313 boreholes to provide a comparison of directly measured salinity with resistivity structure derived from EM inversions. The survey off of Martha's Vineyard was designed to provide the first observational data of offshore groundwater for this area, as the only borehole evidence of freshwater exists onshore Martha's Vineyard and Nantucket. Survey layout is shown in Figure 1.

In both survey locations we recorded seafloor MT and CSEM data using a sparse array of ten broadband EM receivers deployed at 10 to 20 km spacing. The shallow water depths on the continental shelf permitted the additional use of a 336m long surface-towed CSEM transmitter antenna fol-

lowed by four EM receivers at offsets of 600m - 1380m from the transmitter. This allowed us to collect short-offset, surface-towed CSEM data continuously along all profiles. The antenna transmitted an alternating 100 A current using a complex binary waveform with a fundamental frequency of 0.25 Hz that was designed to provide a wider frequency spectrum of high amplitude harmonics than is produced by a simple square wave (Myer et al. 2011). This surface towed system is ideal for detecting resistive freshwater as it was designed for high resolution imaging in the near surface (Sherman et al. 2017). CSEM response functions for frequencies of 0.25 Hz - 48.25 Hz for each surface towed receiver were obtained by processing measured electric field time series as outlined by Myer et al (2011). Data were robustly stacked into 60 sec bins.

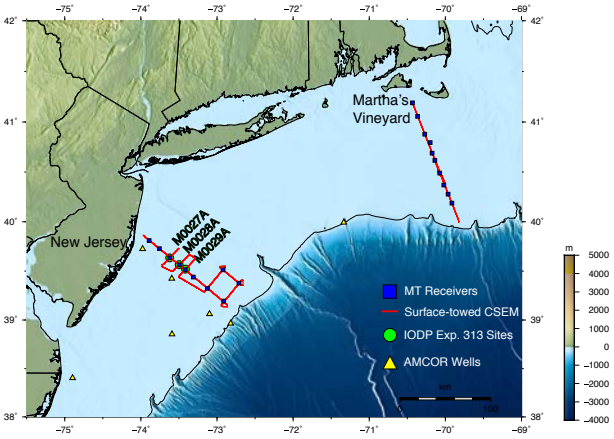


**Figure 1:** Map of electromagnetic survey of the US Atlantic continental shelf. Red lines show the surface-towed CSEM profile. Blue squares show MT receiver locations. IODP Expedition 313 borehole locations are labeled and shown as green circles. Yellow triangles show locations for AMCOR wells

Seafloor MT receivers recorded horizontal electric and magnetic field time series for 3-5 days and were processed into impedance responses using a robust array processing method to estimate impedances (Egbert 1997). Due to the shallow water depths (20 to 150 m) and generally favorable sea state, we obtained good MT responses from $10^{-4}$Hz up to 100 Hz, greatly exceeding the typical maximum recoverable frequency of 0.1-1Hz for broadband receivers deployed at ocean depths of 4 to 1 km, respectively.

## 2D Inversion Results

We inverted our data for 2D isotopic resistivity structure using MARE2DEM (Key 2016), a freely-available goal-oriented adaptive finite-element inversion code for 2D electromagnetic modeling. The surface-towed CSEM data consisted of the 0.75 and 1.75 Hz harmonics and the MT data consists of periods below 100 seconds. In order to evaluate the relative merits of both data types, we carried out independent inversions of the surface-towed CSEM and seafloor MT data, then jointly inverted the two data types together.

Figure 2 shows the three different inversion models for our shore-to-shelf New Jersey profile. In both locations the independent surface-towed CSEM and MT data was fit to root-mean squared misfit (RMS) 1.0 using 1% and 5% error floors, respectively. For the jointly inverted data sets, the New Jersey profile uses MT error floors of 10% and fits the data to RMS 1.0. For Martha's Vineyard, the MT error floors remain at 5% and fit the data to RMS 1.4.

The surface-towed CSEM inversion in Figure 2 identifies a large scale resistive feature in the upper 500 m of sediments from the survey origin to 90 km offshore. The resistor is continuous laterally until 50-60 km position, where it abruptly jumps to shallower depths. In general, the resistive feature is fairly smooth looking, except for a few small scale resistors on the seafloor where the data's lateral and depth resolution is highest.

The MT inversion in Figure 2 also recovers the resistive feature, although it is not as laterally uniform as the CSEM inversion. The magnitude of the resistor is also lower, but this is expected due to the saturation effect of MT responses for a thin resistive layer between conductors. At positions greater than 73 km and depths of around 500 m, the MT inversion recovers an extensive conductive feature about 200 m thick.

The joint inversion shows the same resistivity trend as the independent inversions, but with more sharply defined geometries (see Figure 2). It is possible there are two separate resistive bodies separated at 53 km, rather than an upward shift as the boundary may be smoothed over in our inversion. In the rest of our text we focus on our interpretations on joint inversions results from both survey areas.

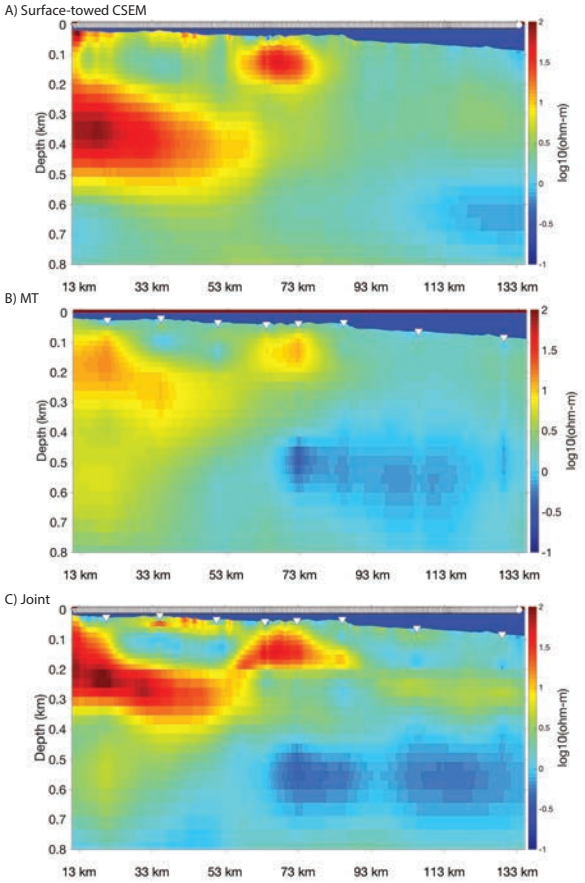


**Figure 2:** Inversion models from (a) surface-towed CSEM data, (b) MT data, and (c) combined surface-towed CSEM and MT data. The vertical scale is distance from shore. The horizontal scale is depth from sea surface. White markers at the top of each figure show the locations of surface-towed CSEM transmitters and receivers. Inverted white triangles on the seafloor show the locations of MT receivers.

## INTERPRETATION

Recent borehole data allow a direct comparison of our inversion model from off New Jersey with chlorinity data from the IODP Expedition 313 (Figure 3). The locations of the high and low resistivity features seen in our inversion correspond well with low and high chlorinity concentrations, respectively. However, due to the diffusion nature of EM soundings, our data cannot resolve the sharply alternating layers of brackish and briny waters observed in the upper 200m of the boreholes. We interpret resistive values (warm colors in Figures 2, 3, and 4) to be indicative of freshwaters and conductive values to be indicative of saltier waters.

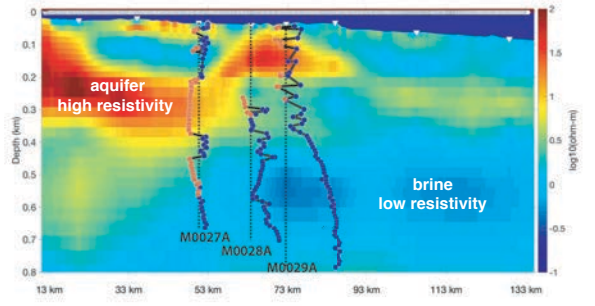


**Figure 3:** New Jersey resistivity shown with overlain chloride concentration data from IODP Expedition 313 borehole data (van Geldern et al. 2013). Orange circles show fresh concentrations and blue circles show salty concentrations. Dashed black lines represent borehole locations.

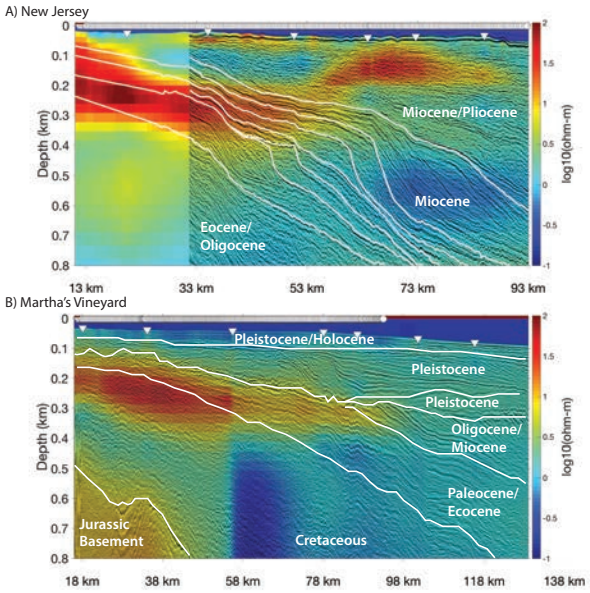


**Figure 4:** Resistivity models for (a) New Jersey and (b) Martha's Vineyard with seismic reflection data and highlighted horizons (white lines). New Jersey seismic data from B. Dugan, personal communication, and picked horizons from M. Steckler, personal communication. Martha's Vineyard seismic data from G. Mountain, personal communication. Picked horizons were estimated based on the seismic interpretation given in Siegel et al (2014).

Joint inversions of shore-to-shelf edge profiles off of New Jersey and Martha's Vineyard (Figure 4) reveal resistive bodies extending out to 93 - 98 km offshore. The highest resistivity values, and therefore freshest pore waters, appear closest to shore for both profiles, indicating this water likely connects and is potentially recharged onshore. When overlaying depth migrated seismic reflection data (G. Mountain, personal communication, B. Dugan, personal communication) and specific sequence boundaries (M. Steckler, personal communication), the freshwater appear stratigraphically capped for both locations. Furthermore, both locations show the terminus of the freshwater colocated with the onset of clinoform structures. Both locations show deeper conductive features that do not correlate with any stratigraphic boundaries.

## CONCLUSION

We have demonstrated marine EM methods successfully map shallow submarine groundwater. Our results constrain the lateral and depth extent of the freshwater in both New Jersey and Martha's Vineyard. In both locations, the fresh water aquifer geometries seem to be structurally controlled by clinoforms and sequence boundaries. Although separated by 300 km, the similarity of the offshore extent of both aquifers suggests the entire shelf in this region may contain abundant freshwater. The lateral and depth constraints on groundwater off the US Atlantic coast provided by this study may be used to guide modeling studies determining the relative importance of stratigraphy, sea level changes, and ice sheet dynamics for paleo-freshwater emplacement.

## ACKNOWLEDGEMENTS

We thank the student volunteers, engineers and technicians from Scripps Institution of Oceanography and Woods Hole Oceanographic Institution and the captain and crew of the R.V. Marcus G. Langseth for a successful research cruise. This work was funded by National Science Foundation Awards 1458392 and 1459035.

## REFERENCES

Cohen, D. et al. (2010), Origin and Extent of Fresh Paleowaters on the Atlantic Continental Shelf, USA, Ground Water, 48(1), 143-158, doi:10.1111/j.1745-6584.2009.00627.x.

Egbert, G. D. (1997), Robust multiple-station magnetotelluric data processing, Geophysics Journal International, 130(2), 475-496.

Hathaway, J. C., C. W. Poag, P. C. Valentine, R. E. Miller, D. M. Schultz, F. T. Manheim, F. A. Kohout, M. H. Bothner, and D. A. Sangrey (1979), U.S. Geological Survey Core Drilling on the Atlantic Shelf, Science, 206(4418), 515-527.

Key, K. (2016), MARE2DEM: a 2-D inversion code for controlled-source electromagnetic and magnetotelluric data, Geophysical Journal International, 207(1), 571-588, doi:10.1093/gji/ggw290.

Lofi, J. et al. (2013), Fresh-water and salt-water distribution in passive margin sediments: Insights from Integrated Ocean Drilling Program Expedition 313 on the New Jersey Margin, Geosphere, 9(4), 1009-1024, doi:10.1130/GES00855.1.

Mountain, G., J.-N. Proust, Expedition 313 Science Party (2010), The New Jersey Margin Scientific Drilling Project (IODP Expedition 313): Untangling the Record of Global and Local Sea-Level Changes, edited by H. C. Larsen and U. Harms, Scientific Drilling, (10, September 2010), 1-9, doi:10.2204/iodp.sd.10.03.2010.

Myer, D., S. Constable, and K. Key (2011), Broad-band waveforms and robust processing for marine CSEM surveys, Geophysical Journal International, 184(2), 689-698, doi:10.1111/j.1365-246X.2010.04887.x.

Post, V. E. A., J. Groen, H. Kooi, M. Person, S. Ge, and W. M. Edmunds (2013), Offshore fresh groundwater reserves as a global phenomenon, Nature, 504(7478), 71-78, doi:10.1038/nature12858.

Sherman D, Kannberg P, Constable S (2017) Surface towed electromagnetic system for mapping of subsea Arctic permafrost. Earth and Planetary Science Letters 460:97-104. doi: 10.1016/j.epsl.2016.12.002

van Geldern, R., T. Hayashi, M. Bottcher, M. J. Mottl, J. A. C. Barth, and S. Stadler (2013), Stable isotope geochemistry of pore waters and marine sediments from the New Jersey shelf: Methane formation and fluid origin, Geosphere, 9(1), 96-112, doi:10.1594/PANGAEA.801732.

# Maine CSEM inversion using rotational invariants and its application to the Black Sea data

Gang Li[2,1], Marion Jegen[1], Sebastian Hölz[1] and Shuangmin Duan[2,1]
[1]GEOMAR Helmholtz Centre for Ocean Research Kiel, Kiel 24148, Germany, ligang0309@gmail.com
[2]College of Marine Geosciences, Ocean University of China, Qingdao 266100, China

## SUMMARY

The GEOMAR's time-domain marine controlled-source electromagnetic (CSEM) data is excited with two perpendicular horizontal dipole polarizations, thus the rotational invariants can be used for better representing the measured horizontal field components, which are independent of the horizontal orientations of both the transmitters (TXs) and the seafloor receivers (RXs). The time-domain CSEM transient electric fields for each RX-TX pair are firstly transformed into the corresponding frequency-domain using the discrete Fourier transform, in which both the low and high frequency parts are selected for a varying frequency range. In this study, we present a frequency-domain Gauss-Newton (GN) one-dimentional (1D) inversion scheme using rotaional invariants, which could be used for interpreting the GEOMAR's CSEM data. It is worth mentioning that the rotational invariants are directly computed in the frequency domain. Synthetic tests show its validity. The developed inversion scheme is also used for interpretation of the CSEM data collected in the Black Sea for gas hydrate estimation.

**Keywords:** Marine electromagnetics; 1D; Inversion; Rotational invariants

# Marine CSEM gas hydrate studies in the Danube Delta, Western Black Sea

K. Schwalenberg[1], R. Gehrmann[2], S. Hoelz[3] and T. Zander[3]
[1]BGR- Federal Institute for Geosciences and Natural Resources, Hannover, Germany, katrin.schwalenberg@bgr.de
[2]University of Southampton, Ocean and Earth Science, UK, r.a.gehrmann@soton.ac.uk
[3]GEOMAR- Helmholtz Centre for Ocean Research, Kiel, Germany, shoelz / tzander@geomar.de

## SUMMARY

Marine CSEM data have been collected in 2014 onboard R/V M.S. MERIAN over seismically inferred submarine gas hydrate targets in the Danube delta fan, western Black Sea, with the goal to derive the sub-seafloor gas hydrate distribution and to provide saturation estimates. The Black Sea is a quasi-closed marginal sea with thick sediment layers. Anoxic conditions and water depths exceeding 1000 m favor the generation of methane and extensive gas hydrate deposits along the continental margins of the Black Sea. Methane venting at the landward edge of the gas hydrate stability zone and the observation of multiple bottom simulating reflectors in the deeper parts of the margins are further expressions of a major hydrocarbon potential.
First results of the CSEM data analysis from a profile (P1) using BGR's seafloor-towed electric dipole-dipole system have been presented at the EMIW 2016. Two-dimensional inversion of this data set revealed highly anomalous resistivities which are partly attributed to low pore water salinities due to sea level low stands in the past, but also require an additional resistive phase, i.e. gas hydrate.
Recently measured pore water salinities from piston cores down to a depth of 30 m from the edge of the hydrate stability field vary between 1 and 4 ppm. Comparison with conductivities derived from short offset CSEM data arrive at a better fit for salinities of 4 ppm.
Data analysis has been going on towards inclusion of continuously towed data in addition to stationary data using Key's 2D inversion code MARE2DEM. The code also allows incorporation of structural constraints from coincident seismic profiles which have been applied to the data. Higher resistivities are observed below a prominent seismic reflector at intermediate depth of 50 m below seafloor which may be a lithological interface. CSEM data from two additional profiles (P2 and P3) have been processed and are now available for the inversion and interpretation. P2 is located close to P1 within a channel levee system in the Bulgarian sector, but shows generally lower resistivities which are still open for discussion. P3 is located further North in the Romanian sector in a slump area at the edge of the hydrate stability field. Even though the gas hydrate stability layer is much thinner, the inverted resistivity values are comparable high to P1. The area was also the focus of a cruise in late 2017 using the MeBo mobile drilling platform, which for the first time provided core samples and physical data down to a depth of 147 m.
In the paper we present new 2D inversion models from the three CSEM profiles using stationary and continuous data as well as structural constraints from seismic. We also derive gas hydrate saturation estimates based on Archie's relation including salinity data from shallow bore holes, porosity information from seismic velocity data, and information available from the MeBo drill sites.

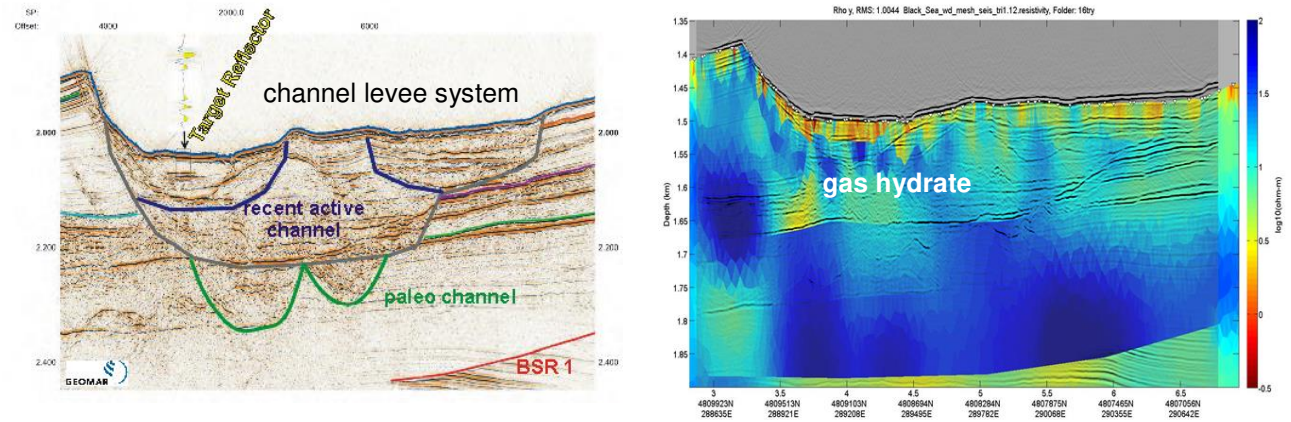


**Figure 1.** Left: seismic section showing interpreted reflectors of the recent and paleo channels, and the recent BSR. Right: 2D resistivity model profile P1 using structural constraints. High resistivities values up to 50 Ωm are partly due to low pore water salinities and point at high gas hydrate saturations

**Keywords:** marine CSEM, submarine gas hydrates, western Black Sea, 2D inversion

# Marine EM on Land: MT Measurements in Mono Lake

S. Constable[1] and J. Peacock[2]
[1]Scripps Institution of Oceanography, sconstable@ucsd.edu
[2]U.S. Geological Survey, jpeacock@usgs.gov

## SUMMARY

Long Valley Caldera and the Inyo-Mono Craters are manifestations of an active volcanic system on the eastern flank of the Sierra Nevada in California, USA. The United States Geological Survey has been using the MT method to study the hydrothermal and magmatic systems associated with this volcanism, but Mono Lake, at the northern end of the Inyo-Mono Crater chain, creates a 20×15 km hole in the land MT data set. This is particularly inconvenient considering that the most recent volcanic feature in the area is the lake's Paoha Island, which emerged only 350 years ago. In 2016, we tested two moored, lake-bottom MT receivers which are based on the ocean-bottom MT instrument developed by Scripps. After encouraging results, in 2017 we conducted a small campaign to collect 21 sites across the lake. Seven instruments were deployed and moved three times at 2-day intervals, and collected good quality data from 100 Hz (limited by sample rate) to 200–3,000 s periods. A preliminary 2D model that includes land stations along with the lake-bottom stations identifies a large conductor on the north side of the lake at a depth of 3 km and extending to 20–30 km deep. This conductor is consistent with a conductor observed on the edge of 3D inversions of the land data, and is probably a hydrothermal system, similar to a conductor seen beneath Long Valley Caldera to the south, underlain by a magmatic system.

**Keywords:** lake MT, magmatic, hydrothermal, marine MT

## INTRODUCTION

Mono Lake lies in the Mono Basin, situated at the eastern edge of the Sierra Nevada in central California near the Nevada border (Figure 1). Mono Basin and Long Valley Caldera, to the south of the basin, are both volcanically active regions. Extending south from Mono Lake is a chain of recent volcanic features called the Inyo-Mono Craters, which which have erupted as recently as 650 years ago. Paoha Island in Mono Lake is the most recent edifice, having emerged from the lake only 350 years ago. Long Valley Caldera lies at the southern end of the string of craters, having erupted 600 $km^3$ of material 0.76 Ma ago, material which now forms the Bishop Tuff which can be identified over 2,000 km from the eruption. Long Valley Caldera continues to be active, with a resurgent dome, many earthquake swarms, and the release of considerable amounts of $CO_2$. These active volcanic systems are not only of geological interest, but pose a threat to the communities of Mammoth Lakes, Bishop, and Lee Vining. For these reasons the United States Geological Survey (USGS) has been collecting magnetotelluric (MT) sites in Long Valley and across the crater chain in order to image the magmatic and hydrothermal systems in this region (Peacock et al., 2015: Peacock et al., 2016). However, the 20×15 km area of Mono Lake is not accessible to routine MT data collection, and so Scripps Institution of Oceanography (SIO) and the USGS teamed up to collect data in the lake using a modified version of an ocean-bottom MT instrument.

## INSTRUMENTATION AND DATA COLLECTION

The ocean-bottom MT instrument described in Constable (2013) consists of a custom, low power, 8-channel, 24-bit logging system that uses a temperature compensated crystal oscillator for timing. The timing oscillator is set using GPS time on deployment, and on recovery drift is measured against GPS time: drift is typically about 1 ms/day. Elec-

tric fields are measured across silver-silver chloride electrodes and magnetic fields are measured using standard multi-turn induction coils with mu-metal cores. Both electric field and magnetometer amplifiers are transformer-coupled chopper amplifiers designed to exploit the low input impedance of electrodes in the marine environment, or to load the output of the induction coils to flatten the open-circuit resonant peak. Orientation on the seafloor is carried out using external compasses that measure pitch, roll, and heading.

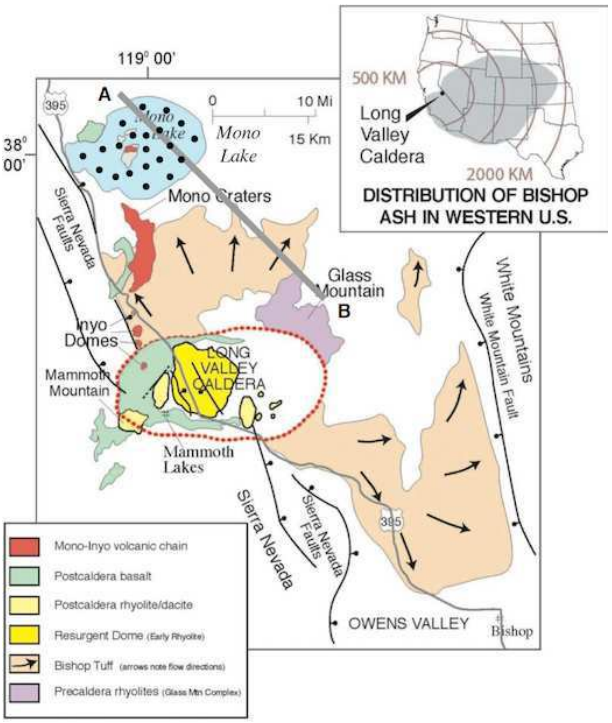


**Figure 1:** Simplified volcanic geology of Mono Basin and Long Valley Caldera, showing the extent of the Long Valley eruption. The approximate location of the lake-bed sites are shown as black dots, and location of the inversion transect shown in Figure 5 is given by **A-B**. Base figure from USGS via Wikipedia.

For the lake-bottom experiments, the deep-sea floatation was removed, along with the acoustic release mechanism. These were both replaced with 60 m of floating rope and a surface buoy to create a moored system that could be deployed and recovered by hand. (The maximum depth of Mono Lake is 48 m.) Motion of the surface buoy was decoupled from the instrument by attaching two 1.5 kg lead diving weights to the mooring rope about 2 m from the instrument. The 10 m electrode separation in the seafloor instrument was reduced to 3 m for the lake-bottom instrument to increase the ease of handling using small water craft. The seafloor instrument will record continuously for about 2 weeks from a pack of internal NiMH batteries, so the instruments could be moved from site to site without bringing them back to shore. The recording schedule of the external compass was modified to collect data every hour for the duration of the deployment, in order to record the changes in orientation when the instruments were moved. The instrument is shown in Figure 2.


**Figure 2:** Lake-bottom MT instrument, showing the various components. The electrodes, which need to be stored wet, have not yet been fitted.

In 2016, we deployed two prototypes of this instrument overnight in Mono Lake near the southern shore in order to test signal to noise ratios. The data were noisy but encouraging, given that the weather was poor (the lake was covered in whitecaps) and the deployment short. We reasoned that with more instruments, longer deployments, and better weather, the approach was viable, and so we returned in 2017 with seven instruments.

For initial deployment, the seven instruments were deployed by inflatable boat (Figure 3) across the lake. The instruments had been started the previous afternoon, and initial deployment only took half a day, taking two instruments out at a time in the boat. After two days, the instruments were recovered and moved to another location, one by one, which again only took half a day. The instruments

were moved for a second time, to occupy 21 sites in all. Finally on the sixth day, the instruments were recovered and the data were downloaded. Two remote reference sites had been installed, using EMI BF-4 magnetometers and the same seafloor data logger, one on the south shore of Mono Lake and one in a quiet location close to the town of Mammoth Lakes.

At seven locations around the lake a conductivity-temperature-depth (CTD) probe was lowered to record water conductivity. There was a thermocline at about 5 m depth, with water conductivity about 7.25 S/m at the surface and 5 S/m below 20 m depth. Water conductivity structure was used in the inversion described below.

**Figure 3:** Two instruments about to be deployed.

## DATA AND INVERSION

Data were processed using the multi-station code of Egbert (1997), which works very well for seafloor instrument arrays similar to the one used here, with the addition of one of the land references included. In spite of only a 3 m dipole, the electric channels were excellent, and the noise is dominated by motion of the instrument on the magnetic channels. For about half the sites this created noise in the responses at around 2 Hz (Figure 4), which is probably a strumming frequency of the instrument or the mooring. In the worst cases, usable data only extend to 200 s periods, but in many cases, such as the site shown in Figure 4, usable data were processed to 1,000 s periods or longer. Two sites had large tilts (of order 45°), probably as a result of deploying on the tufa pinnacles for which Mono Lake is famous, and had to be discarded.

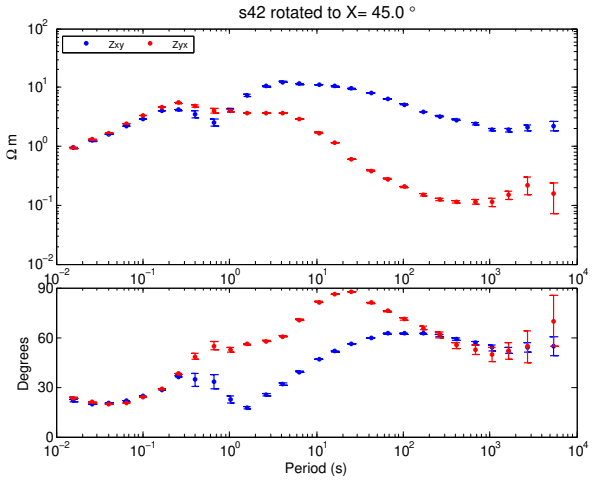


**Figure 4:** An example of the MT response functions from one site, better than average in terms of longest periods, worse than average in terms of motional noise around 2 Hz.

After inspecting polar plots, swift skew, and phase tensors, and considering the local geology, 9 lakebed sites and 13 land sites close to the line **A-B** shown in Figure 1 were rotated into the line and inverted with the MARE2DEM 2D inversion code of Key (2106). The result is shown in Figure 5. Data fit to RMS 1.4 with an error floor of 20%, with the TE resistivities excluded from the land stations to reduce the effects of 3D geology. A large conductor is evident, the top of which shallows to the north of Mono Lake to a depth of 3 km. The base of the conductor is around 25 km and the lowest resistivity about 0.3 $\Omega$m. This conductor is consistent in position, depth, and resistivity with conductor "C3" which appears at the edge of the 3D inversion of Peacock et al. (2015), but the new data show that this conductor extends past the northern edge of the lake and puts a much better constraint on its shallowest depth. The top of the conductor is too conductive and too shallow to be a magmatic system, and is similar to a conductive body seen beneath Long Val-

ley Caldera by Peacock et al. (2016), interpreted as a hydrothermal system. However, the Mono conductor extends to significantly greater depths, which may be a deep magmatic source for the recent volcanism in the area and the shallower hydrothermal systems.

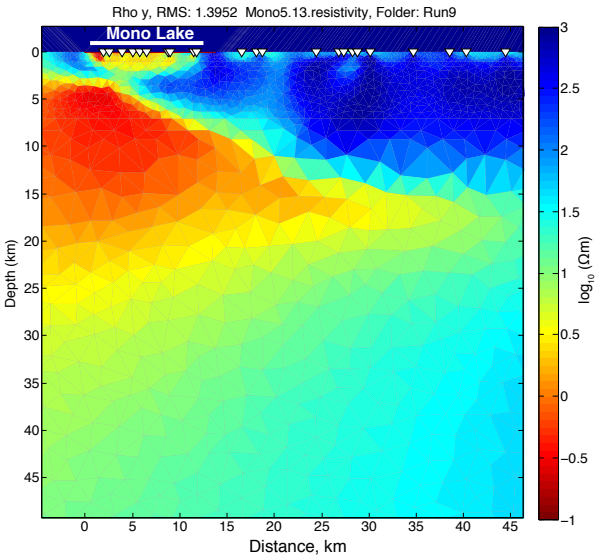


**Figure 5:** Inversion of land and lake-bed data from sites along the line **A-B** shown in Figure 1.

## CONCLUSIONS

Moored versions of the Scripps seafloor electromagnetic receiver provide an effective and efficient method of collecting MT data in shallow lakes. Here, 21 MT sites were collected with an expenditure of 4 half-days of work spread out over 6 days of elapsed time. Such productivity for land MT is difficult to achieve. Our data clearly show that a conductive system identified in earlier 3D land MT inversions extends to the north side of Mono Lake, and is shallower than previously identified. Future work will involve collecting more data on the north side of the lake along with 3D inversion of the data.

## ACKNOWLEDGMENTS

Many thanks to Tom Crowe, our boat provider and operator. Thanks to the USGS interns and the technicians and engineers from the SIO Marine EM Laboratory. Scripps costs for this project were provided by the Scripps Seafloor Electromagnetic Methods Consortium. As always, we thank Gary Egbert and Kerry Key for making their codes available.

## REFERENCES

Constable, S (2013) Review paper: Instrumentation for marine magnetotelluric and controlled source electromagnetic sounding. Geophysical Prospecting 61:505–532

Egbert, GD (1997) Robust multiple-station magnetotelluric data processing. Geophysical Journal International 130:475–496

Key, K (2016) MARE2DEM: a 2-D inversion code for controlled-source electromagnetic and magnetotelluric data. Geophysical Journal International 207:571–558

Peacock, JR, MT Mangan, D McPhee, and DA Ponce (2015) Imaging the magmatic system of Mono Basin, Californai, with magnetotellurics in three dimensions. Journal of Geophysical Research: Solid Earth 120:7273–7289

Peacock, JR, MT Mangan, D McPhee, and PE Wannamaker (2016) Three-dimensional electrical resistivity model of the hydrothermal system in Long Valley Caldera, California, from magnetotellurics. Geophysical Research Letters 43:7953–7962

**Figure 6:** Mono Lake

# MARTEMIS – A New EM Tool for the Detection of Buried Seafloor Massive Sulfides

S. Hölz[1], A. Haroon[1], K. Reeck[1] & M. Jegen[1]
[1] GEOMAR – Helmholtz Centre for Ocean Research Kiel, 24148, Germany (shoelz@geomar.de)

## SUMMARY

Past investigations of seafloor massive sulfides (SMS) focused on actively forming sites. New technologies are needed to explore for SMS deposits which have finished their active phase and are possibly covered by sediments or lava. For this purpose the new marine transient electromagnetic induction system MARTEMIS was developed by GEOMAR.

The system was used for investigations in the Tyrrhenian Sea (Palinuro Seamount) and at the Mid-Atlantic Ridge (TAG area) and proved to be suitable for operations at great water depths (~3600m) in steep and difficult terrain. Calibration measurements in the water column demonstrate that it is possible to acquire high quality data, which is fit to be evaluated in terms of inversions. However, these calibration measurements also demonstrated that great care has to be taken in the design of such an inductive coil system, because relatively small metal bodies may lead to significant static distortions in the measured transients.

Inversion results of data acquired at the Palinuro Seamount show a conductive layer in the vicinity of a previously drilled, buried SMS occurrence and serve as proof of principle of the system. Results also indicate that the conductive SMS unit is indeed a confined layer with limited thickness between 3 – 5m, which was not known from drilling. In a similar manner, results also hint at an unknown mineralization at depth in a second area of the Palinuro Seamount and also disclosed several mineralizations in the vicinity of the TAG area. The synopsis of results demonstrates that the MARTEMIS system is a suitable tool to find and characterize buried SMS occurrences, which are no longer associated to any hydrothermal activity.

**Keywords:** seafloor massive sulfides (SMS), transient electromagnetics (TEM), marine resources

## INTRODUCTION

At present, the investigation of seafloor massive sulfides (SMS) is strongly limited by the available technology to the detection of actively forming sites, since detection of SMS deposits mainly relies on plume detection of active hydrothermal venting in the water column and seafloor morphological observations. While these methods have proven to be valuable for active sites, they do not allow the detection of deposits which are no longer associated to any hydrothermal activity and are possibly covered by sediments or lava. Therefore, new technologies are necessary which allow for the detection of buried SMS, which are no longer connected to any hydrothermal activity.

In land-based exploration, it has been common practice for several decades to use electromagnetic methods to detect and characterize massive sulfide deposits. However, when turning to marine investigations only a few electromagnetic experiments have ever been conducted on SMS, e.g. by Cairns et al. (1997) on the TAG hydrothermal mound or by Kowalczyk (2008) on the Solwara SMS deposits. In Swidinsky et al. (2012) our workgroup has proposed to use the transient electromagnetic (TEM) method and demonstrated that the TEM method is in principle not only useful for the detection of a deposit under a sediment cover but can also yield valuable information about its depth and potentially also its thickness.

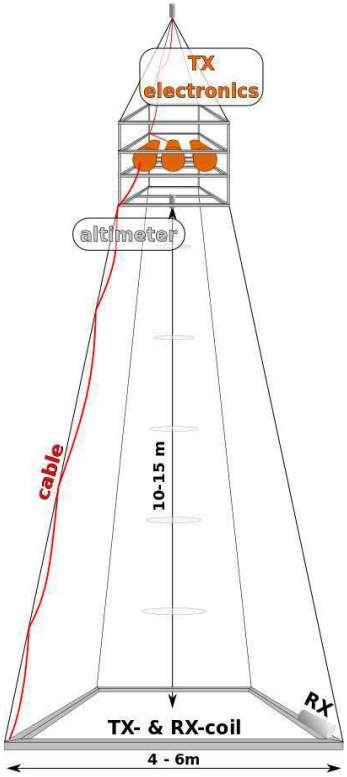


*Figure 1: Sketch of MARTEMIS coil system.*

Here, we will present results obtained with GEOMAR's new marine transient electromagnetic induction system (MARTEMIS), which were acquired over known and assumed SMS sites with no active hydrothermal activity.

## METHODS

The MARTEMIS system (Figure 1) is a coincident loop TEM system for the detection and characterization of conductive seafloor features like SMS. It is characterized by:

- adjustable coil size depending on size of A-frame (e.g. 4x4m$^2$ – 6x6m$^2$ ),
- transmitter currents up to 60A into one or two windings,
- operation of coil close to seafloor (2-10m),
- continuous measurement,
- operation at speeds up to 0.7kn.

The design of the system with a lower frame (holding the coincident transmitter and receiver coils) and an upper frame (holding the transmitter electronics and the altimeter) ensures that conductive metal parts (e.g. pressure housings) are at a sufficiently large distance to the sensor coils in order to minimize distortion effects.

The maximum operation depth of the system is mainly limited by the length of the ship's winch cable and the maximum depth rating of the pressure housings (currently 6000m).

Additional sensors can be mounted to the system, e.g. two extra pairs of electrodes to the coil frame to measure the ambient electrical field.

## EXPERIMENTS & RESULTS

### Palinuro Seamount

The Palinuro Seamount (Figure 2), which is located about 75km off the coast of Italy at a water depth of about 600m in the Tyrrhenian Sea, was the research target during two cruises (POS483, 2015; POS509, 2017; both R/V Poseidon). Previous investigations had found up to 5m of massive sulfides in drilling cores, partially under several meters of sedimentary cover, in a small area of about 45m x 27m (Petersen et al. 2014). Thus, the seamount was chosen as suitable target for testing the MARTEMIS system.

In 2015, TEM measurements with the MARTEMIS system showed anomalous responses (red circles in Figure 2, **A**) in the vicinity of the area where SMS had previously been recovered in drilling cores (black rectangle). Calibration measurements within the water column show that measured transients are only distorted at times earlier than ~1ms, but later times up to 20ms match the expected theoretical full space responses and are, thus, suitable for inversion (Hölz et al. 2015).

1D inversions of TEM data (Figure 3) were carried out and confirm the existence of a buried layer of conductive material (red, ~10S/m) in the vicinity of the previous drilling sites (**A**), which we interpret as SMS layer beneath sedimentary cover. Additionally, a conductive layer (**B**) was detected at greater depth (~15–20m), hinting at a so far unknown mineralization. At this depth the layer is at the detection limit of the system.

In 2017, follow-on investigations showed increased heatflow values and gravity cores containing sulfide rich sediments (sites **B** & **C**), which provided ground truthing and substantiate the interpretation of EM measurements (Hölz, 2017). An extended TEM data set with ~900 stations along ~9km of profile were also measured across the structure. Evaluation of this data set is still work in progress. First results of self-potential measurements and additional EM experiments were recently published and can be found in Safipour et al. (2017a, b; 2018).

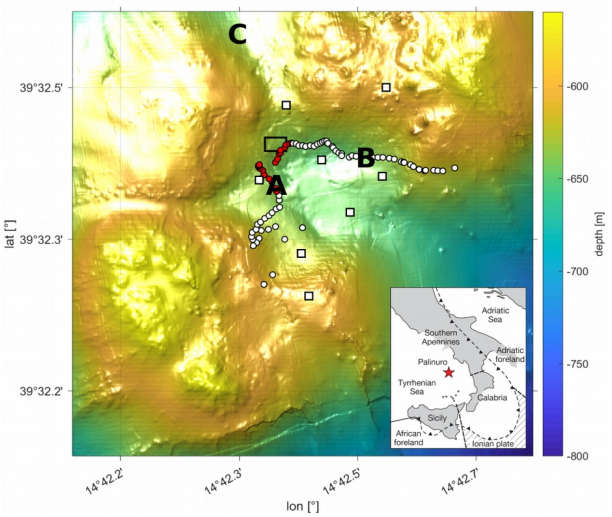


*Figure 2: Bathymetric map of Palinuro Seamount with area outlining locations with SMS recovery from drilling (black rectangle), 700m long profile line of MARTEMIS system (circles), stationary OBEM receivers (squares) and marked areas A - C with anomalous EM responses.*

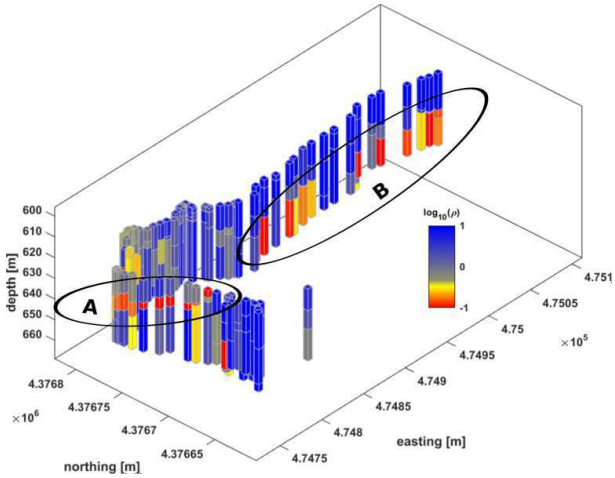


*Figure 3: 1D inversion results of TEM measurements, conductive features (ρ~0.1Ωm, red) are indicative of SMS occurrences.*

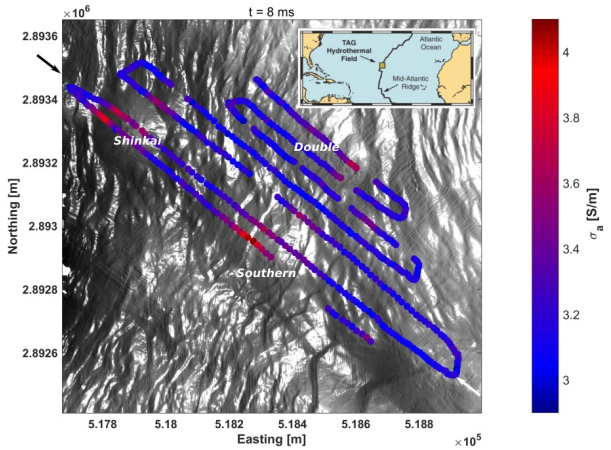


*Figure 4: Bathymetric map of working area 3-Mounds. Colored dots show apparent conductivity (Swidinsky & Weiss, 2017) along the track of the MARTEMIS system. Anomalies are evident in the region of the known mounds.*

### TAG Area

In 2016, regional scale experiments were carried out in the vicinity of the TAG (Trans-Atlantic Geotraverse) hydrothermal field during cruise JC138 (R/V James Cook).

One of the experiments was carried out along an 8km long profile line in the working area *3-Mounds* at a water depth of ~3600m (Figure 4). Calibration measurements in the water column revealed significant distortions, which were only recognized after the experiment. In subsequent testing the problem was traced back to additional weights, which had been attached onto the coil frame during this experiment. Theoretical considerations and modeling show that these distortions can be considered to be static (similar in Schamper et al. 2014) and that calibration measurements within the water column may be used to correct for the distortions.

Apparent conductivities show anomalous values in the vicinity of the three mound structures (Figure 4). 1D inversion results (Figure 5) along a selected profile show conductive features at the western flanks of Shinkai and Southern Mound. Laboratory investigations confirm that such high conductivities require the presence of high grade SMS (Spagnoli et al. 2016).

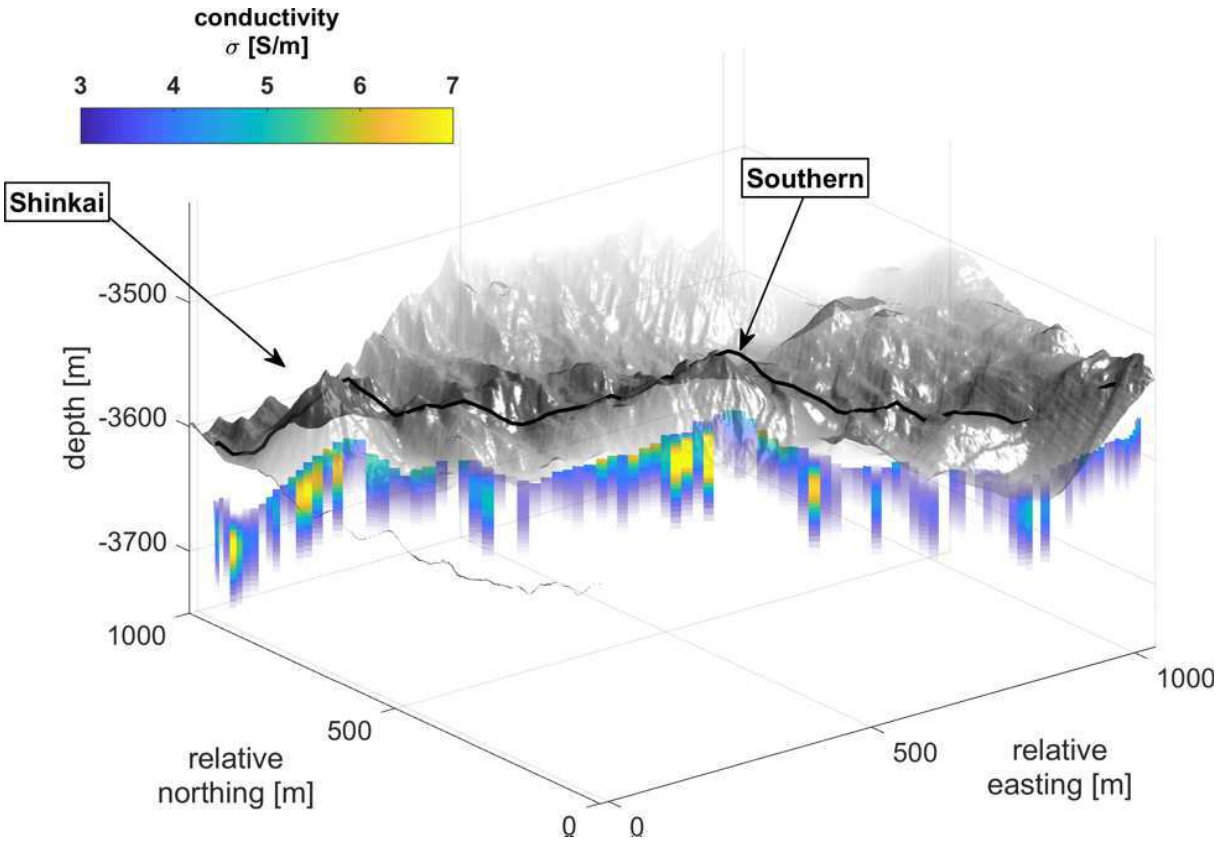


*Figure 5: 3D view of bathymetry with the track line of the MARTEMIS system (black line) and stitched 1D inversion results of TEM measurements (shifted down for better visibility) along profile 6 (marked by arrows in Figure 4). Conductive features (yellow) are evident on the western flanks of Shinkai and Southern Mound. Low conductivities (<3S/m) are blanked out because the system has no sensitivity to resistive features.*

## CONCLUSION

The MARTEMIS coil system designed at GEOMAR has been built as a tool for the investigation of sediment covered SMS, which are no longer connected to any hydrothermal activity, thus, being impossible to find with conventional detection methods. A first test of the system at the Palinuro Seamount in 2015 served as proof of principle and also demonstrated, that the system may not only be used for the detection of conductive anomalies, but may also yield information about the geometrical characteristics (e.g. thickness and depth of conductor).

Subsequent experiments with the system showed that it may also be used in difficult environments like the Mid-Atlantic Ridge, where water depth of around 3600m and Alpine like bathymetry poses severe challenges for the experimental design.

The evaluation of data has shown that calibration measurements in the water column are a viable asset for the later evaluation of data, since they can help to verify the correct functionality of the system or may help to identify and remove static distortion effects in the data.

## ACKNOWLEDGEMENTS

Work presented here received funding from the European Union (grant 604500 - Blue Mining).

## REFERENCES

Cairns, G, Evans, R & Edwards, RN (1996) A time domain electromagnetic survey of the TAG hydrothermal mound. Geophysical Research Letters, 23: 3455-3458.

Hölz S. (ed., 2017) RV POSEIDON Fahrtbericht / Cruise Report POS509 - ElectroPal 2: Geophysical investigations of sediment hosted massive sulfide deposits on the Palinuro Volcanic Complex in the Tyrrhenian Sea. GEOMAR Helmholtz-Zentrum für Ozeanforschung, Kiel, Germany, 63pp. DOI 10.3289/GEOMAR_REP_NS_39_2017

Hölz S, Jegen M, Petersen S & Hannington M (2015) How to Find Buried and Inactive Seafloor Massive Sulfides using TEM. Extended abstract to UMC Conference, Tampa Bay, Florida, USA.

Kowalczyk, P (2008) Geophysical prelude to first exploitation of submarine massive sulfides. First Break, 26: 99-106.

Petersen S, Monecke T, Westhues A., Hannington M, Gemmell JB, Sharpe R, Peters M, Strauss H, Lackschewitz K, Augustin N, Gibson H & Kleeberg R (2014) Drilling shallow-water massive sulfides at the Palinuro volcanic complex, Aeolian Island arc, Italy. Economic Geology: 109, 2129-2158.

Safipour R, Hölz S, Halbach J, Jegen M, Petersen S & Swidinsky A (2017a) A self-potential investigation of submarine massive sulfides: Palinuro volcanic complex, Tyrrhenian Sea. Geophysics, 82, A51-A56.

Safipour R, Hölz S, Jegen M & Swidinsky A (2017b) On electric fields produced by inductive sources on the seafloor. Geophysics, 82(6): E297-E313.

Safipour R, Hölz S, Jegen M & Swidinsky A (2018) A first application of a marine inductive source EM configuration with remote electric dipole receivers: Palinuro Seamount, Tyrrhenian Sea. Geophysical Prospecting, accepted. DOI 10.1111/1365-2478.12646.

Schamper S, Auken E. & Sørensen K (2014) Coil response inversion for very early time modelling of helicopter-borne time-domain electromagnetic data and mapping of near-surface geological layers. Geophysical Prospecting, 62: 658-674.

Spagnoli G, Hannington M, Bairlein K, Hördt A, Jegen M, Petersen S & Laurila T (2016) Electrical properties of seafllor massive sulfides. GeoMarLett, 36: 235 - 245.

Swidinsky A, Hölz S & Jegen M (2012) On mapping seafloor mineral deposits with central loop transient electromagnetics. Geophysics, 77: E171-E184.

Swidinsky A & Weiss C (2017) On coincident loop transient electromagnetic induction logging. Geophysics, 82 (4): E211-E220.

# Adapting Better Interpolation Methods to Model Amphibious MT Data Along the Cascadian Subduction Zone.

A. Blake Parris[1], C. Gary Egbert[2], C. Kerry Key[3] and C. Dean Livelybrooks[4]
[1]University of Oregon, blakeparris16@gmail.com
[2]Oregon State University, egbert@coas.oregonstate.edu
[3]Columbia University, kkey@ldeo.columbia.edu
[4] University of Oregon, dlivelyb@uoregon.edu

**SUMMARY**

The Magnetotelluric Observations of Cascadia using a Huge Array (MOCHA) experiment provides amphibious data useful for imaging subducted fluids from trench to mantle wedge corner. When using MOD3DEM(Egbert et al. 2012), a finite difference inversion package, we have encountered problems inverting, particularly, sea floor stations due to the strong, nearby conductivity gradients. As a work-around, we have found that denser, finer model grids and intermediary lower conductivity layers near the land-sea interface produce better inversions, as characterized by reduced data residuals. This is partly to be due to our ability to more accurately capture topography and bathymetry. We are experimenting with improved interpolation schemes that more accurately track EM fields across cell boundaries, with an eye to enhancing the accuracy of the simulated responses and, thus, inversion results.

We are adapting how MOD3DEM interpolates EM fields in two ways. The first seeks to improve how fields are interpolated across a conductive boundary by adapting Shantsev's(2014) extra interpolation term that corrects the discontinuity in the derivative of the electric field across the conductive boundary. Electric fields are interpolated using a tri-linear spline technique, where weights are determined for the eight nearest electrical field estimates creating a kind of weighted average for the field. We modify these weights to include a term that corresponds to the discontinuity in the derivative of the electric fields caused by large differences in conductivity at a boundary. This enhances the accuracy of the interpolated fields calculated by the forward solver.

In the second method we introduce a new planar geometry capable of tracking sloping conductivity interfaces, determined by bathymetry and topography, and within a normally rectilinear grid, and tested for now using a simplified Matlab version of the forward model routines of the Mod3DEM(Egbert 2011) inversion code. This new geometry allows us to more accurately model large conductivity-contrasting boundaries such as the land-sea interface or the air-land interface. We rotate into a coordinate system defined by the local, tilted plane using the singular value decomposition (SVD). The interpolation is done in this system, using the plane to more accurately define where the conductivity boundaries occur. We then use a QR decomposition to create coefficients that are used to interpolate the fields from a Yee grid to a station on the new interface.

Using both the adapted conductivity discontinuity term and the new planar interface we intend to more accurately estimate RMS misfits while inverting MT data, thus leading to more accurate conductivity models for Cascadia and other tectonic settings.

**Keywords:** Inversion, Interpolation, Cascadia, Mod3DEM

# Quantification and reduction of platform immanent bias factors on frequency and time domain coil data.

K. Reeck[1], H. Müller[2] and S. Hölz[3]
[1]Geomar Helmholtz Centre for Ocean Research, kreeck@geomar.de
[2]Federal Institute for Geosciences and Natural Resources
[3]Geomar Helmholtz Centre for Ocean Research

**SUMMARY**

Electromagnetic systems rely on the use of non-conductive materials in proximity of the sensor to minimize bias effects on their sensitivity and measured data. Additionally, for marine sensors used for deep sea surveys, rigidity, compactness and the handling of the platform is essential. Thus commonly a trade-off between rigid, cost-effective and non-conductive materials (e.g. stainless steel vs. fiberglass composites) has to be found. In case of the BGR's GOLDEN EYE frequency domain coil system (developed at the University of Bremen), the compact and rigid design is achieved by a circular fiberglass platform inhabiting several titanium pressure housings. Geomar's MARTEMIS time domain system trades the compact design for a clear separation of up to 15 m between an upper fiberglass frame, holding most critical titanium system components, and its coil and receivers.

For this study, an experimentally verified 3D finite element model was developed in COMSOL Multiphysics to analyze and quantify the static influence of conducting pressure housings on the sensitivity of a frequency and time domain coil system and the effectiveness of calibration procedures to minimize the distortions. In addition, we examine dynamic variations of the conductive components' positions relative to the sensor in field datasets and discuss their effect on the results.

The experiments do not only show the significance of the static bias on the inversion results, produced by high conducting components, but also the efficiency of a system calibration against the calculated response in a known environment. The remaining bias as a function of seafloor conductivity can be minimized by optimizing the dimensions and positioning of the titanium housings and thus reducing the influence on the inversion results. The dynamic variations due to system instabilities however lead to an unpredictable signal bias demanding a rigid structure, heave compensation mechanisms and a careful handling of the system.

**Keywords:** COMSOL, finite-element-modelling, controlled source electromagnetics, bias, calibration

# Reducing electromagnetic noise induced by short-period ocean waves in marine MT data sets using wavelet analysis

Baoqiang Zhang, Jianxin Pei
College of Marine Geosciences, Ocean University of China, Qingdao, Shandong, China, peijx@163.com

## SUMMARY

The marine magnetotelluric (MT) data may be distorted by the electromagnetic (EM) noise induced by short-period ocean waves across the Earth's magnetic field. In this presentation, we present a normalized evaluation system for selection of optimal mother wavelet, and a procedure for determining the highest level of wavelet decomposition and the target levels in wavelet domain is presented. The feasibility of the proposed method has been demonstrated on both the synthetic data and the measured marine MT data.

**Keywords:** Marine MT; EM noise; Ocean waves; Wavelet analysis; Optimal mother wavelet; De-noising

## INTRODUCTION

The induced electromagnetic (EM) signal by short-period ocean waves across the Earth's magnetic field is one of the main noise sources in the marine magnetotelluric (MT) data. Short-period ocean waves may generate magnetic field of several tens of nT and electric field of several tens μV/m. The frequency band of EM noise lie mainly in the range 0.05-0.5Hz. The electromagnetic noise should be removed from the observation during the data processing. In this paper, we propose a method for reducing the EM noise induced by the short-period surface waves based on the wavelet analysis. The feasibility of the proposed method has been demonstrated on both the synthetic data and the measured marine MT data.

## METHODOLOGY

Let $\psi(t)$ be the mother wavelet, an orthogonal wavelet basis can be constructed (Daubechies, 1990)

$$\psi_{a,b}(t) = \frac{1}{\sqrt{|a|}}\psi\left(\frac{t-b}{a}\right) \quad (1)$$

in which, $a \neq 0$, $b \in R$. $a$ is scale factor, and $b$ is a translation factor.
The discrete wavelet transform (DWT) and inverse transform are defined as

$$C_{j,k} = \sum_{t=-\infty}^{\infty} f(t)\psi_{j,k}^{*}(t) \quad (2)$$
$$f(t) = \sum_{-\infty}^{\infty}\sum_{-\infty}^{\infty} C_{j,k}\,\psi_{j,k}(t) \quad (3)$$

The selection of mother wavelet function as well as the decomposition level is a key factor in wavelet analysis. We combined 4 types of indexes, signal-to-noise ratio ($\mathrm{SNR}$), root mean square error ($\mathrm{RMSE}$), correlation coefficient ($\mathrm{R}$), and smoothness ($\mathrm{r}$) into a normalized evaluation system.

The EM noises are processed by using well-known 55 types of discrete mother wavelets, respectively. The $\mathrm{SNR_i}$, $\mathrm{RMSE_i}$, $\mathrm{R_i}$ and $\mathrm{r_i}$ related to the $\mathrm{i^{th}}$ mother wavelet are calculated. Then each type of indexes is normalized for eliminating the influence of dimension on different types of indexes, which makes 55 values of each type of index be within [0,1]. Thus, the best mother wavelet reaches 1 while the worst gets 0. The calculation formula for normalization are

$$p_{k1}(i) = \frac{k1(i) - \min(k1)}{\max(k1) - \min(k1)} \quad (3)$$
$$p_{k2}(i) = \frac{max(k2) - \mathrm{k2}(i)}{\max(k2) - \min(k2)} \quad (4)$$

where $\mathrm{k1}$ indicates $\mathrm{SNR}$ or $\mathrm{R}$, $\mathrm{k2}$ indicates $\mathrm{RMSE}$ or $\mathrm{r}$.
The normalized evaluation system of $\mathrm{i^{th}}$ mother wavelet is

$$p(i) = p_{SNR}(i) + p_{RMSE}(i) + p_R(i) + p_r(i) \quad (5)$$

Obviously, p is distributed in [0,4], and it means that larger the value of p, more effective the selected mother wavelet is. Note that the proposed method requires that pure signal is known. In practice, the mother wavelet selected through synthetic data is used for measured MT data processing.
Because wavelet analysis only deals with detailed coefficients after DWT and the induced noise of short-period ocean waves is a narrow-band spectrum in frequency domain, hence the wavelet decomposition scale is increased until the lowest frequency component of noise is decomposed into detailed coefficients of one or adjacent several levels. The level corresponding to the largest scale is defined as highest wavelet decomposition level, and the level of detailed coefficients that contain noise is considered as target level. The frequency band represented by approximate coefficients and detailed coefficients of each level after wavelet

decomposition is shown in Table 1. Assuming that the sampling frequency of signal is $f_s$ and frequency band of noise is $[f_l, f_h]$, which is known or estimated before the processing, and the target levels are distributed from level $J_{min}$ to $J_{max}$. It meets that $f_l$ is larger than $f_s/2^{J+1}$, namely lower boundary of frequency band is represented by detailed coefficients of highest level, thus

$$J = \text{ceil}[\log_2(f_s/f_l) - 1] \quad (6)$$

where ceil(.) is ceiling function to ensure $J$ is integer and noise is not leaked. The detailed coefficients of highest level contain the components of noise, thus $J_{max} = J$. Similarly, $f_h$ is smaller than $f_s/2^{J_{min}}$, namely upper boundary of frequency band represented by detailed coefficients of level $J_{min}$

$$J_{min} = \text{floor}[\log_2(f_s/f_h)] \quad (7)$$

where, floor(.) is floor function to ensure $J_{min}$ is integer.

**Table 1**. Frequency band represented by detailed and approximate coefficients of each level after wavelet multiscale decomposition

| level | approximate coefficients | detailed coefficients |
|---|---|---|
| 1 | $[0, f_s/2^2]$ | $[f_s/2^2, f_s/2^1]$ |
| 2 | $[0, f_s/2^3]$ | $[f_s/2^3, f_s/2^2]$ |
| ⋮ | ⋮ | ⋮ |
| $i$ | $[0, f_s/2^{i+1}]$ | $[f_s/2^{i+1}, f_s/2^i]$ |
| ⋮ | ⋮ | ⋮ |
| $J$ | $[0, f_s/2^{J+1}]$ | $[f_s/2^{J+1}, f_s/2^J]$ |

Assuming that the energy of the noise is compressed into a minority of small-amplitude detailed coefficients and conversely a large amount of large-amplitude detailed coefficients represents the useful signals. The detailed coefficients below determined threshold value are abandoned, downweighted or retained by using a designed shrinkage function, thus the noise is eliminated and main features of the useful signal are preserved. The de-noised signal can be reconstructed by inverse DWT with approximate coefficients at highest level $J$ and detailed coefficients at all levels including the modified detailed coefficients at target levels.

The effectiveness of denoise processing also relies on the threshold algorithm and shrinkage function. Heursure algorithm (A. K. Verma and N. Verma, 2012) and an improved compromise function between soft and hard shrinkage (Xu et al., 2004) are used to deal with target levels.

## SYNTHETICAL DATA

We simulate a set of time series of magnetic noise induced by short-period ocean waves and then add that to a simulated set of pure time series of marine MT signals. The sampling frequency is 10Hz and the length of time series is 10min. The parameters of the 1-D marine model are shown in Figure 1.

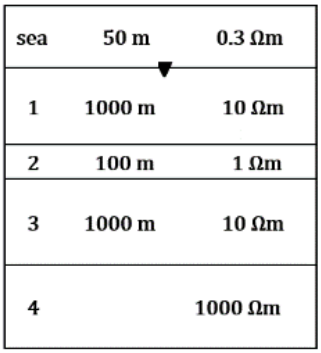


**Figure 1**. 1-D marine model

Figure 2 shows the time series and amplitude spectrum of simulated pure magnetic signal and the signals before and after de-noising. Noise spreads out in entire time interval of magnetic signal and presents a feature of short-period and quasi-sinusoidal, but lies in a narrow band of 0.08-0.16Hz. The magnetic field increases by 1-2 orders of magnitude and the SNR decreases to 1.3904.

Both the highest decomposition level and target level are 6. After decomposition and processing using Dmey wavelet, noise in time domain disappears and the de-noised signal is extremely closer to pure signal. Note that the method can preserve the original features of marine MT data at the specific frequency band and leave noise free data sections unchanged in frequency domain (Figure 2).

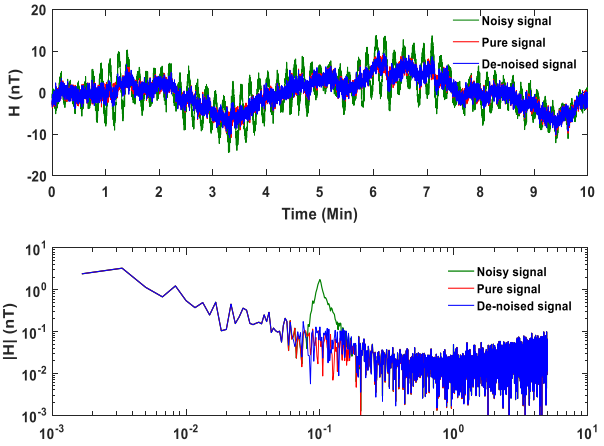


**Figure 2.** Time series and amplitude spectrum of simulated pure signal and the signals before and after de-noising

Figure 3 shows the apparent resistivity and phase obtained by the simulated data without noise and with noise as well as after de-noising. Apparent resistivity for polluted data reduces by several orders of magnitude and phase is wildly oscillatory nearby the theoretical values at frequency band of 0.08-0.16Hz. After removal of noise with the proposed method, apparent resistivity appears reasonably and anomalous singularly low-resistivity is effectively eliminated. Apparent resistivity for de-noised data is closer to that for the noise free data.

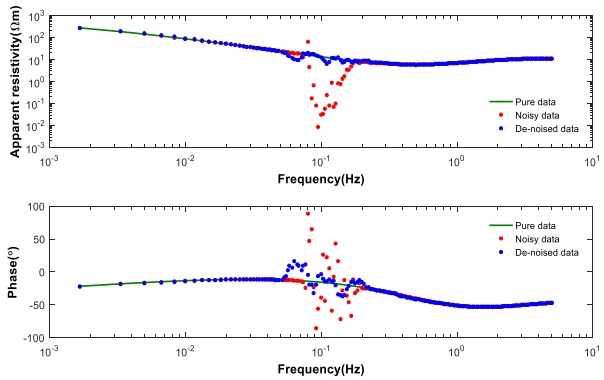


**Figure 3.** Apparent resistivity and phase for simulated data without noise and with noise as well as after de-noising.

## MEASURED DATA

The removal procedure has been applied to process marine MT data observed in China Yellow Sea. The sampling frequency is 10Hz. The seawater is about 20m. The time series and amplitude spectrum of horizontal components are shown in Figure 4 and Figure 5. One can see that in both the time and frequency domains the magnetic field is obviously polluted and strong short period disturbances appear. The power spectrum shows a sharp peak around 7s, which corresponds closely to the period of short-period ocean waves in China Yellow Sea in summer (Chen et al., 2006). The spectral peak is considered to be caused by the short-period ocean waves.

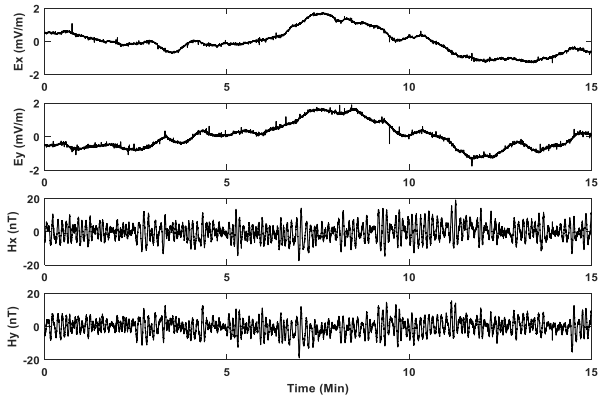


**Figure 4.** The time series of horizontal components of measured marine MT data.

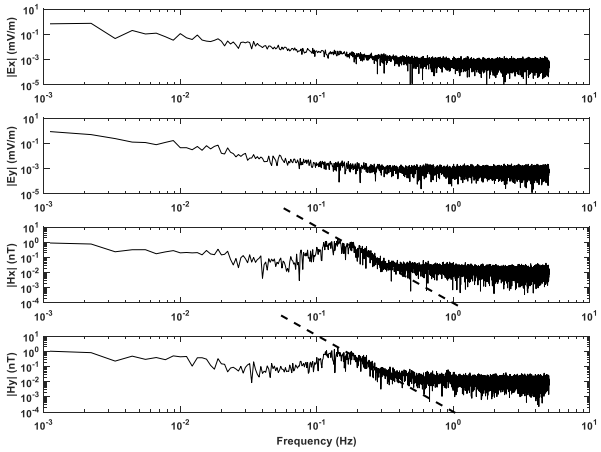


**Figure 5.** The amplitude spectrum of horizontal components of measured marine MT data

The highest decomposition level is 6 and target levels are level 5 and level 6. Both Hx and Hy are decomposed and processed by using Dmey wavelet. From Figure 6, one can see that the short period noise is obviously removed. Both Hx and Hy become stable, and the propsed method may preserve the features of marine MT data at the specific frequency band of noise-related and leave noise free data sections unchanged in frequency domain.

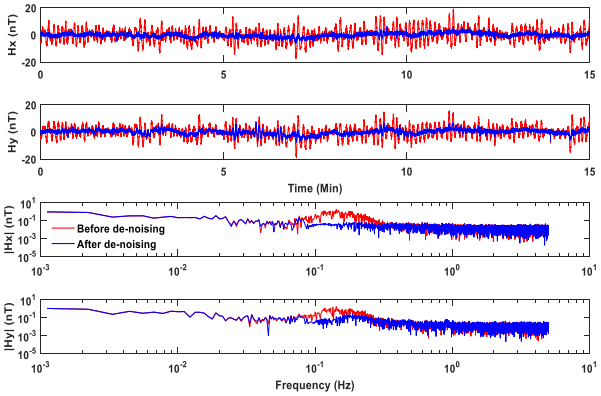


**Figure 6.** Time series and amplitude spectrum of measured Hx and Hy before and after de-noising.

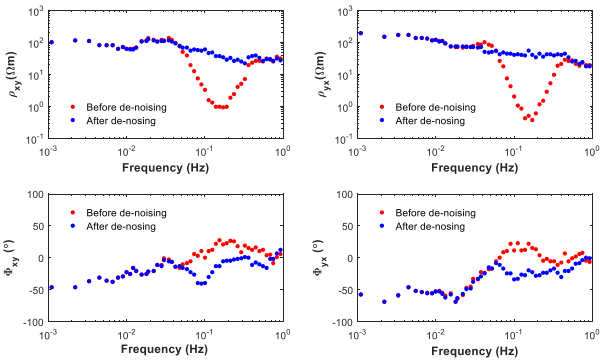


**Figure 7.** Apparent resistivity and phase for measured marine MT data before and after noise removal.

Figure 7 shows apparent resistivity and phase obtained by using both the measured data and de-nosing p data.

## Conclusions

The induced EM noise due to short-period ocean waves spreads out in entire time interval of marine MT and has a feature of short-period and quasi-sine and a narrower-band in frequency domain. The apparent resistivity may reduce by several orders of magnitude, causing an unreasonably low resistivity and phase is wildly oscillated.

After applying the proposed wavelet analysis method and procedure wavelet analysis, EM noise may be removed and reasonable results obtained. The noise is decomposed into the detailed coefficients of a certain level or adjacent several levels without redundant decomposition and the target levels can be accurately located by the proposed method. The method can preserve the original features of marine MT data at the specific frequency band of noise-related and leave noise free data sections unchanged in frequency domain.

## Acknowledgements

The work was funded by the National Natural Science Foundation of China (41130420 and 41174091) and the National Major Project of China (2011ZX05008-006-30).

## References

Chen, H., Hua, F., Yuan, Y., (2006). Seasonal characteristics and temporal variations of ocean wave in the Chinese offshore waters and adjacent sea areas. Advances in Marine Science, 24(4), 407–415. (in Chinese)

Daubechies I., (1990). The wavelet transform, time-frequency localization and signal analysis. IEEE Transactions on Information Theory. 36(5), 961-1005.

Lilley, F. E. M., Hitchman, A. P., Milligan, P. R., et al., (2004). Sea-surface observations of the magnetic signals of ocean swells. Geophysical Journal International. 159(2), 565-572.

Phillips, O.M., (1977). The dynamics of the upper ocean. Cambridge Univ. Press, Cambridge.

Verma, N., Verma, A. K., (2012). Performance analysis of wavelet thresholding methods in denoising of audio signals of some indian musical instruments. International Journal of Engineering Science & Technology. 4(5), pp. 2047–2052.

Xu, C., Zhao, R., Gan, B., (2004). Wavelet Analysis and its Application. Science Press, Beijing. pp.108-111. (in Chinese).

Ye, A., Li, F., (1992). Physical Oceanography. Qingdao Ocean University Press, Qingdao. pp. 334-448. (in Chinese)

# Removing orientation dependence and galvanic distortions in marine MT data by the quadratic equation: application to data from Gulf of California, México

A. Montiel-Álvarez[1], J.M. Romo[1], E. Gómez-Treviño[1] and S. Constable[2]

[1] Ciencias de la Tierra, CICESE, Ensenada, B.C., México;
montiel.aideliz@gmail.com; jromo@cicese.mx; egomez@cicese.mx
[2] Scripps Institution of Oceanography, La Jolla, California, USA; sconstable@ucsd.edu

**SUMMARY**

In marine magnetotelluric surveys, it is not possible to orient the measurement instruments as it is usually done in land surveys. To know the orientation, the ocean-bottom instruments have compasses that sometimes do not work correctly or are affected by interference due to induction coils or batteries. A wrong orientation of the measurements can seriously mislead the interpretation, so the application of alternative processing methodologies is needed.

One of the main lines of research in magnetotellurics has been to develop methodologies to remove the dependence of strike and the effect of other galvanic distortions. One of those methodologies is the invariant solution of a quadratic equation, which provides two complex resistivities that probe to be independent of strike and twist.

Here we present a comparison between the conventional response estimation and the solution of the quadratic equation to marine MT data. We show the effectiveness of this methodology and the additional advantages of applying it to marine MT data.

The data set was acquired as part of a marine geothermal exploration project in the central part of the Gulf of California, México, a zone with aligned submarine volcanic mounts. We present the final resistivity models, where a clear lateral contrast in resistivity may indicate a limit between oceanic and thinned continental crust.

**Keywords:** Marine magnetotellurics, strike dependence, galvanic distortions, geothermal exploration.

# Study on Gas Hydrate Targets in the Danube Delta with the Sputnik Controlled-Source Electromagnetic System

Shuangmin Duan[1], Sebastian Hölz[1] and Marion Jegen[1]
[1]Geomar, Wischhofstrasse 1-3, 24148, Germany. sduan@geomar.de

**SUMMARY**

A marine controlled source electromagnetic (CSEM) experiment was conducted over gas hydrate targets in the Danube Delta off the coasts of Bulgaria and Romania in early 2014 during cruise (MSM35 on R/V Maria S. MERIAN, part of the German SUGAR Project) was aimed to study submarine gas hydrates as a source of methane and possible sink for CO2 sequestration. Two working areas in water depths of ~1500m and ~600m were studied. Multiple BSRs and velocity anomaly are observed in both work areas, which may indicate the presence of gas hydrate or free gas. In work area 1, 12 receiver (RX) stations were positioned along two parallel, NE -SW striking profiles consisting of six stations each and with spacing between stations of about 300 m and a separation of the two profiles of about 500 m. Transmissions with the Sputnik transmitter (TX) system, which has two perpendicular horizontal TX polarizations, were then conducted at 81 different locations along three profiles with lengths between 2.5-3km each. A similar experiment with 11 RXs and 49 TXs was carried out in work area 2.

The acquired data were first processed to yield transient rotational invariants for each RX-TX pair. The transients were then inverted in terms of 1D inversion and 1D common-mid point (CMP) inversions. In work area 1, the inversion result show the resistivity anomaly at a depth of ~70m (Sugar channel) and ~250m (above BSR). In work area 2, resistivity increase at depth ~50m and deeper is observed from the inversion result. Comparison between the resistivity model and seismic data shows good consistence. Since low pore-water salinities are not sufficient to explain the high resistivities, high saturations of gas or gas hydrates are the likely cause. Based on the drilling holes and using the Archie's Law, we make gas hydrate saturation estimates for work area 1, which may give a better understanding and provide suggestions for the gas hydrate distribution and concentration.

**Keywords:** CSEM, gas hydrate, rotation invariants

Title: Studying offshore geothermal prospects using MT and CSEM methods

During the last few decades EM methods have been extensively used for detecting geothermal resources in terrestrial environments. However, a considerable number of potential geothermal prospects can be extended offshore, given that high heat flow values are found along plate tectonic boundaries and hot spots. Mexico has great potential for exploiting this clean and renewable resource, and for this reason an intensive study to assess potential geothermal resources in the Wagner Basin of the Northern Gulf of California was conducted combining EM and heat flow measurements. Our study employed three different EM approaches: MT, seafloor CSEM, and the recently developed surface-towed transmitter and receiver system called Porpoise CSEM that had been previously used to map Artic permafrost. The results obtained show low resistivity areas where there are known faults, in particular the two principal faults controlling the subsidence of the basin. Furthermore, the high heat flow measurements also correlate with low resistivity values, which expand the area where high heat flow anomalies might be found. Combining different EM techniques allow us to better constrain the electrical properties and helped us identify possible offshore geothermal targets in the Northern Gulf of California.

# Technology of marine magnetotelluric sounding in transition zone

D. Epishkin[1], A. Yakovlev[1,2] and D. Yakovlev[1]
[1]Nord-West Ltd
[2]Moscow State University

**SUMMARY**

A new technology of marine magnetotelluric sounding has been developed. This technology provides an opportunity to do exploration at shallow depth in transition zone of sea and ocean. To do investigation by this technology we need to measure only one of two components of horizontal electric field vector. Measurement of magnetic field must be performed within the investigation area and simultaneously on the shore. Acquisition tests at shallow depth have shown efficiency of the proposed technology.

**Keywords:** magnetotelluric, marine geophysics

## INTRODUCTION

At the moment there are quite a lot of successful examples of marine magnetotelluric (MT) investigations in the deep ocean (the depth of the sea reached hundreds of meters or even kilometers) (Constable et al., 1998). However, we can study only large regional structures in this case. Due to the fact electromagnetic field in the water column decay fast at the high frequencies we are becoming unable to investigate the upper part of a geological cross-section.

From this perspective, MT sounding at shallow sea has the advantage of a wider level of available information. With a decrease in the thickness of the water layer, it becomes possible to study smaller depths. For example, in case of performing MT sounding at a shallow depth (about 10-50 meters) we can study the near-surface geological structures (first tens of meters) so it is possible to carry out engineering studies. Regardless, MT sounding in the transit zone of the seas and oceans has not yet been widely spread due to difficulties encountered during its implementation. There are 1) high level of noise from surface waves of the sea and 2) low productivity of existing technologies. Widely employed technique of marine magnetotellurics is designed for working in deep sea environment and is not oriented for shallow marine investigations. Furthermore, the deep sea MT receivers are heavy and very expensive.

Earlier some attempts were made to carry out MT soundings in shallow water. The article (Ueda et al., 2014), for example, gives a description of a such survey. … But noise level for measurement at shallow depths (about 10 meters) was strong enough to damage the impedance estimates.

In an attempt to overcome the aforementioned difficulties, we are proposing a new technology to perform MT soundings at shallow depth of the sea.

## PROPOSED TECHNOLOGY

The proposed technology has the following features (fig. 1, 2):

- Only one of two components of the horizontal electric field is measured ($E_x$). In this case some information is lost, but it becomes easy to lay out long measuring electric dipoles, so the level of signal is increased. Also the productivity of the work is increased significantly;
- Length of measuring lines is about 100 meters;
- Measurements are made with a small step (from 100 to 300 meters);
- Measuring equipment are combined into a single continuous line, which reaches 1 kilometer or more. Equipment is laid out on the seabed by unfolding from vessel moving along the profile;
- The magnetic field is measured simultaneously at several points on the sea bottom (near the electric lines) and additionally on the land near the survey area. Records of magnetic field on the sea bottom are used to calculate impedances, then overland records let us separate the signal from the noise by remote reference technic (Gamble, 1979);
- Both on land and at sea, two horizontal components of the magnetic field are measured ($H_x$, $H_y$);

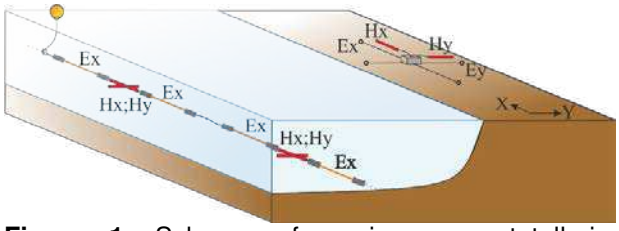


**Figure 1.** Scheme of marine magnetotelluric sounding in transition zone

**Figure 2.** Nord-West experimental marine MT equipment on the ship deck

**Testing**

To understand the possibilities and limitations of proposing technology, experimental and methodical investigations were performed at Black sea in April - June 2017 (fig. 3). The aim of these works was testing of measuring equipment, development of low noise sensors, development of shipboard launching / lifting operations.


**Figure 3.** Area of experimental measurements at Black sea

The measurements were carried out in the sea at a small distance from the shore (up to 5 kilometers). The depth of the sea in the work area varied from 10 to 25 meters. Remote reference site was installed on land near the work area (15 kilometers).

Experimental works at Black sea showed that it is possible to obtain reliable marine data at shallow depths. For example, figure 4 gives a comparison of typical coherences between orthogonal components of electric and magnetic fields for measurements in the sea and on the land. Values close to one indicates high data quality. Decrease in coherence tell us about low signal / noise ratio. It is obvious that the quality of the marine data is comparable to the quality of the ground data in almost the entire considered frequency range. Only at high frequencies (from 10 to 300 Hz) coherency level of marine data slightly less than on shore.

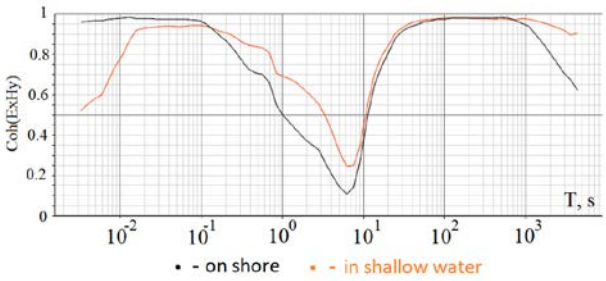


**Figure 4.** Coherence between orthogonal components of electric and magnetic field. Black line – land measurements; red line - marine measurement

Figure 5 shows the comparison of apparent resistivity curves in the sea and on shore. As we see, quality is very similar in the entire frequency range despite the differences in the coherence level.

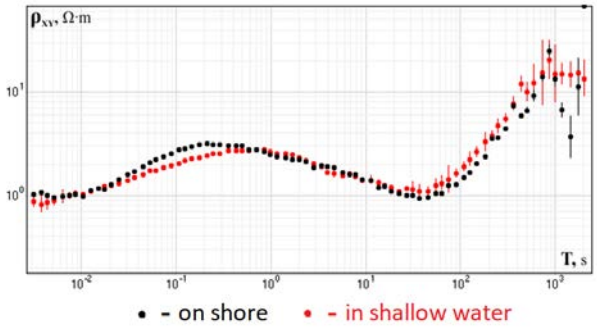


**Figure 5.** Typical apparent resistivity curves. Black dots – land measurement; Red dots – marine measurement

**"Belyi island" survey**

In the summer 2017 a full-scale marine MT survey was successfully performed in Kara Sea (Russia). Work area was located 20 kilometers to the north-west from the Yamal peninsula. The depth of the

sea in this region was 10 – 20 meters. The remote reference site was situated on the island Belyi (the northern end of the Yamal peninsula). It was carried out 240 successful measurements in total.

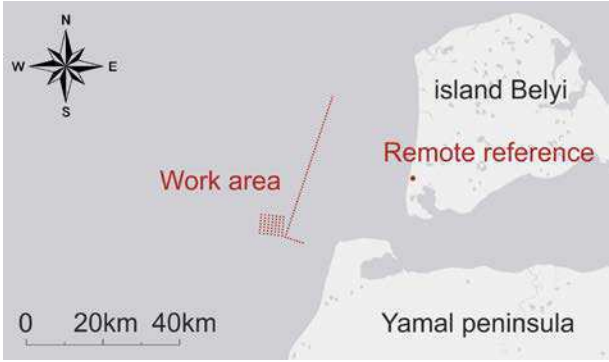


**Figure 6.** A map showing the project points of the survey in relation to the Yamal peninsula and Beliy island

Under favorable weather conditions, it was possible to obtain high-quality data. The figure 7 shows one of such curves carried out in the absence of sea disturbance

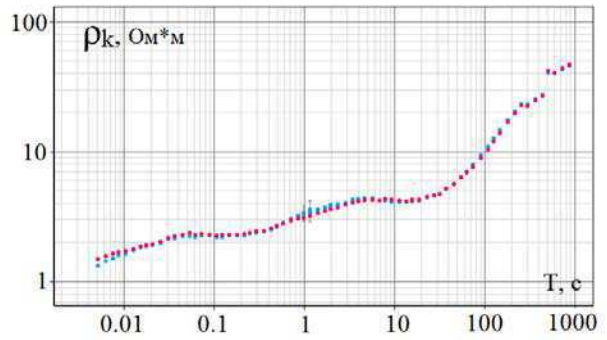


**Figure 7.** Example of apparent resistivity curve carried out at the bottom of Kara sea near the Yamal peninsula

**Data processing algorithms**

To process data, we used EPI-KIT software (Epishkin, 2016). However, we took into account that processing of marine data obtained by the considered technology has number of features.

Since we measure only one of two horizontal electric components ($E_x$), it is possible to estimate only two impedance tensor elements from equation below:

$$E_x = H_x \boldsymbol{Z_{xx}} + H_y \boldsymbol{Z_{xy}}$$

To improve the quality of these estimations we use a number of robust statistical procedures such as M-estimation, coherency threshold etc. and remote reference method (Egbert G, Livelybrooks D, 1996).

The accurate positioning of magnetic coils on the sea floor turned out to be practically impossible, hence the actual azimuth direction of the recorded magnetic field component should be also measured and taken into account in the data processing algorithm.

If such information is not available, then it is necessary to calculate sensor orientation in some way. For example, in “Belyi island” survey according to a priori information we assume that resistivity structures are 1-D, so it is appropriate to use the maximum coherency criterion to estimate the rotation angle for magnetic field. We need to find rotation angle $\alpha$ with maximum coherency between $E_x$ and rotated $H_y(\alpha)$:

$$Coh^2\left(E_x H_y(\alpha)\right) = \frac{\left|\overline{E_x {H_y}^*(\alpha)}\right|^2}{\left|\overline{E_x E_x^*}\right| \ \left|\overline{H_y(\alpha) H_y(\alpha)^*}\right|}$$

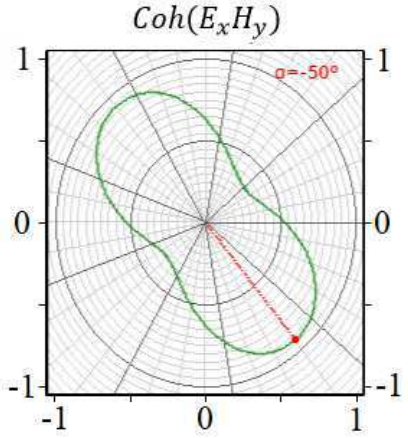


**Figure 8.** Polar diagram showing the coherence level between components $E_x$ and $H_y$ for different rotation angles of horizontal magnetic vector. For this example maximum coherency is observed at the rotation angle $\alpha$ of -50 degrees

Exact time synchronization between recording MT units is necessary for good data quality and is commonly secured by using temperature-compensated crystal oscillators coupled with GPS receiving systems, which applicability in marine environment is rather limited. The absence of GPS signal leads to noticeable desynchronization during the several hours of MT record. Figure 9 shows time dependence of phase characteristic at frequency 300 Hz during the record. We corrected the time series according to the speed of phase shift at high frequencies (fig. 10).

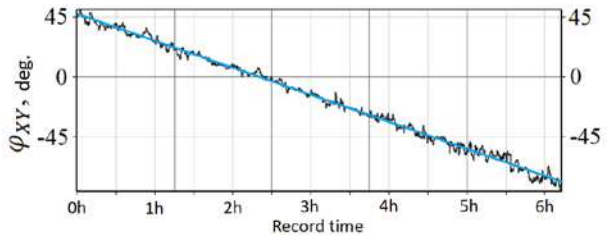


Figure 9. Phase shift on high frequency (300 Hz) during the record time caused by absence of GPS signal. A linear shift is observed

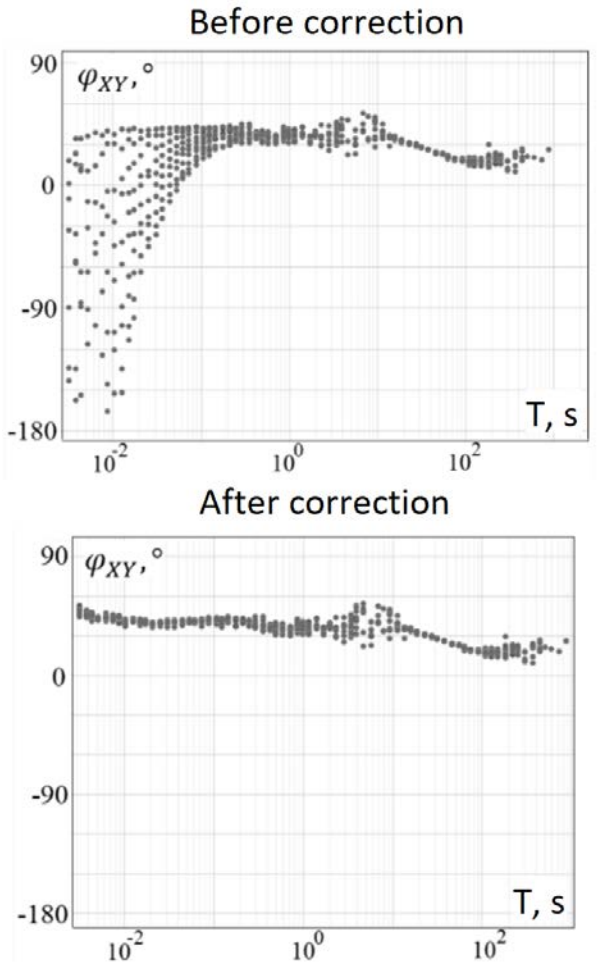


Figure 10. Phase curves before and after correction. Observed data was divided into 10 independent fragments.

## CONCLUSIONS

The new technology of marine shallow magnetotelluric sounding was proposed: the corresponding equipment, processing algorithms, operating procedures were developed.

The following tasks were solved:

- Increasing level of the signal and lessening step along the profile through the usage of cabled system
- EM modeling and determination of the possibility of a one-dimensional interpretation of the obtained resistivity curves
- Estimation of azimuth of electrical lines and orientation of magnetic sensors
- Correction of EM time series due to loss of synchronization between recording MT units during the record

The technology was tested and first results were obtained.

## REFERENCES

Constable S, Orange A, Hoversen M, Morrison F (1998) Marine magnetotellurics for petroleum exploration. Geophysics 63: 816-825

Egbert G, Livelybrooks D (1996) Single station magnetotelluric impedance estimation: coherency weighting and the regression M-estimate. Geophysics 61: 964-970

Epishkin DV (2016) Improving magnetotelluric data-processing methods. Moscow University Geology Bulletin 71: 347-354

Gamble TD, Goubau WM, Clarke J (1979) Magnetotellurics with a remote magnetic reference. Geophysics 44: 53-68

Ueda T, Mitsuhata Y, Uchida T, Marui A, Ohsawa K (2014) A new marine magnetotelluric measurement system in a shallow-water environment for hydrological study. J.Appl.G 100: 23-31

# Unextractable partial melt in the oceanic asthenosphere: Evidence from new geophysical constraints

Kate Selway[1] and J. P. O'Donnell[2]
[1]Department of Earth and Planetary Sciences, Macquarie University, Sydney, kate.selway@mq.edu.au
[2]Institute of Geophysics and Tectonics, University of Leeds, j.p.odonnell@leeds.ac.uk

**SUMMARY**

For decades, a debate has been active over whether the seismic low velocity zone (LVZ) in the oceanic asthenosphere is due to a small amount of partial melt or high hydrogen contents. MT models of old, stable oceanic asthenosphere can also generally be interpreted in terms of either elevated peridotite hydrogen contents or a small amount of partial melt. New experimental data have greatly improved constraints on seismic attenuation, showing that attenuation is not affected by hydrogen but is strongly affected by oxygen fugacity and grain size. Experimental data have also improved estimates of the effect of small amounts of partial melt on seismic and electrical properties. We combine these experimental constraints with seismic and MT data from the stable oceanic asthenosphere. Results show that the seismic LVZ cannot be caused by high hydrogen contents but is likely to be caused by a small (~0.1%) volume of partial melt. If corresponding peridotite hydrogen contents are moderate (~100 ppm), this volume of partial melt is consistent with the MT data. In the deeper asthenosphere, seismic velocities increase, becoming faster than those predicted from the experimental data, but electrical resistivities continue to decrease, consistent with increasing melt or hydrogen contents. We explain these observations with a model whereby melting at mid-ocean ridges extends to approximately the base of the LVZ (~200 km), reducing the hydrogen content of the asthenosphere to this depth. While most of the melt is extracted at the ridge, a small fraction (0.1%) is unextractable and is carried with the asthenosphere as it convects away from the ridge. At greater depths, the unmelted peridotite retains a higher hydrogen content, explaining the low electrical resistivities. The high seismic velocities at these depths are likely caused by low seismic attenuation due to low oxygen fugacities and large grain sizes.

**Keywords:** Asthenosphere, partial melt, hydrogen, low-velocity zone

# Using marine controlled-source electromagnetics to study potential offshore groundwater: Canterbury Basin, New Zealand

Zahra Faghih[1], Bradley A. Weymer[1], Marion Jegen-Kulcsar[1], Shuangmin Duan[1], Amir Haroon[1], Sebastian Hölz[1], Katrin Schwalenberg[2], Aaron Micallef [3], Joshu Mountjoy[4], Susanne Woelz[4]

[1]GEOMAR – Helmholtz Centre for Ocean Research Kiel, 24148, Germany, zfaghih@gmail.com, bweymer@geomar.de, mjegen@geomar.de, sduan@geomar.de, aharoon@geomar.de, shoelz@geomar.de,
[2]Bundesanstalt für Geowissenschaften und Rohstoffe (BGR), 30655, Hannover, Germany, Katrin.Schwalenberg@bgr.de
[3]Marine Geology & Seafloor Surveying, Department of Geosciences, University of Malta, 2080, Malta, aaron.micallef@um.edu.mt
[4]National Institute of Water and Atmospheric Research Ltd, Private Bag 14901, Wellington, New Zealand, Joshu.Mountjoy@niwa.co.nz, susi.woelz@niwa.co.nz

**SUMMARY**

Continental shelves are the submarine edges of the continental crust and in some areas have been shown to contain freshwater aquifers beneath the seafloor. During the Quaternary, continental shelves experienced maximum exposure to meteoric water during the Last Glacial Maximum. Offshore groundwater systems are slowly adjusting toward a new equilibrium in present-day conditions as a result of rising sea-level. Information regarding the location, characteristics and dynamics of offshore groundwater systems and whether they can be used sustainably as a potential source of drinking water may be obtained by applying a range of geophysical techniques including marine controlled-source electromagnetics (CSEM) and multichannel seismics. However, the methods applied to map the extent, volume and connectivity of offshore aquifers are still in the experimental phase. One promising geophysical tool to study offshore groundwater is the CSEM method. CSEM is capable of mapping the spatial variations of saline and fresh water zones in the sub-seafloor. Currently, there are only a few studies that have successfully applied marine CSEM to quantify offshore groundwater aquifers. This study constitutes a new attempt in using CSEM to detect the offshore groundwater at large spatial scales (around 100 km).

Here we show selected results from a 300 km long CSEM line survey carried out in the Canterbury Basin along a siliclastic passive continental margin, offshore the South Island of New Zealand. The study area contains one of the farthest offshore groundwater reservoirs and was investigated during IODP Expedition 317, which provided complementary data from cores, borehole logs and geochemical pore water analyses. CSEM data were collected along 7 profiles during 9 deployments using a seafloor-towed CSEM system. Four survey lines were acquired close to IODP site U1353, an area where the inferred low-salinity zone is located at a depth of approximately 50 m beneath the seafloor. Three additional survey lines were collected outside of the region to determine the lateral extent of the groundwater aquifer(s).

Processing and inversion results of two CSEM lines are selected to examine the capability of the CSEM technique to map offshore groundwater aquifers. One line crosses U1353, and the other is shifted around 50 m NE from the IODP site U1353. 1D inversion results and 2D resistivity sections show a shallow resistive anomaly in the upper 100 meters, which is interpreted as the shallow aquifer in accordance with IODP borehole data. Comparison between IODP borehole data and the CSEM lines point towards the presence of a shallow aquifer within 100 m depth beneath the seafloor. We also show a compression of the CSEM lines with concurrent seismic lines which were acquired during the same cruise and discuss how seismic and CSEM data can best be combined for a refined data interpretation with regard to aquifer characterization.

**Keywords:** Marine CSEM, offshore groundwater, Canterbury Basin

# Volcanic activity of Nishinoshima volcano in Izu-Bonin arc estimated by VTM and OBEMs observation

N. Tada[1], K. Baba[2], Y. Hamano[3], H. Ichihara[4], H. Sugioka[5], T. Koyama[6] and M. Takeo[7]

[1]Japan Agency for Marine-Earth Science and Technology, norikot@jamstec.go.jp
[2]Earthquake Research Institute, The University of Tokyo, kbaba@eri.u-tokyo.ac.jp
[3]Japan Agency for Marine-Earth Science and Technology, hamano@jamstec.go.jp
[4]Earthquake and Volcano Research Center, Nagoya University, h-ichi@seis.nagoya-u.ac.jp
[5]Graduate School of Science, Kobe University, hikari@pearl.kobe-u.ac.jp
[6]Earthquake Research Institute, The University of Tokyo, tkoyama@eri.u-tokyo.ac.jp
[7]Earthquake Research Institute, The University of Tokyo, takeo@eri.u-tokyo.ac.jp

**SUMMARY**

Nishinoshima is a volcanic island located about 900 km south from the main land of Japan. The volcano started eruptive activity in November, 2013. We conducted electromagnetic observation on the seafloor around the Nishinoshima using 1 VTM (Vector tsunameter) and 4 OBEMs (Ocena bottom electromagnetometers) from October 2016 to May 2017. VTM got the data during the whole of this time, while OBEMs observed for a maximum of two months. While the eruption activity of the Nishinoshima had not been identified during the first two months, the tilt data of VTM and OBEMs changed from 13th November to 20th November. At the same time, the total magnetic intensity changed a lot at two sites which were settled on the north side and east side of the island.

Tilt data can include both crustal movement and instrumental movement itself, but there is no significant instrumental movement except one OBEM according to the record of three-component fluxgate magnetometer. The tilt changes occurred in the middle of November were recorded at four sites, which means that the tilt changes were caused by crustal movement.

The time variation of the total magnetic intensity were calculated at each site using VTM, which is the farthest site from the Nishinoshima, as a reference site. Whereas the total magnetic intensity of the north site increased, that of the east site decreased. These variations were about 10 nT, and these changes were consistent with thermal demagnetization occurred inside the island.

The large variations of the tilt and total magnetic intensity were related to volcanic activity of the Nishinoshima and might be caused by the movement of magma. Moreover, the large variations were occurred five months before the Nishinoshima restarted eruption activity.

**Keywords:** Volcanic island, Ocean bottom magnetometer, Vector tsunameter, tilt change, magnetic field variation